Surface mass balance modeling of the Greenland ice sheet

Sensitivity and uncertainty of the energy balance model BESSI

Tobias Zolles

Thesis for the degree of Philosophiae Doctor (PhD)
University of Bergen, Norway
2022

UNIVERSITY OF BERGEN

Surface mass balance modeling of the Greenland ice sheet

Sensitivity and uncertainty of the energy balance model BESSI

Tobias Zolles

Thesis for the degree of Philosophiae Doctor (PhD)
at the University of Bergen

Date of defense: 17.06.2022

Year: 2022

Title: Surface mass balance modeling of the Greenland ice sheet

Name: Tobias Zolles

Print: Skipnes Kommunikasjon / University of Bergen

Preface

This dissertation for the degree of philosophiae doctor (PhD) has been submitted to the Department of Earth Science at the University of Bergen. The research in this thesis was part of the project "Modeling Englacial Layers and Tracers in ice-sheets " (MELT, reference number 231354), which was supported by the Trond Mohn Stiftelse.

The thesis was conducted entirely at the University of Bergen and supervised by Andreas Born. The Bjerknes Centre of Climate Research in Bergen made networking with other PhD students and researchers working in climate research easier. Through the CHESS research school it was possible to participate at various interesting courses and workshops. I had the opportunity to stay one month at the ice-core drilling site EASTgrip to study surface processes of snow and get better understanding of the surface mass balance in Greenland.

Acknowledgements

The University of Bergen served as a good host institution through my entire PhD. I would foremost like to thank my supervisor Andreas Born, for the opportunity to work on this project and the constant support provided. He gave me the chance to tailor the project to my interests and was understanding for my needs throughout my entire working time. It was a pleasure to work with him and that we finally got a bigger working group together by the end of my time in Bergen.

The entire glaciology group was supportive and lot of fun in the short period we shared the working environment. I would like to thank Andreas for getting two super motivated interns to us, with Katharina Maike Holube and Peter Wegmann. Katharina did an outstanding job working with me on the surface mass balance projections for Greenland, always being very keen on trying out my ideas and giving me the feeling of not working alone all the time and it was fun to supervise her. I want to thank Peter for the two reasons, for improving BESSI's efficiency and his interest in my knowledge on snow processes, and the activities we did together to keep me motivated through the last month of my thesis. Thanks for almost a year in the same working group, Therese Rieckh, Rebekka Frøystad and Konstanze Haubner. Alexios Theofilopulos was sharing my office and the PhD worries through the entire time with me, I will never forget the occasional earthquakes he caused to the table ;).

I want to thank all the members of BSI Seiling, from my first experiences with my office mate at that time Lukas Becker to becoming a Skipper and teaching new ones; we made it Natacha Fabregas. I want to thank my friends in Bergen who I shared offices with, good times, adventures and outdoor trips. Thanks Lander Crespo in particular for it.

Last, but not least come my friends from home and my family. Without my skiing buddies from Innsbruck, Adrian Schmidt, Julius Bär, Daniel Thorlakson und Moritz Müller I probably would not have made it through Covid times, and I am looking forward to ski with them again. My parents Karl and Irene Zolles, and my sister Isabella Zolles, were always supportive and had an open ear for me, you are the best. Lastly, Irina Kraft for everything, good times in Bergen, teaching me to sail, sailing, and exploring the world together, hope to see you soon.

Abstract

The surface mass balance is the main connection between the atmospheric climate change and the evolution of Greenland ice sheet over the next century. This thesis focuses on the development of surface mass and energy balance model for simulations of timescales above a century. The Ber*ge*n Snow SImulator (BESSI) needs to compromise between the necessary complexity to resolve the relevant physical processes and the computational costs of the model. There were three main studies published for the PhD focusing on model sensitivity, uncertainty assessment, transferability in space and time, and the modeling of the surface mass balance until the end of the current century.

BESSI is an energy balance model that accounts for snow albedo decay, vapor fluxes and sub-surface water percolation and refreezing. The sensitivity of the surface mass balance towards the individual free model parameters was assessed for a cold and a warm period for the first publication of this thesis. The dominant factor during the warm period are uncertainties associated with the long-wave radiation and clouds, while during the cold climate of the last glacial maximum, sublimation and deposition cannot be neglected. BESSI provides useful SMB simulations over the entire Greenland ice sheet, but the uncertainties associated with the long-wave radiation are better reduced by relying on climate data input.

The influence of the boundary climate conditions was studied next. The ice sheet is relatively stable to temporal variability changes, if the absolute range of change stays the same. Nevertheless, simulations based on a climatology instead of variable climate lead to a drastic overestimation of the surface mass balance. Climatologies have small amounts of daily snowfall, which lead to an increased snow albedo. A possible solution to obtain a good forcing for BESSI, and likely other surface mass balance models, is by distributing the precipitation based on the real temporal and spatial precipitation patterns.

After the thorough sensitivity and climate dependency study, the surface mass balance of Greenland over the current century was simulated. There are multiple different climate scenarios, depending on the chosen behavior of humans over the current century. The climate projections for each scenario are available from the Climate Model Intercomparison Project (CMIP6). The surface mass balance of the Greenland ice sheet was modeled for multiple model-scenario combinations. For the majority of the simulations the surface mass balance decreases until 2100, but the uncertainty in the projected SMB value is large. The biggest contributor to the uncertainty is the climate model uncertainty and not the selected scenario.

List of publications

Paper I[1]

Tobias Zolles and Andreas Born. 2021 **Sensitivity of the Greenland surface mass and energy balance to uncertainties in key model parameters**, *The Cryosphere* **15.6: 2917-2938.**, doi: doi.org/10.5194/tc-15-2917-2021

Paper II[1,2]

Tobias Zolles and Andreas Born. 2021 **How does a change in climate variability impact the Greenland ice-sheet surface mass balance?**, *The Cryosphere Discussions*, doi: doi.org/10.5194/tc-2021-379

Paper III[1]

Holube, Katharina M., Tobias Zolles, and Andreas Born. 2022 **Sources of uncertainty in Greenland surface mass balance in the 21st century**, *The Cryosphere* **16, 315–331, 2022**, doi: doi.org/10.5194/tc-16-315-2022

[1]Paper I-III are published under an open-access license which permits use and distribution (including reprint) in any medium, provided the original work is properly cited and no modifications or adaptations are made.

[2]Paper II is currently subject to an open review process

Two more papers were published during the PhD thesis using the model BESSI, but are not included in the thesis as Paper A I is a model intercomparison project and only BESSI simulations were contributed to the study. Paper A II was previously included in a PhD thesis by S. Rutledal, but was resubmitted including model simulations with BESSI recently.

Paper A I

Xavier Fettweis, Stefan Hofer, Uta Krebs-Kanzow, Charles Amory, Teruo Aoki, Constantijn J Berends, Andreas Born, Jason E Box, Alison Delhasse, Koji Fujita, Paul Gierz, Heiko Goelzer, Edward Hanna, Akihiro Hashimoto, Philippe Huybrechts, Marie-Luise Kapsch, Michalea D King, Christoph Kittel, Charlotte Lang, Peter L Langen, Jan Lenaerts, Glen E Liston, Gerrit Lohmann, Sebastian H Mernild, Uwe Mikolajewicz, Kameswarrao Modali, Ruth H Mottram, Masashi Niwano, Brice Noël, Jonathan C Ryan, Amy Smith, Jan Streffing, Marco Tedesco, Willem Jan Van de Berg, Michiel Van den Broeke, Roderik SW Van De Wal, Leo Van Kampenhout, David Wilton, Bert Wouters, Florian Ziemen, Tobias Zolles. 2020 **GrSMBMIP: intercomparison of the modelled 1980–2012 surface mass balance over the Greenland Ice Sheet**, *The Cryosphere* **14,11, 3935-3958, 2022**, doi: doi.org/10.5194/tc-14-3935-2020

Paper A II

S. Rutledal, M.H. Simon, L. Menviel, T. Zolles, H. Haflidason, A. Born, S.M.P. Berben, and T.M. Dokken. 2021 **Atlantic inflow into the Nordic Seas at the onset of the Last Glacial Maximum promotes open-ocean conditions and Fennoscandian Ice Sheet growth**, *Science Advances* **under review**

Contents

1 Introduction

The cryosphere is reacting to the global climate. While currently glaciers are the main contributor to global sea level rise the big ice sheets on Greenland and Antarctica will be the dominating component by the end of the century (IPCC 2021). Reducing the uncertainty in ice sheet evolution projections is one of the main challenges for sea level projections. Greenland and Antarctica have existed throughout the last glacial cycle and the last interglacial-glacial cycle, and their past evolution may serve as an analogue for the current warming (*Greve et al.*, 1999; *Van de Berg et al.*, 2011; *Plach et al.*, 2019). Furthermore, past climate information is stored in the ice and can be reconstructed using isotope analysis (e.g. *Dansgaard et al.*, 1969; *Augustin et al.*, 2004; *Masson-Delmotte et al.*, 2015). With the re-constructed climate conditions the evolution of the past ice sheets can be modeled. The main interaction between the atmospheric climate and the ice sheet is via the surface mass and energy balance. This thesis focuses on the development of a surface energy and mass balance model, the Ber*g*en Snow SImulator (BESSI), to simulate the atmosphere-ice interaction.

Surface mass balance models have a wide range of complexity. Simple models rely only on temperature and precipitation to calculate the surface mass balance (SMB) (*Braithwaite*, 1995; *Cuffey and Marshall*, 2000; *Ohmura*, 2001; *Hock*, 2003; *Fürst et al.*, 2015; *Goelzer et al.*, 2016). They are often referred to as temperature index, or degree day models (PDD), as the amount of surface melt is depending on a fixed melt factor and the days above a certain temperature threshold. PDD was enhanced to also account for changes in solar radiation on multiple occasions (enhanced temperature index, insolation-temperature melt (ITM)) (e.g. *Pellicciotti et al.*, 2005; *Van Den Berg et al.*, 2008; *Robinson et al.*, 2010, 2011), which is highly relevant for simulations of the glacial cycle with its drastic changes to the orbital configuration and solar insolation. The second common type of SMB models are energy balance models, which calculate the surface energy balance based on multiple atmospheric parameters. Due to the increased data requirement, they were first applied on the point scale close to a weather station which provided all the data necessary (*Brock et al.*, 2000; *Greuell and Smeets*, 2001; *Lefebre*, 2003; *Bougamont et al.*, 2005). Distributed energy balance models are frequently used to model the SMB now (*Klok and Oerlemans*, 2002, 2004; *Hock and Holmgren*, 2005; *Box et al.*, 2012). *Hock* (2005) provides a wide review of the history and status of SMB modeling. Lastly, regional climate models are used to model the SMB together with multiple atmospheric quantities. Over Greenland examples are HIRHAM5 (*Lucas-Picher et al.*, 2012), RACMO (*Noël et al.*, 2018) and MAR (*Fettweis et al.*, 2005). The RCMs may include very complex snow models to calculate the SMB, like SNOWPACK or CROCUS (*Bartelt and Lehning*, 2002; *Vionnet et al.*, 2012), but which on their own fall into the category of energy balance models.

With the increasing complexity of the above mentioned groups of temperature index, energy balance and regional climate models, not only the computational costs increase but also the data requirement. Most long time simulations of the ice sheets are relying on temperature index based methods for the SMB, as only precipitation and atmospheric temperature are needed (*Fürst et al.*, 2015; *Goelzer et al.*, 2016). Temperature can be reconstructed using ice or marine cores, while precipitation is harder to reconstruct.

Additionally, the uncertainties in the precipitation forcing are hard to quantify in such an approach and the validity of the temperature index parameterization for different time periods than the one calibrated for is questionable (*Beven and Binley*, 1992; *MacDougall et al.*, 2011; *Li*, 2020). ITM does account for orbital changes of the solar radiation, but still suffers from a similar calibration problem (*Robinson et al.*, 2010, 2011). On the other side, the regional climate models are too computationally demanding to model longer time periods, and also require full global climate model data as forcing at a sub-daily resolution. They have been applied successfully to different time periods, but are not feasible to be run over longer time scales (*Plach et al.*, 2019; *Agosta et al.*, 2019).

Energy balance models are expected to be better suited to be used for different time periods than PDD-models, because individual physical processes are modeled and changes in atmospheric variables other than temperature can be accounted for. Despite their potential gain, they may still suffer from over-fitting during the calibration period, unresolved physical processes, or too simple parameterizations (e.g. *Beven and Binley*, 1992; *Prinz et al.*, 2016; *Zolles et al.*, 2019). Given the data requirement and computational constraints efficient energy balance models are quite good candidates to be used for ice sheet models. Today most ice sheet models rely on PDD/ITM which was shown to be inferior for certain climate models (*Bauer and Ganopolski*, 2017). Over the last years multiple energy balance models were developed to fill this gap, e.q. BESSI, SEMIC, and dEBM (*Born et al.*, 2019; *Krapp et al.*, 2017; *Krebs-Kanzow et al.*, 2018, 2021). Given the long time scales that are to be modeled simplifications compared to state of the art energy balance models for glaciers have to be done. BESSI does not resolve the diurnal cycle, but has a multi-layer sub-surface scheme, turbulent fluxes and variable albedo routines as well as firn densification. dEBM does not resolve any of the turbulent fluxes, but accounts for the daily cycle. SEMIC parameterizes the daily cycle of temperature and therefore can resolve the melt-refreezing cycle, but the subsurface layers are not resolved and no densification occurs.

Even energy balance models have to be calibrated before being used. The free model parameters are to be fixed in the calibration step. This could either be done relative to measurements or other models. During the calibration the model parameters are adjusted to fit the data of the calibration period. This may result in an effect called over-fitting, parameters may take values that are too specific for the calibration period or may compensate for effects which the model does not include (*Beven*, 1989; *Beven and Binley*, 1992). Calibrated parameters may not be consistent through time. Furthermore, the model may also be calibrated against multiple objectives leading to multiple solutions and parameter combinations (*Rye et al.*, 2012; *Zolles et al.*, 2019). A cross-validation procedure could be used to quantify the effect of over-fitting. It has been shown for another energy balance model that the free model parameters found during calibration from on year to another vary drastically for alpine glaciers (*Zolles et al.*, 2019). It is expected that the variation will be even larger for time periods further apart, with a varying climate like over a glacial cycle. To reduce the effects of over-fitting and check for the applicability of BESSI for the glacial cycle, a proper uncertainty and sensitivity analysis is helpful. Throughout this thesis sensitivity is considered to be the variance of the model output (e.g. SMB) as function of the uncertainty ranges in the model input (parameters, forcing) (*Zolles et al.*, 2019). Given the large range of physical reasonable values for multiple free model parameters more model solutions may exist. A reduction in the amount of model free parameters based on a thorough sensitivity analysis reduces

the effects of over-fitting, saves computational costs and reduces the effect of parameter correlation (*Spear and Hornberger*, 1980; *Saltelli et al.*, 2000; *van Griensven et al.*, 2006; *Zolles et al.*, 2019).

Multiple techniques to analyze the model sensitivity exist: local one at a time (OAT), gradient based, regression analysis or variance based. OAT techniques are most commonly used due to low computational cost and complexity, but require an estimate of the optimal parameter settings as every parameter is disturbed from the one optimal combination (*Gurgiser et al.*, 2013). To assess the parameter sensitivity under different climate conditions, other techniques may be better suited. First, due to the lack of calibration data the optimal parameter setting is not known, and it may as well vary for the different climate conditions. Second, some free model parameters in BESSI are not continuous, but rather switches enabling different albedo or turbulence schemes. Therefore, a variance based technique was used. The global sensitivity analysis developed by *Saltelli et al.* (2010) had previously been applied to snow and glacier models (*Sauter and Obleitner*, 2015; *Zolles et al.*, 2019). The sensitivity analysis provides a deeper understanding of the used model, its sensitivity to the free model parameters, insights into the model tuning processes, the key model parameters and which input to be optimized first. Furthermore, free model parameters showing a low sensitivity could be fixed to any value within the range to reduce computational costs for optimization and reduce parameter correlation. Nevertheless, the technique comes at a high computational cost with a requirement of more than 10.000 simulations in the case of BESSI.

An energy balance model does not only have uncertainties in its free model parameters, but also in the climate forcing (*Walsh et al.*, 2008). The high arctic is a particular uncertain region for climate model simulations (*Cai et al.*, 2021). The uncertainty for climate reconstructions is even larger. Given the uncertainty in climate reconstructions during the glacial cycle, they had not been part of the sensitivity analysis of Paper I (*Hargreaves et al.*, 2013). The energy balance model requires proper climate forcing data. The amount, temporal and spatial resolution, and quality of available data becomes less the further away from present day the data is needed. For the last 40 years the extensive reanalysis products of the ECMWF ERA-interim and ERA5 provide a usable forcing over the Greenland ice sheet (*Uppala et al.*, 2011). Global circulation models (GCMs) offer data of similar resolution and may have a similar climatology than the reanalysis data, though biases over Greenland are larger than for most other regions (*Watanabe et al.*, 2012). GCMs are also available for short snaps of the last glacial cycle and could act as possible forcing for energy balance models (*Bauer and Ganopolski*, 2017; *Plach et al.*, 2019). Furthermore, glaciological models were often forced using climate reconstructions based on the glacial index, which interpolate a cold and a warm climate state based on a temperature proxy, most commonly an ice core (*Greve et al.*, 1999; *Forsström et al.*, 2003; *Niu et al.*, 2019, e.g.). The problem of the GCMs and the reconstructed climate data is that the inter-annual variability is different from the reanalysis data. Proxies even often show no variability below centennial resolution. The SMB may be sensitive to the inter-annual variability (*Bougamont et al.*, 2005; *Donat-Magnin et al.*, 2020) and using climatological forcing may impact the model results. The effect of climatological averages and reduced inter-annual variability is studied in Paper II.

1.1 Data and methods

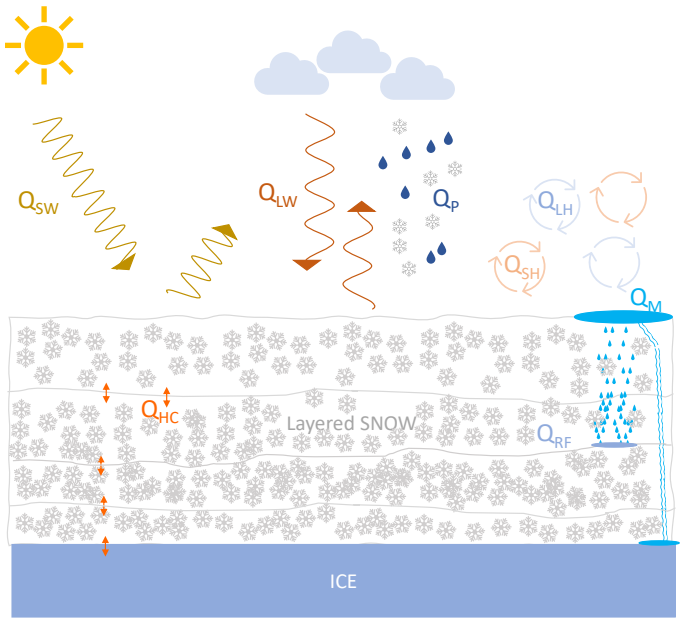

Figure 1.1: The schematic energy fluxes at the surface of a snowpack on ice. The solar radiation is partly reflected depending on the snow albedo (Q_{SW}). The sky and clouds as well as the snow surface emit thermal/long-wave radiation (Q_{LW}). Rain and snow are associated with the precipitation heat flux Q_P. Via turbulence sensible heat Q_{SH} and latent heat Q_{LH} are exchanged. If the energy fluxes lead to melting ($Q_M > 0$), it can percolate, runoff or refreeze (Q_{RF}). The subsurface furthermore conducts heat (Q_{HC}).

This PhD-thesis was part of the Modeling Englacial Layers and Tracers in ice sheets (MELT). The overarching aim is to model the Greenland ice sheet over an entire glacial cycle, and validate it with radio-stratigraphy and ice core data (*Sime et al.*, 2014; *MacGregor et al.*, 2015). The SMB is one of the key components of ice sheet models. Over such long time scales as an entire glacial cycle small uncertainties and biases can lead to drastic results in the evolution of the ice sheet. The Ber*g*en Snow SImulator was in its first iteration developed by *Imhof* (2016) at the University of Bern. It was a surface mass balance subroutine used in conjunction with a simple ice sheet model (*Neff et al.*, 2016). The previously used version of BESSI by *Imhof* (2016) showed dramatic overestimation of the SMB during the last glacial maximum (LGM) in the dry zones like the Tibetan Plateau. To avoid similar errors in the modeling of the SMB over Greenland, BESSI was developed further to include different albedo schemes, variable output as well as accounting for the turbulent latent heat flux. The changes implemented were thoroughly tested and the model sensitivity assessed.

Surface energy balance models compute the surface energy balance (SEB) at the surface:

$$Q_i + Q_M = Q_{SW} + Q_{LW} + Q_{SH} + Q_{LH} + Q_P \tag{1.1}$$

where Q_i is the internal energy of the ice (temperature) and Q_M the energy available

for melting. The energy changes due to the short-wave/solar radiation Q_{SW}, the long-wave/thermal radiation Q_{LW}, turbulent fluxes for sensible Q_{SH} and latent Q_{LH} heat, and the heat supplied by precipitation Q_P. The energy either leads to an increase of the snow/ice temperature or melting. The meltwater starts down to percolate into lower layers once the maximum water holding capacity is reached. The meltwater may then either refreeze Q_{RF}, or percolate further until it is treated as runoff if the lowest layer is saturated. The subsurface is subject to heat conduction Q_{HC}. All fluxes mentioned above are parameterized in BESSI, which also accounts for densification of the snow. An in-depth description of the individual processes is given in *Born et al.* (2019) and Paper I of this thesis.

BESSI is a surface energy and mass balance model that runs on daily time scales and can run about 150 years/h. A recent parallelized version can achieve up to 100 years/min. The model requires input of atmospheric temperature, humidity, short-wave and long-wave (optional) radiation, and precipitation. All studies within this thesis were run on a 10×10 km grid, that includes all of Greenland. The climate data used for the different studies are ERAinterim (ECWMF (*Uppala et al.*, 2011)), CCSM4 for the LGM (*Brady et al.*, 2013), and CMIP6 (*Eyring et al.*, 2016).

1.2 Thesis outline

The thesis is composed of three main papers studying a) the sensitivity of BESSI, b) the impact of climate variability on the SMB c) the SMB of the Greenland ice sheet in the 21st century.

Paper I, *Sensitivity of the Greenland surface mass and energy balance to uncertainties in key model parameters*

The study assesses the sensitivity of the distributed surface mass balance model BESSI over two periods during the last glacial cycle. Additionally, BESSI was improved by including multiple albedo schemes and the turbulent latent heat flux. The sensitivity method used is a variance based technique that is independent of prior model tuning and an optimal parameter setting. The method had so far been applied in cryospheric studies only twice. The global sensitivity analysis determines the model sensitivity over the entire free model parameter space, but is computationally expensive, leading to more than 16.000 simulations of 500 model years for this study.

Two distinct time periods were chosen for the sensitivity modeling, with present day as representative forcing for warm conditions, and the last glacial maximum for cold conditions. The two extremes of the glacial cycle provide a reasonable assessment of the sensitivity through time. The sensitivity and uncertainty quantification will provide a better understanding of applicability of energy balance models through time. BESSI is most sensitive to the long-wave radiation parameterization and the associated parameters under present day conditions, but the sensitivity towards the snow albedo as well as the turbulent latent heat flux are of similar importance in some regions of Greenland. While the turbulent latent heat flux has very little influence under present day climate conditions on the Greenland-wide integrated SMB, it is the dominant sensitivity component during the colder LGM, due to reduced air temperature and less over-all melting

the impact of the long-wave radiation decreases for the glacial. The sensitivity of the Greenland-wide SMB is distinctly different from a regional basis. The turbulent latent heat flux has a low impact on the total SMB during the current climate, but over the entire glacial cycle it has to be included. Due to the large uncertainty associated with the parameterization of long-wave radiation and clouds, it is desirable to use these directly from a climate model for SMB modeling of the glacial cycle.

Paper II, *How does a change in climate variability impact the Greenland ice sheet surface mass balance?*

The surface mass balance model requires atmospheric climate data as an input, which can be weather forecasting data, global or regional circulation model data, reanalysis data, weather station data, or reconstructed climate data. The quality and temporal as well as the spatial resolution of the data varies. With BESSI being developed mainly for simulations of longer time scales (centennial and longer), data is often of lower resolution. Climate reconstructions only provide an average climate state, ranging from yearly to multi-centennial, depending on the used proxies, method and time period. Also the General Circulation Models, if it all do only agree in the average climate but not the internal temporal variability. Paper II studies the uncertainties arising from those climate averages in comparison to fully transient forcing. The last forty years of present day climate are chosen, as temperature rises over this time period. Such a trend may not be visible in proxy data of multi-decadal resolution, but may impact the SMB response.

A simple reordering procedure is applied first to assess the impact of climatic trends and inter-annual variability on the SMB. The order of warm and cold years during almost 500 years of present day climate has less than 5% influence on the SMB over the entire ice sheet, though around the equilibrium line and the dry north-west it is larger. The temporal variability beyond inter-annual timescales has therefore only a minor importance for the SMB. In a next step the inter-annual variability was removed completely and only climatological averaged data used as forcing. The SMB is drastically (40%) overestimated. Due to small amounts of precipitation every day in the climatological data, the albedo is overestimated by the model. The study investigates this further and suggests a potential solution how to create forcing data from an average climate which is functional with BESSI, and similar SMB models.

Paper III, *Sources of Uncertainty in Greenland Surface Mass Balance in the 21st century*

Based on the results of the two previous studies BESSI is applied to the current century over Greenland. Using the CMIP6 climate projection ensemble of 26 global circulation models, the SMB until 2100 was simulated for four different Shared Socioeconomic Pathways (SSP (IPCC 2021)). The SSPs are closely related to the CO_2 emission scenarios. The SMB over Greenland decreases for all SSPs, but there is a significant difference between the individual climate models. Despite them all showing a positive temperature trend over Greenland, the SMB does not decrease for all in a similar manner. With a variance decomposition, we could identify that the biggest source of uncertainty for the Greenland SMB are the climate models and only then followed by the SSPs/emission scenarios. The uncertainty related to the free model parameters in BESSI is marginal in

comparison, leading to the overall conclusion that the uncertainties in the climate data is the main issue related to SMB modeling over Greenland.

1.3 Contributions at scientific meetings

Tobias Zolles. Parameter uncertainty of energy and mass balance glaciological models. *Snow Modeling Workshop*; 2017-10-10 - 2017-10-12, Finse, Norway.

Tobias Zolles and Andreas Born. Parameter uncertainty of energy and mass balance glaciological models. *IASC Workshop on the Dynamics and Mass budget of Arctic glaciers*; 2019-01-21 - 2019-01-23, Geilo, Norway.

Tobias Zolles and Andreas Born. The need for water vapor fluxes in long-term modeling of the Greenland ice sheet. *EGU General Assembly 2019*; 2019-04-07 - 2019-04-12, Vienna, Austria.

Tobias Zolles and Andreas Born. The uncertainty of average precipitation forcing. *IASC Workshop on the dynamics and mass budget of Arctic glaciers* ; 2020-01-28 - 2020-01-30, Obergurgl, Austria.

Katharina Meike Holube, Tobias Zolles, and Andreas Born. Sources of Uncertainty in Greenland Surface Mass Balance in the 21st century. *EGU General Assembly 2019 digital*; 2021-04-19 - 2021-04-30, Vienna, Austria (digital)

Sensitivity of the Greenland surface mass and energy balance to uncertainties in key model parameters

Tobias Zolles and Andreas Born
Department of Earth Science, University of Bergen, Bergen, Norway
Bjerknes Centre of Climate Research, Bergen, Norway
The Cryosphere, 15, 2917–2938, 2021
doi: doi.org/10.5194/tc-15-2917-2021

The Cryosphere, 15, 2917–2938, 2021
https://doi.org/10.5194/tc-15-2917-2021

The Cryosphere Open Access EGU

Sensitivity of the Greenland surface mass and energy balance to uncertainties in key model parameters

Tobias Zolles[1,2] **and Andreas Born**[1,2]

[1]Department of Earth Science, University of Bergen, Bergen, Norway
[2]Bjerknes Centre for Climate Research, Bergen, Norway

Correspondence: Tobias Zolles (tobias.zolles@uib.no)

Received: 22 October 2019 – Discussion started: 14 November 2019
Revised: 30 March 2021 – Accepted: 25 April 2021 – Published: 28 June 2021

Abstract. We investigate the sensitivity of a distributed glacier surface mass and energy balance model using a variance-based analysis, for two distinct periods of the last glacial cycle: the present day (PD) and the Last Glacial Maximum (LGM). The results can be summarized in three major findings: the sensitivity towards individual model parameters and parameterizations is as variable in space as it is in time. The model is most sensitive to uncertainty related to atmospheric emissivity and the down-welling longwave radiation. While the turbulent latent heat flux has a sizable contribution to the surface mass balance uncertainty in central Greenland today, it dominates over the entire ice sheet during the cold climate of the LGM, in spite of its low impact on the overall surface mass balance of the Greenland ice sheet in the modern climate. We conclude that quantifying the model sensitivity is very helpful for tuning free model parameters because it clarifies the relative importance of individual parameters and highlights interactions between them that need to be considered.

1 Introduction

Of the many challenges to accurately simulate past variations in the volume of the Greenland ice sheet (GrIS) and to project its future contribution to sea level rise, recent studies agree that the uncertainty associated with surface mass balance (SMB) is among the most important (Aschwanden et al., 2019; Plach et al., 2019).

Models to calculate SMB cover a whole range of complexities from empirical index models that only account for air temperature (Ohmura, 2001; Zemp et al., 2019) or temperature and solar radiation (Bintanja et al., 2002; Van Den Berg et al., 2008; Robinson et al., 2011) to coupled atmosphere–snow models that simulate the snowpack in multiple layers and give a full representation of the atmospheric circulation, based on physical first principles (Lehning et al., 2002; Fettweis, 2007; Noël et al., 2018). On this spectrum, the empirical models perform well for the observational period and when the temperature sensitivity of the SMB is well known (Fettweis et al., 2020), but they are difficult to constrain for temporal and spatial climate variations and become unreliable for conditions outside their relatively narrow tuning interval (van de Berg et al., 2011; Plach et al., 2019). There is a lack of constraint in empirical models even though their low computational requirements make them attractive for the long integration times that are needed to simulate continental ice sheets. Their shortcomings severely limit the usefulness of their results. On the other hand, detailed snow models and especially those coupled with regional atmosphere models are computationally too expensive to run for long periods of time. This situation motivated the development of models that balance the defensible representation of the relevant physical processes with computational efficiency (Krapp et al., 2017; Krebs-Kanzow et al., 2018; Born et al., 2019).

In this study, we use the BE*rge*n Snow SImulator (BESSI), a model that is designed to include all relevant physical mechanisms with reasonable detail but is specifically prepared for long integration times by reducing its computational requirements and by strictly conserving mass and energy (Born et al., 2019). Adding to the original model version, we now include three different parameterizations for snow aging based on Oerlemans and Knapp (1998), Aoki

et al. (2003), and Bougamont et al. (2005). The turbulent latent heat flux is now also simulated. For this study the model domain was reduced to Greenland at a resolution of 10 km, but all model changes are also applicable to the original setup.

Multiple studies have investigated the impact of the turbulent latent heat flux on the surface mass balance (Box and Steffen, 2001; Box et al., 2004; van Den Broeke et al., 2008; Cullen et al., 2014; Noël et al., 2018). They find a relatively small impact of the vapor fluxes on the Greenland ice sheet total mass balance ($\approx 5\,\mathrm{Gt\,a^{-1}}$; Cullen et al., 2014), but their local impact can be up to 20 % of the annual accumulation (Box et al., 2004). The importance of the vapor flux is difficult to assess for different climatic settings because, as Box and Steffen (2001) have shown, the choice of the calculation method impacts the results greatly in regions of low mass flux like the dry interior zone of Greenland. This is exacerbated by the fact that turbulent latent heat fluxes are mostly negative in winter under the present climate conditions and positive in summer, so the sign of the net flux may change with a different climate. During the colder climate of the glacial a much larger impact of the turbulent latent heat flux can be assumed, similarly to the much greater importance it currently has in Antarctica (e.g., Gallet et al., 2014; van Wessem et al., 2018). A parameterization based on the bulk method by Rolstad and Oerlemans (2005) has been added to BESSI to simulate the turbulent latent heat flux.

To assess the sensitivity of the new parameterizations and that of BESSI overall, we employ a variance-based approach (Saltelli et al., 2000, 2006, 2010; Sauter and Obleitner, 2015) that has previously been used to quantify the sensitivity of glacier and ice models (Aschwanden et al., 2019; Bulthuis et al., 2019; Zolles et al., 2019). We extend the sensitivity analysis used by Zolles et al. (2019) to provide spatial patterns of sensitivity indices. Following our model's design goal to be used over timescales of glacial cycles and accounting for potentially different sensitivities under different climate boundary conditions, we analyze two large ensembles with a total of 16 500 simulations, for the present-day (PD) climate and for that of the Last Glacial Maximum (LGM). The result is rich information on what parameters and parameterizations have the largest impact on the model's performance and how this sensitivity varies in different regions of Greenland and over time. Knowing the sensitivity also enables a better calibration of the model parameters as the knowledge prevents or reduces over-fitting to a particular study location or time (Beven, 1989).

The revised model is described in Sect. 2. The distributed sensitivity analysis of multiple model output variables in relation to model parameters, including those for the new parameterizations for turbulent latent heat flux and snow aging, is presented in Sect. 3. After that, we discuss our findings in Sect. 4 and conclude in Sect. 5.

2 Model description and study setup

The study uses the efficient mass and energy balance model BESSI, which is designed to simulate the mass balance over long timescales (Born et al., 2019). The energy exchange between the snow and the atmosphere is altered in the model version used here, while the subsurface and internal processes are unchanged from the previously published version. The following model was enhanced to include the turbulent latent heat flux and multiple more-complex snow albedo schemes were added. The model description given in the following focuses entirely on the interaction between the snow surface and the atmosphere. For the numerical description and other subsurface processes like firnification and heat conduction, see Born et al. (2019).

The model setup used here has a 10 km grid for the domain of Greenland. The vertical dimension is discretized based on the mass with up to 15 layers in the snowpack (Born et al., 2019). The mass of each layer is 100–500 $\mathrm{kg\,m^{-2}}$. Each cell has a default maximum of $300\,\mathrm{kg\,m^{-2}}$, but due to melt and refreezing the mass may decrease or increase, respectively. Cells above $500\,\mathrm{kg\,m^{-2}}$ or below $100\,\mathrm{kg\,m^{-2}}$ are split or merged, respectively, to restore the default maximum value. Simulations require daily input of air temperature, total precipitation, and solar radiation and its reference height. Humidity is an optional input which is required if the turbulent latent heat flux is computed. All variables are interpolated to the 10×10 km model grid using bi-linear interpolation. The air temperature is the only meteorological input which is vertically downscaled to the firn model topography using a temperature lapse rate of $6.5\,\mathrm{K\,km^{-1}}$ for the PD and $8.55\,\mathrm{K\,km^{-1}}$ for the LGM. The output written by the model may be adjusted by the user, who can select values ranging from daily over monthly to annual timescales. Output variables include surface mass balance; melt of snow; melt of ice; runoff; refreezing; albedo; turbulent latent heat flux; and a mask containing snow, land, ice, and water as well as the 3-dimensional grid values for snow mass, snow density, snow temperature, and liquid water mass.

2.1 Surface energy fluxes

The energy exchange between the surface and the atmosphere comprises five different processes, of which the precipitation and the turbulent latent heat flux (vapor flux) also imply a change in mass: the shortwave radiation (Q_{SW}), the longwave/thermal radiation (Q_{LW}), the turbulent sensible heat flux (Q_{SH}), the turbulent latent heat flux (Q_{L}), and the heat flux associated with precipitation (Q_{P}).

The total surface flux can be expressed as

$$c_{\mathrm{i}} m_{\mathrm{s},1} \left.\frac{\partial T}{\partial t}\right|_{\mathrm{surface}} + Q_{\mathrm{M}} = Q_{\mathrm{i}} + Q_{\mathrm{M}} = Q_{\mathrm{SW}} + Q_{\mathrm{LW}} + Q_{\mathrm{SH}} + Q_{\mathrm{L}} + Q_{\mathrm{P}}\,, \quad (1)$$

where the left-hand side denotes the resulting temperature change of the snow/ice (Q_i) and the available energy for melting (Q_M) if the melting point is reached. Due to the implicit scheme the model uses, no melt is calculated at first, only energy fluxes and temperatures (even above 273 K). The actual melt is then calculated explicitly at each time step as the excess heat above the melting point. The mass flux of the water vapor is also calculated explicitly.

2.1.1 Shortwave radiation and albedo parameterization

The energy input to the surface from solar radiation is calculated by using a broadband albedo value:

$$Q_{SW} = (1-\alpha)\cdot SW_{in}\,, \tag{2}$$

where α denotes the surface albedo, either α_s for snow or α_i for ice, and SW_{in} is the incoming short-wave radiation at surface height. The albedo value is assumed constant with respect to the solar incidence angle but undergoes temporal and spatial variations depending on surface properties. We implement four albedo parameterizations of different complexity to simulate the snow albedo. They all have a common maximum albedo value for fresh snow (α_{fs}) and minimum value for aged snow (firn α_{fi}), and ice albedo (α_i), but they vary in how they calculate the aging.

1. Constant. This simple parameterization only uses constant values for dry snow ($\alpha_s = \alpha_{fs}$ $T_s < 273$ K), wet snow ($\alpha_s = \alpha_{fi}$ $T_s = 273$ K), and ice (α_i). This parameterization has been used before in BESSI (Born et al., 2019).

2. Oerlemans and Knapp (1998). This parameterization assumes an exponential decay with time of the fresh snow albedo to a final value of old snow albedo (Oerlemans and Knapp, 1998):

$$\alpha_s = \alpha_{fi} + (\alpha_{fs}-\alpha_{fi})e^{(\frac{t_{fs}-t}{t^*})}, \quad t^* = \begin{cases} 30\,\mathrm{d}, & T_s < 273.15\,\mathrm{K} \\ 5\,\mathrm{d}, & T_s = 273.15\,\mathrm{K}, \end{cases} \tag{3}$$

where t_{fs} denotes the last day of snowfall and t the current day (time step) with t^* as the characteristic time in days. This or similar parameterizations are usually optimized for the decay rate t^* using observations of albedo or mass balance (e.g., Oerlemans and Knapp, 1998; Klok and Oerlemans, 2004; Bougamont et al., 2005). The very fast decay at the melting point was chosen to account for our very large upper grid box (0.28–1.4 m depending on the mass and density of the box), as the heat capacity of the entire large box may delay the melting on the top of the surface layer. Equation (3) does not consider shallow snowpacks, where underlying ice or dirty firn albedo may reduce the albedo.

3. Bougamont et al. (2005). These authors modified the parameterization by Oerlemans and Knapp (1998) specifically for the Greenland ice sheet by introducing a snow-temperature-dependent decay rate:

$$t^* = \begin{cases} 100\,\mathrm{d}, & T_s < 263\,\mathrm{K} \\ 30\,\mathrm{d} + 7\,\mathrm{d}\cdot(273.15\,\mathrm{K} - T_s), & 263\,\mathrm{K} \geq T_s < 273.15\,\mathrm{K} \end{cases} \tag{4}$$

Equation (4) results in the same t^* of 30 d as that of Oerlemans and Knapp (1998) (Eq. 3) up to the melting point (273.15 K). This parameterization furthermore introduces an additional wetness-dependent albedo decay in the case of wet snow, which assumes a thin layer of water at the surface according to

$$\alpha_s = \alpha_{fi} - (\alpha_{fi}-\alpha_s)\cdot e^{(\frac{-w_{surf}}{w^*})}. \tag{5}$$

Here w_{surf} denotes the thickness of the water layer and w^* is a characteristic water layer thickness. Since BESSI does not explicitly simulate water at the surface, we adapted the liquid-water-dependent part using a simple linear parameterization. The decay rate increases depending on the liquid water content ζ (see Sect. 2.2 for details about the liquid water content):

$$t^* = 15 - 14\cdot\frac{\zeta}{\zeta_{max}}\,\mathrm{d}, \quad T_s = 273.15\,\mathrm{K}. \tag{6}$$

4. Aoki et al. (2003). The final albedo parameterization available in the model uses both temperature- and time-dependent decay rates. There is a linear dependency on temperature in each time step, and this parameterization is therefore not exponentially dependent on the time since the last snowfall.

$$\alpha_s(t) = \min\{\alpha_s(t-1) - ((T_s - 273.15\,\mathrm{K})\cdot k + c),\ \alpha_{fi},\ \alpha_s(t-1)\}, \tag{7}$$

where t and $t-1$ are the current and the previous time step, α_s is the snow albedo, and $k = 1.35\times10^{-3}\,\mathrm{K}^{-1}$ and $c = 0.0278$ are two empirically based constants. The values are based on averaged values from Aoki et al. (2003) for different spectral bands. To account for a faster decay in a wet snowpack, the albedo is linearly decreased based on the liquid water content of the topmost layer:

$$\alpha_s(t) = \alpha_s(t) - (\alpha_s(t) - \alpha_{fi})\cdot\frac{\zeta}{\zeta_{max}}. \tag{8}$$

If the layer is fully saturated with water, the snow albedo instantly drops to its minimum value. This is done in addition to Eq. (7) at each time step. The albedo increases when new snowfall occurs, but instead of resetting it to the fresh snow value, this albedo is incrementally increased depending on the amount of fresh snow to account for thin layers of snow and the penetration of shortwave radiation into the older subsurface:

$$\alpha(t) = \alpha(t-1) - (\alpha_{fs}-\alpha_{fi})\cdot(1-\exp\frac{-d}{d^*}), \tag{9}$$

where d is the amount of new snow and the characteristic snow depth d^* is at 3 cm (Oerlemans and Knapp, 1998).

2.1.2 Longwave radiation

The longwave radiation is a simple parameterization based on the Stefan–Boltzmann law:

$$Q_{LW} = \sigma(\epsilon_{atm}T_{atm}^4 - \epsilon_s T_s^4), \tag{10}$$

where σ is the Stefan–Boltzmann constant and T_{atm} and T_s are the 2 m air and snow surface temperature, respectively. The emissivity of snow/ice ϵ_s is constant at 0.98. Incoming longwave radiation only depends on the actual air temperature and the atmospheric emissivity ϵ_{atm}, as the only free model parameter. The lack of confidence in cloud cover of climate models in particular during the last glacial cycle led to this decision. Though more complex empirical relations exist (e.g., Listion and Elder, 2006), their applicability for other timescales is questionable. We therefore refrain from using these empirical relationships despite the importance of cloud cover, moisture, and aerosols. ϵ_{atm} varied over a broad range of 0.6–0.9 following the previous configurations of BESSI or similar models (Greuell and Konzelmann, 1994; Busetto et al., 2013; Born et al., 2019). Emissivity values spanning from 0.6 to 0.9 may in reality occur simultaneously in different regions of the Greenland ice sheet, but in the current configuration there is only a single atmospheric emissivity value over the entire ice sheet.

2.1.3 Turbulent sensible heat flux

The calculation of the turbulent latent heat flux is based on a bulk method (Braithwaite, 2009) which was applied previously on Greenland as a residual method (Rolstad and Oerlemans, 2005). This method assumes a constant turbulent exchange coefficient (C_h) for sensible heat over time and space. The only dependency in the previously published parameterization is on the local wind speed u and air temperature T_{atm}:

$$Q_{SH} = \rho_{air} c_p C_h u (T_{atm} - T_s) = D_{SH}(T_{atm} - T_s), \quad (11)$$

where ρ_{air} is the density of air and c_p the heat capacity of air. Since BESSI does not use wind speed as an input field, we simplify the equation with a single free model parameter: the turbulent heat exchange coefficient D_{SH} which is the subject of the sensitivity analysis. The values given in Table 1 assume an average wind speed of $5\,m\,s^{-1}$ if compared to the reported values by Braithwaite (2009). The variation in parameter D_{SH} therefore accounts for both the variability in average wind speed and the efficiency of the exchange C_h.

2.1.4 Turbulent latent heat flux

The previous version of BESSI did not include turbulent latent heat flux. The new model version includes an optimal turbulent latent heat flux subroutine as part of the setup. The implementation is analog to the turbulent sensible heat flux (Eq. 11):

$$Q_L = 0.622\ \rho_{air} L_v C_h u (e_{air} - e_s) p^{-1} = D_{LH}(e_{air} - e_s), \quad (12)$$

where D_{LH} is the turbulent latent heat exchange coefficient and e is the water vapor pressure. The parameterization is based on the bulk formulation of Rolstad and Oerlemans (2005) with the latent heat of vaporization L_v and the air pressure p. The latter is calculated from the standard pressure at sea level for each grid point. While Rolstad and Oerlemans (2005) assume the same exchange coefficient C_h for vapor and sensible heat, Greuell and Smeets (2001) have previously shown that the roughness lengths and the exchange coefficient for momentum and vapor are not necessarily equal. Nevertheless, the parameters D_{LH} and D_{SH} are inherently connected by the surface structure (snow/ice) and the wind speed. To account for the correlation as well as some degree of freedom, our setup uses two free model parameters determining D_{LH}, the turbulent exchange coefficient for sensible heat D_{SH}, and $r_{lh/sh}$, which are defined by

$$D_{LH} = r_{lh/sh} \cdot 0.622 L_v D_{SH} / c_p\ . \quad (13)$$

In the setup of our study there are three parameters determining the turbulent latent heat flux. The ratio ($r_{lh/sh}$) accounts for different exchange rates for water vapor and sensible heat. D_{SH} is the absolute exchange strength (roughness, wind, stability). The additional parameter (χ_{QL}) switches the simulation of the turbulent latent heat flux on and off.

2.1.5 Precipitation heat flux

The heat supplied by precipitation depends on the atmospheric temperature, which we assume to be in balance with the precipitation. An atmospheric temperature of 273.15 K is the limit of solid precipitation. In the case of snowfall the solid mass of the topmost grid cell of the snowpack increases by the amount of snow and the heat added to this box is

$$Q_{P,snow} = P \rho_w c_i (T_{atm} - T_s) \quad (14)$$

while rain is added as liquid water mass to the same cell:

$$Q_{P,rain} = P \rho_w c_w (T_{atm} - 273.15\,K), \quad (15)$$

where P is the amount of precipitation and ρ_w and c_w are the density and heat capacity of water. If the rain freezes or percolates further down, the corresponding exchange of latent heat is calculated during the balance calculation as outlined in the next section.

2.2 Subsurface percolation and refreezing

Only a brief overview of the subsurface routine is given in this paper. Full details are available in Born et al. (2019). The water-holding capacity of each layer determines the percolation. The maximum liquid water content ζ_{max} is the parameter subject to the sensitivity analysis:

$$\zeta = m_w / m_s \frac{1}{\rho_w \left(\frac{1}{\rho_s} - \frac{1}{\rho_i} \right)}, \quad (16)$$

where m_w, m_s and ρ_w, ρ_s, and ρ_i are the masses and densities of water, snow, and ice. If the liquid water content ζ exceeds ζ_{max}, the liquid water mass percolates to the next cell below or is treated as runoff when it leaves the bottom cell.

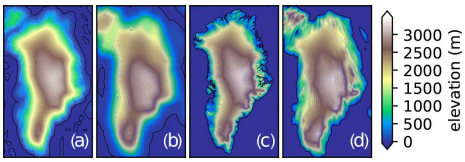

Figure 1. The climate model topography for the PD **(a)** is from the ERA-Interim data set, and that for the LGM **(b)** is from the CCSM4 simulation. The model topography used for the PD is ETOPO **(c)**, and ICE-6G is used for the LGM **(d)**. For the plot all topography below 5 m was considered sea level for the climate models.

2.3 Global sensitivity analysis

Setup and theoretical background

We assess the model sensitivity of and uncertainty in BESSI for two different time periods to verify its applicability over the whole glacial cycle. The present-day (PD) period uses the ERA-Interim reanalysis data (Uppala et al., 2011) ranging over 38 years from 1979 to 2017. Our Last Glacial Maximum (LGM; 21 000 years before present) simulations are forced with 30 climate years of the Community Climate System Model version 4 (CCSM4) (Brady et al., 2013). The simulated LGM has an annual mean temperature over the entire model domain of 249 K/−24 °C, while the current climate is relatively warm with an annual mean of 262 K/−11 °C. The entire model domain was chosen as the ice sheet has different shapes in the two climate states. The precipitation averages are around 400 kg m^{-2} for the LGM and 570 kg m^{-2} for the PD. The annual mean solar radiation is about 10 % higher for the LGM, though the seasonal cycle deviates drastically from the PD. The surface mass balance model uses a static topography, which is based on ETOPO (Amante and Eakins, 2009) for the PD and on ICE-6G (Peltier et al., 2015) for the LGM (Fig. 1). There is an interpolation artifact in the PD simulation in the far northwest, but as no ice is present in this region of Greenland, it does not influence the analysis. BESSI was run for 500 years with the same forcing data looping the forcing data back and forth (1979–2017–1979–2017, etc.) to account for the long response time of the firn cover. After 400 years the firn cover was dynamically (density) and thermodynamically (temperature) stable, even in the regions of very low accumulation. The analyses shown here are entirely based on the last 100 years of every simulation.

Global sensitivity analysis (GSA) is a variance-based method that allows for an assessment of the model sensitivity over the entire parameter space. In contrast to other sensitivity methods, it assesses the full parameter space simultaneously. The method has been applied previously to snowpack (Sauter and Obleitner, 2015) and recently to alpine glacier modeling (Zolles et al., 2019). The method is based on algorithms developed by Saltelli et al. (2000, 2006, 2010), utilizing the setup of the ensemble hypercube (Sobol et al., 2007). To compute both sensitivity indices, the estimator from Sobol et al. (2007) was used. The probabilistic framework provides an estimate of the sensitivity of the model output to the individual input variables, including parameters and data. The GSA is independent of model calibration and tuning. The model output Y is a function of the input parameters X_i: $Y = f(X_1, X_2, .., X_n)$. There are two normalized values that quantify the model sensitivity for each input parameter X_i: the first- or main-order sensitivity index S_{Xi} and the total sensitivity index S_{Ti} of parameter X_i. The first order index denotes the sensitivity of the model towards the parameter X_i only, while the latter includes all the interactions of X_i:

$$S_{Xi} = \frac{V_{Xi}(E_{X-i}(Y|X_i))}{V_Y}, \tag{17}$$

$$S_{Ti} = \frac{E_{X-i}(V_{Xi}(Y|X_{-i}))}{V_Y}, \tag{18}$$

where E is the expectation value of a given observable such as the SMB. V_Y is the total variance of the given variable, and V_{Xi} the variance that only depends on the input parameter X_i. X_{-i} denotes the whole parameter space excluding any variation in X_i. The first-order index calculates the mean model output $(E_{X-i}(Y|X_i))$ for each representation of X_i and then assesses the sensitivity by calculating the variance for all values of X_i.

The total index can be compared to the local sensitivity index that is often determined around the optimal model setting, but the GSA presented here does not rely on a predetermined optimal parameter setting. $V_{Xi}(Y)$ varies the parameter X_i along its dimension but is computed for all possible points of the parameter space instead of for the optimal one. For the detailed algorithm refer to Saltelli et al. (2010). As under-sampling is assumed because of the relatively low numbers of simulations, bootstrapping is applied to the ensemble and multiple sensitivity values are reported. Both indices are normalized with the variance of the whole ensemble V_Y. We are limiting the detailed discussion to the total index S_{Ti}, as BESSI is a highly correlated model.

We are using nine free model parameters (Table 1). The initial ensemble was generated using a Sobol sequence which consisted of 2000×9 members for the PD and 1000×9 members for the LGM. This sequence spans a 9-dimensional unit hypercube. For computing both sensitivity indices the estimator from Sobol et al. (2007) was used. It splits the initial sequence into two subsets, **A** and **B**, each consisting of one-half of the initial sequence (1000×9 or 500×9). Then an additional set of matrices $\mathbf{B}^i_A$, which are based on the matrix **B** where the values for parameter X_i are replaced with those from subset A, are created. The matrices **A**, **B**, and $\mathbf{B}^i_A$ are then used to estimate the model sensitivity. A detailed description of the algorithm can be found in Sobol et al. (2007) and Saltelli et al. (2010). The whole ensemble consists of $N \cdot (2 + k)$ members, with N being the base sample (1000 in

Table 1. The parameter ranges for the free model parameters are broad and based on previously published values (Born et al., 2019). The firn albedo may not exceed the fresh snow albedo, and its value was limited to 0.65 during the LGM. All parameters are distributed following a pseudo-random Sobol sequence.

No.	Name	Abbreviation	Range	Unit	Reference
1	Fresh snow albedo	α_{fs}	0.65–0.9		Cuffey and Paterson (2010)
2	Firn albedo	α_{fi}	0.45–0.7 (0.65)*		Cuffey and Paterson (2010)
3	Ice albedo	α_{i}	0.3–0.4		Cuffey and Paterson (2010)
4	Turbulent heat exchange coefficient	D_{SH}	5–25	$\mathrm{W\,m^{-2}\,K^{-1}}$	Braithwaite (2009)
5	Ratio of sensible and latent heat flux	$r_{\mathrm{lh/sh}}$	0.5–1.2		
6	Emissivity of the air	ϵ_{atm}	0.6–0.9		Greuell (1992)
7	Switch for turbulent latent heat flux	χ_{QL}	on/off		
8	Albedo module	χ_α	constant, Aoki		Aoki et al. (2003); Born et al. (2019)
			Bougamont		Bougamont et al. (2005)
			Oerlemans		Oerlemans and Knapp (1998)
9	Maximum liquid water content	ζ_i	5–15	% pore volume	Greuell (1992); Born et al. (2019)

* The firn albedo may not exceed the fresh snow albedo.

the case of the PD) and k the number of parameters (nine; Table 1).

The full ensemble for the present-day climate has 11 000 members; that for the LGM climate has 5500. The initial hypercube with a length of [0,1] in each dimension is linearly transformed to the intervals given in Table 1, with the exception of the latent heat flux switch and the albedo module. These two parameters have two and four discrete values, respectively, and the parameter space is split equally between them. The model simulations are carried out with the generated parameter matrix. We are using bootstrapping to estimate the sensitivity indices. For each bootstrap Eqs. (17) and (18) are evaluated. Finally, we report the mean sensitivity indices and their standard deviation. The results were checked for consistency ($\sum S_{Xi} \leq 1$, $S_{Xi} \leq S_{Ti}$). The ensemble size used during the LGM is at the absolute lower limit of applicability for GSA, as the standard deviation of the sensitivity indices is large (Fig. A1). The GSA works well for the SMB, latent heat flux, and melt, sometimes with increased uncertainty, but fails for the 10 m firn temperature for example. Due to the larger ensemble, the confidence in the PD ensemble is higher but not by a large enough margin to justify the additional computation time relative to the 5500 members of the LGM ensemble. BESSI is a complex model with all parameters interacting, and S_{Xi} provides less information. Therefore, the results mainly focus on the total sensitivity index S_{Ti}.

The GSA was computed for five different outputs: albedo, vapor flux, snowmelt, surface mass balance, and surface temperature, which are based on average yearly sums for SMB, melt, and vapor flux or temporal averages for albedo and temperature over 100 years. Surface temperature results are uncertain, and only tendencies can be extracted as the surface temperature is largely influenced by the annual cycle and fresh snowfall on an ice surface.

3 Results

3.1 Global sensitivity analysis – GSA

GSA in the present day (PD) over elevation bands. The main focus of the results is on the surface mass balance, and discussion is limited to the total sensitivity index (S_{Ti}), due to limited information that can be extracted from S_{Xi} in complex models. The sensitivity of the SMB for different elevation classes for the present-day ice sheet is shown in Fig. 2. In the region from 0–1000 m the largest sensitivity is associated with the parameter uncertainty in the atmospheric emissivity ϵ_{atm} with a normalized total sensitivity index of about 0.8. The second-most-influential parameter is the turbulent heat exchange coefficient D_{SH}, followed by the snow albedo (Fig. 2a). The general features are similar up to 2000 m (Fig. 2b), with a slight decrease in the sensitivity to D_{SH}. In regions above 2000 m (Fig. 2c, d, e) the SMB is sensitive to a much wider range of parameters: the atmospheric emissivity, the fresh snow α_{fs} and firn albedo α_{fi}, the choice of albedo module χ_α, the turbulent heat flux coefficient D_{SH}, and the turbulent latent heat flux switch χ_{QL}. While the importance of χ_{QL} increases with elevation, the importance of α_{fi} decreases. The sensitivity of the fresh snow albedo α_{fs} increases up to 0.4 at 2500 m but not further. With the increasing sensitivity of multiple parameters, the relative sensitivity to ϵ_{atm} decreases, leading to χ_{QL} being almost equally important in the region with the highest average elevation. The local SMB in regions above 2000 m is impacted by multiple parameters, while the integrated mass balance is dominated by the atmospheric emissivity, with the snow albedo and turbulent fluxes having a minor influence.

Spatial pattern of GSA in the PD. The global sensitivity maps for all parameters are displayed in Fig. 3. The GSA was calculated for each grid cell individually. The general trends are similar to the elevation averages, but the spatial pattern

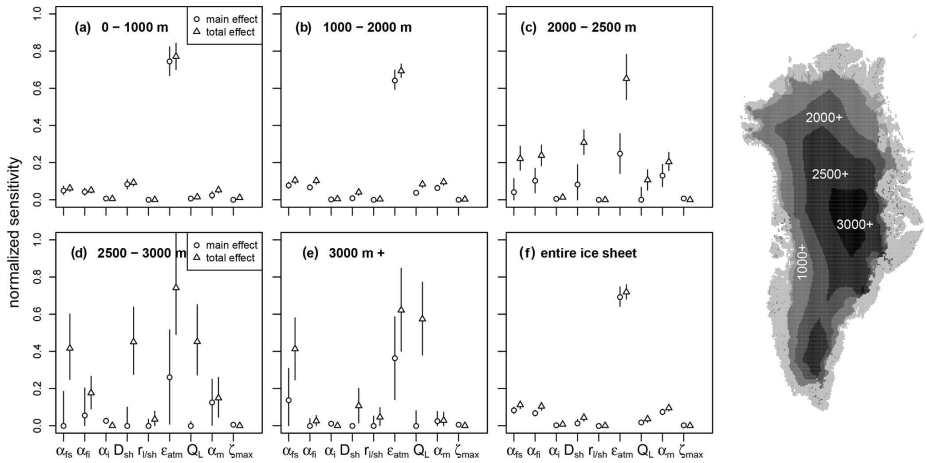

Figure 2. The global sensitivity analysis of the PD SMB provides the main-order effect (circle) and the total effect (triangle). The main-order effect shows the model sensitivity to the parameter alone, and the total includes its interaction with other parameters (Sect. 2.3). The two indices are displayed for all nine parameters over the different elevation bands ranging from 0–1000, 1000–2000, 2000–2500, and 2500–3000 to above 3000 m and for the entire ice sheet. The symbol represents the mean value of the sensitivity index with the bars as $\pm 1\sigma$. The elevation bands of the present-day topography over Greenland are displayed on the right; the analysis is only performed for cells where ice is present. A similar figure for the LGM is found in the Appendix (Fig. A1).

shows important additional details (Fig. 2). The SMB is sensitive to ϵ_{atm} over the entire ice sheet. The SMB is also sensitive to χ_{QL} in the interior of Greenland, and χ_{QL} can be considered a sensitive parameter for most of the ice sheet apart from the regions of very high melt. In the interior of very high elevation, the most sensitive of the three snow-albedo-related parameters is the one for fresh snow α_{fs}, while at elevations below 2000 m, the firn snow albedo α_{fi} and the chosen type of albedo parameterization χ_{α} is more important, the latter in particular in the northeast, where fresh snowfall is infrequent. The SMB is sensitive to D_{SH} at the ice caps in the west and on the ice sheet above 1500 m; only at the top of the ice sheet is its influence reduced. The ice albedo α_{i} plays a minor role in the north but is generally of very low impact. Additionally, ζ_{max} as well as $r_{\mathrm{lh/sh}}$ is of minor importance.

The dominance of ϵ_{atm} is a result of the change in total heat flux associated with its parameter uncertainty. At an annual average air temperature of $-10\,^{\circ}\mathrm{C}$, a change in the atmospheric emissivity from 0.6 to 0.9 increases the heat flux by $80\,\mathrm{W\,m^{-2}}$, while a change in albedo from 0.9 to 0.6 only increases the energy input by $40\,\mathrm{W\,m^{-2}}$ for typical values of solar radiation annual averages. Similarly, the sensible heat flux is smaller than the other heat fluxes over most of the ice sheet (monthly averages from -20 to $+50\,\mathrm{W\,m^{-2}}$ with $D_{\mathrm{SH}} = 12\,\mathrm{W\,m^{-2}\,K^{-1}}$), so even a doubling will not be larger than the change in atmospheric emissivity on an annual basis. The relatively low impact of the ice albedo α_{i} is due to the small exposure time and the small parameter range. An ice albedo change of 0.3 to 0.4 will at most result in an annual average energy change of 10–$20\,\mathrm{W\,m^{-2}}$, but the ice is never exposed for the whole year. Rather the date of ice exposure, which is a result of the energy fluxes prior to its exposure and associated with an surface albedo change from 0.55–0.9 to 0.3–0.4, is much more important. The SMB in regions above 1000 m is sensitive to the snow albedo, which in turn is a function of snowfall, snow temperature, and the chosen albedo parameterization. Each albedo model treats these processes differently. While the basic one only distinguishes between dry and wet snow, the others account for snow aging ranging from time over time–temperature to time–temperature–wetness dependency. The choice of albedo model is not important in the interior of Greenland, as temperatures are low, albedo decay is slow, and the snow does not get wet. At slightly lower elevations there is an interplay of the fresh snow albedo α_{fs} and firn albedo α_{fi} and the chosen decay parameterization χ_{α}, with a larger impact of the fresh snow albedo, as snowfall is not frequent and decay rates at around $-10\,^{\circ}\mathrm{C}$ are of the order of a few weeks (Sect. 2.1.1). An exception is found in the northeast, which is characterized by the driest climate on Greenland. The less frequent precipitation and therefore albedo resetting explains a larger dependency on the decay rate and the choice

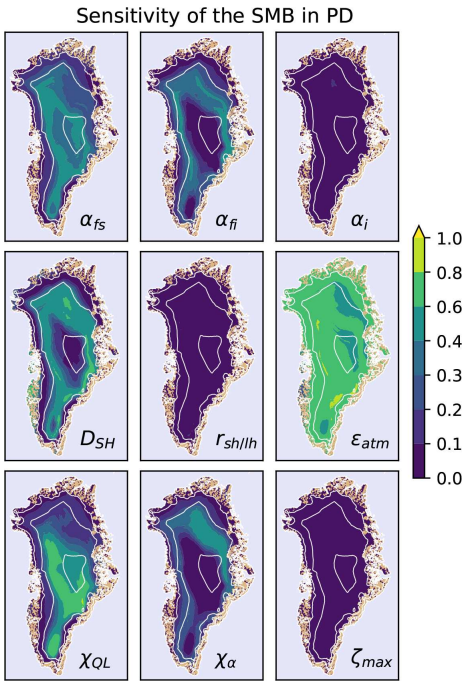

Figure 3. Global sensitivity in the PD. The total sensitivity index of the SMB of every parameter for the PD is displayed for every ice-covered grid cell. The ice-free land is in brown; the ocean is in light blue; 1000 m contours are in white. The sensitivity is largest for the atmospheric emissivity ϵ_{atm}, followed by the fresh snow and firn albedo $\alpha_{\mathrm{fs/fi}}$, the turbulent heat exchange coefficient D_{SH}, and the latent heat flux switch χ_{QL}. The SMB is not sensitive to the ice albedo α_{i}, the ratio of the turbulent exchange coefficients $r_{\mathrm{lh/sh}}$, and the liquid water content ζ_i. The maps do not include uncertainty, but the uncertainties in the sensitivities are of the same order of magnitude as shown in Fig. 2.

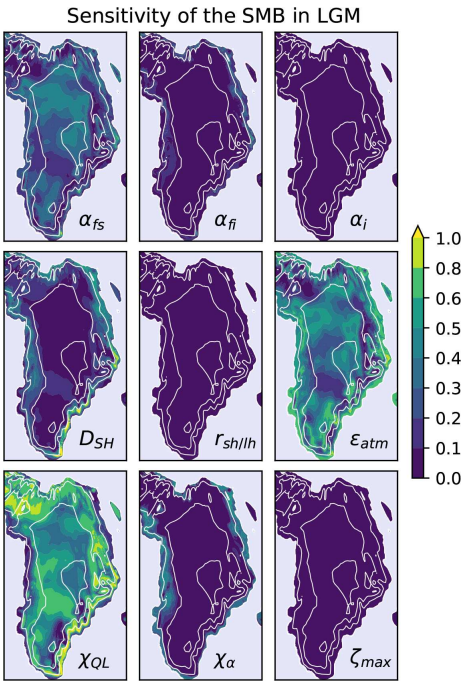

Figure 4. Global Sensitivity in the LGM. The total sensitivity index of the SMB of every parameter for the PD is displayed for every ice-covered grid cell. The ice-free land is in brown; the ocean is in light blue; 1000 m contours are in white. The total sensitivity index of the surface mass balance for the LGM is more variable than during the PD. The model shows the greatest sensitivity towards χ_Q and the atmospheric emissivity ϵ_{atm} followed by the fresh snow albedo α_{fs}. Firn albedo α_{fi} and the albedo module χ_α as well as the turbulent exchange coefficient D_{SH} are important around the margin. The SMB during the LGM shows almost no sensitivity towards the other parameters.

of albedo module. The northeast of Greenland is furthermore an area higher up on the Greenland ice sheet where χ_{QL} is less important. Due to the low amount of precipitation, the SMB is quite sensitive to changes in the surface energy balance (SEB). Ensemble members with very high energy balance (low albedo, high emissivity) lead to a melting state, which results in very large changes in SMB relative to the small changes associated with condensation and sublimation. The large impact of D_{SH} at the western coast is due to the large air–surface temperature difference, while in the interior of Greenland the atmospheric temperature is much closer to the snow surface temperature.

Spatial pattern of GSA at Last Glacial Maximum (LGM). The sensitivity of the SMB in the LGM shows similar features as in the PD but is shifted to lower elevations (Fig. 4). During the much colder and dryer LGM the lowest region shows an increased importance of the choice of the snow albedo module. The turbulent latent heat flux switch χ_{QL} is already as important as the atmospheric emissivity ϵ_{atm} above 1000 m, and the fresh snow albedo α_{fs} is almost as important above 2000 m. The ice-sheet-integrated SMB shows strong sensitivity to atmospheric emissivity ($S_{T_{\chi_{\mathrm{QL}}}} \approx 0.3$–$0.7$), the turbulent heat flux coefficient (up to 0.8, coastal), the latent heat flux switch ($S_{T_{\chi_{\mathrm{L}}}}$ mostly > 0.4), and the snow

albedo ($S_{T_\alpha} \approx 0.3$) (Fig. 4) during the LGM. The liquid water content $\zeta_{\max}$, the ice albedo α_{i}, and the ratio of latent and sensible heat exchange coefficient $r_{\mathrm{lh/sh}}$ only marginally impact the SMB in either of the two climate states (Figs. 3 and 4). On the local scale χ_{QL} followed by ϵ_{atm} and α_{fs} is the main sensitivity component in the LGM (Fig. 4). The sensible heat flux exchange coefficient D_{SH} is important along the margin with the largest impact in the southeast. The firn albedo and the albedo module are sensitive parameters along the margin, apart from the precipitation-heavy south and southeast, where frequent snowfall resets the albedo.

The increased importance of χ_{QL} is a result of a much colder and dryer climate. The SMB is positive over most of Greenland during the LGM, even for parameter combinations leading to a high energy input. In the absence of melt, the only change to the SMB is due to sublimation and hoar formation. The dry climate also favors higher sublimation than in the PD. The vapor flux (sublimation) is mainly a net heat loss for the surface in the LGM. The surface temperature via the Clausius–Clapeyron relation has an exponential impact on the turbulent latent heat flux, resulting in a greater model sensitivity towards the atmospheric emissivity than the actual exchange coefficient D_{SH} (Eq. 13). The incoming longwave radiation is also the largest energy source for the surface. The large impact of D_{SH} in the southeast is due to the large temperature difference between the surface and the air. The southeast is dominated by intense precipitation and rather warm air masses even during the LGM. There is a precipitation gradient from the western coast to central Greenland: the least precipitation is found in the west of Greenland and the south of Ellesmere Island due to circulation changes due to the presence of the Laurentide ice sheet over North America in the LGM (not shown). Therefore, the albedo module is more important on the western than on the eastern margin as frequent precipitation, which is mainly snowfall during the LGM, increases the albedo more frequently. The lower model sensitivity in the LGM towards ϵ_{atm} is mainly a result of the lower air temperature with annual averages being around 10 K lower, resulting in less incoming longwave radiation and a lower absolute impact of the emissivity.

Sensitivity of other output variables in addition to SMB. We also studied the sensitivity of other model variables, namely the surface albedo, turbulent latent heat flux, snowmelt, and surface temperature. The corresponding figures (which are similar to Figs. 3 and 4) are included in the "Additional information". The global sensitivity for the annual average albedo during the PD period is mainly influenced by the fresh snow albedo parameter, with only minor importance of the firn albedo, ice albedo, the choice of the albedo module, and the atmospheric emissivity at the ice sheet margin. As a result, the snow albedo should not be tuned with BESSI without incorporating the atmospheric emissivity in addition to the direct albedo-related parameters (Fig. GSA_albedo_ERAi/LGM in the "Additional information").

Besides the switch (χ_{QL}) which disables the turbulent latent heat flux Q_{L} completely, the turbulent latent heat flux is most sensitive to the atmospheric emissivity ϵ_{atm} followed by the turbulent heat flux exchange coefficient D_{SH}, mainly around the margins (Fig. A3). Around the margin the ratio of turbulent sensible and latent exchange coefficients $r_{\mathrm{lh/sh}}$ plays a minor role ($S_{ti} \approx 0.1$). The turbulent latent heat flux is also sensitive to the snow-albedo-related parameters ($\alpha_{\mathrm{fs/fi}}$, χ_α) in the north. The turbulent latent heat flux Q_{L} is sensitive to neither the maximum liquid water content $\zeta_{\max}$ globally nor the ice albedo and $r_{\mathrm{lh/sh}}$ in the interior of the ice sheet. As the effect of $r_{\mathrm{lh/sh}}$ on the turbulent latent heat flux as well as on the SMB is low, using similar exchange coefficients for moment, temperature, and water vapor is justified within this framework. In the LGM, Q_{L} shows an increased sensitivity to α_{fs}, while the D_{SH} is less important around the margin, due to lower atmospheric temperatures and slower albedo decay (not shown). The albedo module and the firn albedo play almost no role in either case.

The average snow temperature is mainly influenced by ϵ_{atm}, α_{fs}, D_{SH}, and χ_{QL}, though uncertainties in the sensitivity are rather large due to temperature resetting in the event of snowfall on ice or shallow snowpacks.

Snowmelt is closely linked to the SMB and shows similar sensitivities to those reported for the SMB. Just as expected, the impact of the latent heat flux switch is lower as it is mainly important in regions with an absence of melt (Fig. 3).

3.2 Ensemble statistics

PD regional parameter dependencies. The GSA highlights the surface mass balance as the variable most sensitive to atmospheric emissivity and the latent heat flux switch irrespective of background climate. The GSA method has the drawback that it gives no information about the sign and absolute magnitude of the SMB changes. Physical processes and associated parameters, which result in either surface heating or cooling, will be analyzed based on ensemble statistics explained in the following. On the other hand, an increase in albedo and a decrease in atmospheric emissivity always lead to an increase in surface mass balance. The ensemble statistics also give additional information about parameter sensitivities which were well analyzed with GSA. We split Greenland into 11 different regions for the PD and 13 for the LGM (2 more around Ellesmere Island) based on elevation, ice divides, geography, and climatological similarity for this analysis. In particular most of the west coast shows similar behavior and is therefore only a single region (Fig. 5). This is a regional spread of the elevation bands used in Fig. 2. For each region the parameter range is split into 20 equally spaced intervals for which the 5 %, 25 %, 33 %, 50 %, 66 %, 75 %, and 95 % quantiles are calculated. The binning is necessary as the ensemble was not created with parameters at regularly

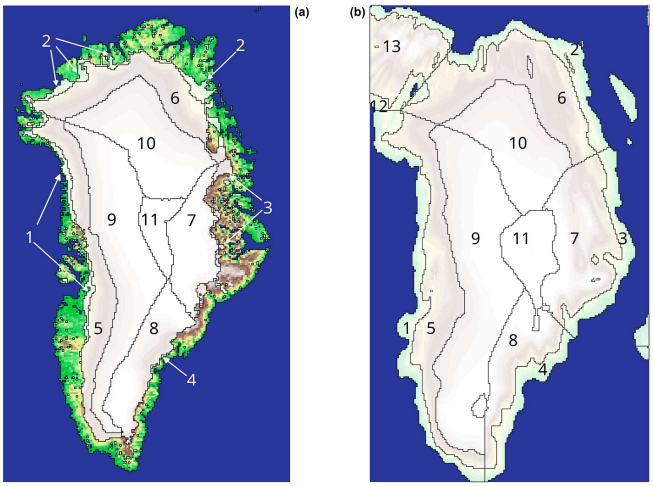

Figure 5. Greenland is split into 11 regions based on elevation, geographic, and climatic similarity for the PD **(a)** and the LGM **(b)**. There are four different sections with SW–W, N, E, SE, and the area around Ellesmere island for the LGM. Each section is split into three elevation bands ranging from 0–1000–2000–3000 m. During the present day there are three regions in the west and north from 0–1000–2000–3000 m (1, 5, and 9; 2, 6, and 10). The southeast and east regions are precipitation driven, and the change in SMB with altitude is less developed; therefore 1000–3000 m is joined to one region (4, 8; 3, 7). There is one additional region in the center which is at elevations above 3000 m (11). Ice-covered areas are in white with slight elevation shading in the background. The ice-free area is based on elevation coloring with green as the lowest and brownish the highest.

spaced intervals. The most interesting features are seen for the parameters where the effect changes sign depending on the atmospheric conditions, like for the turbulent heat exchange coefficient. We discuss the selected region 5 and the turbulent latent heat flux in depth here, while the complete set of figures is included for reference in the "Additional information".

In Fig. 6 the impact of the various parameters on the PD SMB is shown for region 5, the western region of Greenland ranging from 1000–2000 m where the equilibrium line for the present-day ice sheet is located. The dominant parameter is the atmospheric emissivity ϵ_{atm}. Over the range of plausible values, ϵ_{atm} reduces the median of the SMB by almost 800 kg m^{-2}. The atmospheric emissivity and the SMB are inversely correlated, and the relationship is nonlinear with greater effect at larger values. The spread of the ensemble, i.e., the variance of the SMB as a result of other parameters, increases too. The increase in the SMB with the snow-albedo-related parameters α_{fi} and α_{fs} is smaller and the width of the distribution decreases (panel a, b), as even very low albedo parameter values do not necessarily lead to a negative SMB in the western region. An increase in D_{SH} slightly reduces the median SMB, but the spread decreases. Ice albedo α_{i}, liquid water content ζ_{max}, and $r_{\mathrm{lh/sh}}$ have almost no impact. The SMB increases in the presence of turbulent latent heat flux due to the heat loss of sublimation in region 5. With all albedo modules the ensemble has a wide spread, but the variation is smallest for the time-dependent decay (Oerlemans and Knapp, 1998) which also has the highest median mass balance, as it neither has an instant albedo drop upon reaching the melting point (constant) nor accounts for the liquid water mass in the snowpack. The parameterization based on temperature, wetness, and time has the lowest median SMB.

The strong impact of the emissivity on the surface energy balance and therefore also on SMB is due to the larger annual average of the incoming longwave radiation relative to the shortwave, precipitation, and turbulent fluxes. In the PD climate, the largest energy source for the snow is incoming longwave radiation. As atmospheric emissivity ϵ_{atm} decreases, less energy is available for melt in region 5. In the absence of melt, surface mass balance response is only due to the sublimation, and since the vapor flux has a modest absolute impact on the SMB, the spread of the ensemble is low. Vice versa, at large ϵ_{atm} values, warming, as well as potentially early melting of the snowpack, occurs in many grid cells, leading to a positive feedback effect with lower albedo. In agreement with the GSA (Fig. 3) the firn albedo

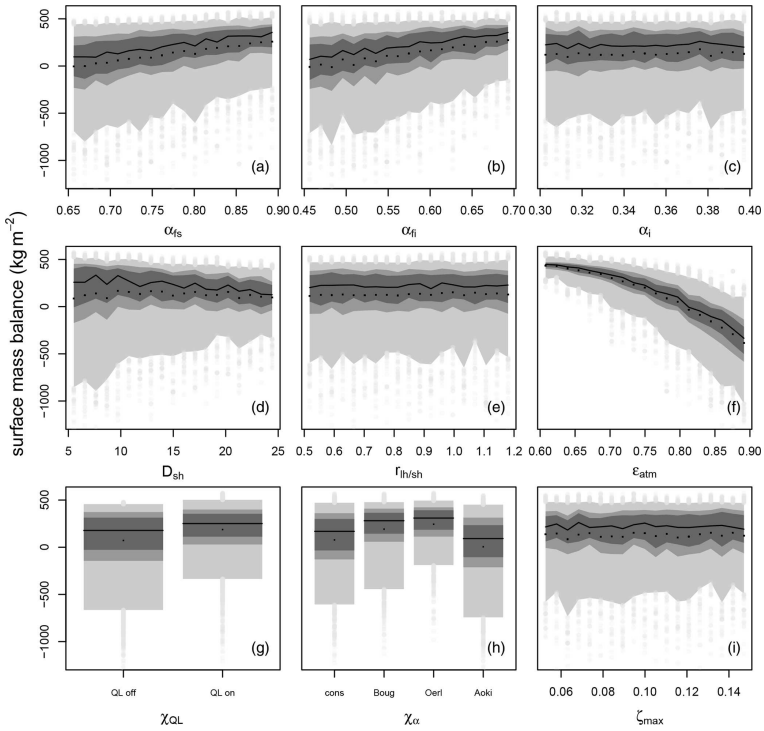

Figure 6. The ensemble statistics for the surface mass balance for region 5 (west 1000–2000 m) in the PD. The 5th and 95th, 25th and 75th, 33rd and 66th, and 50th quantiles are displayed in progressively darker shading. Black points represent the ensemble mean, and the grey points correspond to the rest of the ensemble, apart from outliers (max five per bin allowed), which are removed to improve readability. Each plot represents the range of one parameter with α_{fs}, α_{fi}, and α_i in the top row; D_{SH}, $r_{lh/sh}$, and ϵ_{atm} in the middle; and $Q_{Lon/off}$, χ_α, and ζ_{max} at the bottom. As $Q_{Lon/off}$ and χ_α have two and four discrete values, respectively, the parameter range is not split into 20 intervals.

α_{fi} is almost as important as fresh snow albedo α_{fs}. The equilibrium line altitude (ELA) is located in region 5, and snow temperatures are rather warm, resulting in a large impact of snow albedo decay and its parameterization. The constant albedo parameterization spreads more than 1000 kg m^{-2}, as the albedo is very sensitive around the ELA, changing instantly from α_{fs} to α_{fi} when the snowpack reaches the melting point, while the albedo parameterizations based on Oerlemans and Knapp (1998) and Bougamont et al. (2005) have a temporal decay relative to the instant one in the constant case. Bougamont et al. (2005) have a snow-temperature-dependent increased decay rate, which is even more pronounced in the wet case, leading to an ensemble that is less skewed than those of the constant case and Aoki et al. (2003). The last albedo parameterization decays faster than the other two at warmer temperatures, leading to lower albedo than for all other albedo parameterizations before the melting point is reached. Additionally, there is a difference between the models in the case of snowfall.

Differences in the LGM regional parameter dependencies. During the LGM the western region between 1000–2000 m (not corresponding to the identical geographical area in the PD due to topographic differences) shows positive but low SMB with a lower spread of the ensemble (Figs. 7, A2). The climate in the west of Greenland in the LGM is characterized by a much lower air temperature, slightly more annual mean radiation, and lower precipitation. There are three distinct differences to in the PD:

1. The lower air temperature reduces the impact of ϵ_{atm} and produces a more positive SEB.

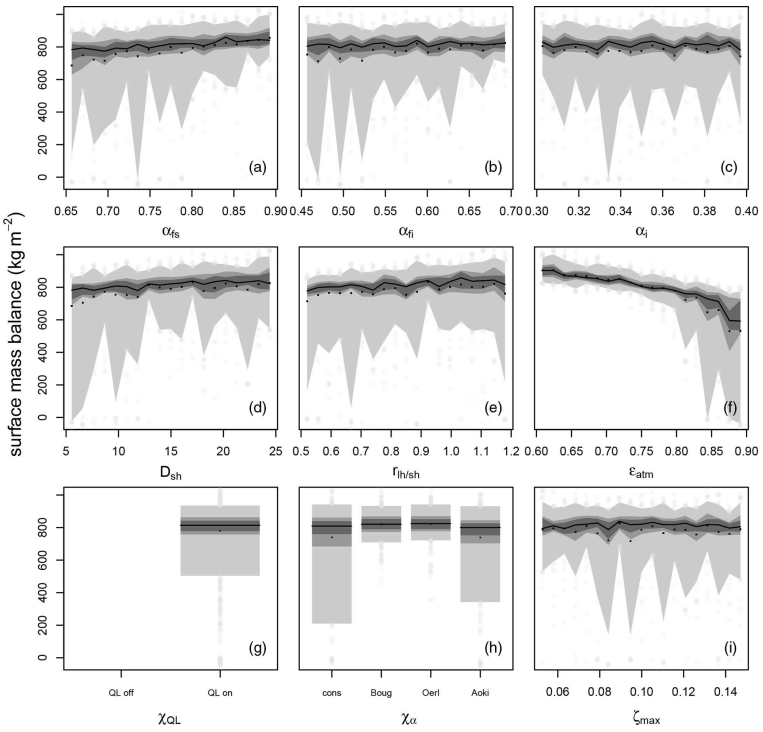

Figure 7. The ensemble statistics for the surface mass balance of the Q_{Lon} sub-ensemble for region 5 (west 1000–2000 m) in the LGM. The 5th and 95th, 25th and 75th, 33rd and 66th, and 50th quantiles are shown in progressively darker shading. Black points represent the ensemble mean, and the grey points correspond to the rest of the ensemble, apart from outliers (max five per bin allowed), which are removed to improve readability. Each plot represents the range of one parameter with α_{fs}, α_{fi}, and α_{i} in the top row; D_{SH}, $r_{\mathrm{lh/sh}}$, and ϵ_{atm} in the middle; and $Q_{\mathrm{Lon/off}}$, χ_α, and ζ_{max} at the bottom. As $Q_{\mathrm{Lon/off}}$ and χ_α have two and four discrete values, respectively, the parameter range is not split into 20 intervals. Figure A2 shows a similar plot for the entire LGM ensemble.

2. The impact of α_{fi} and χ_α is drastically reduced. The importance of α_{fs} increases relatively to ϵ_{atm} (Fig. 7). The incremental increase in snow albedo with snowfall gives slightly lower albedo in the dry climate. The colder snowpack due to a more positive SEB has a slower snow albedo decay (for the albedo subroutines which parameterize the decay), no melting, and almost no impact of associated parameters.

3. Enabling the latent heat flux results in a decrease in SMB, as sublimation prevails in the LGM over the entire year. However, in the absence of melt the increase in sublimation results in a mass loss, rather than the reduced melt via cooling due to sublimation during the PD conditions. Furthermore, the non-linearity in the SMB in the LGM almost vanishes for ϵ_{atm} and α_{fs} as there is hardly any melt and associated snow–ice albedo feedback.

Impact of the turbulent heat flux exchange coefficient on the SMB as an example for the PD. The SMB dependency on the turbulent heat flux coefficient D_{SH} varies over the different regions (Fig. 8). The turbulent sensible heat flux may be either a heat loss or a heat gain for the surface depending on the difference between atmospheric and surface temperature, which is why we present a deeper look into the related parameter (the figures for all other parameters are available in the "Additional information"). Only the sub-ensemble with an active turbulent latent heat flux ($\chi_{\mathrm{QL-on}}$) is shown in Fig. 8 because in regions without melt, 50 % of the simula-

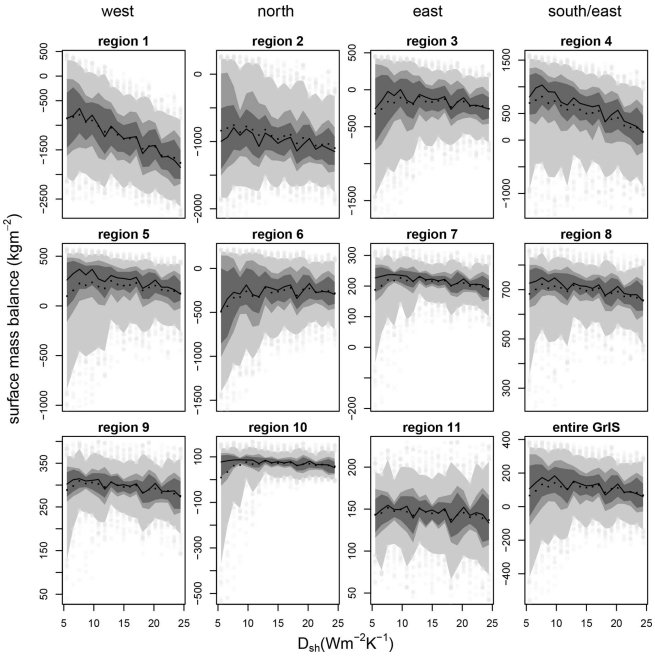

Figure 8. The dependency of the SMB on the turbulent heat exchange coefficient D_{SH} is displayed in a similar manner to in Fig. 7 for the PD. The shading represents the different quantiles: 5th and 95th (light grey), 25th and 75th (grey), 33rd and 66th (dark), and the median (solid black line). The black dots are the ensemble mean based on 20 intervals. The panels are sorted by elevation and regions, with the lowest elevation (0–1000 m) in the top row and the highest elevation at the bottom. Each column is related to a region in Greenland: W, N, E, SE–S (Fig. 5).

tions (χ_{QL-off} sub-ensemble) will show a similar SMB. The overall width of the SMB distribution decreases with altitude. The lowermost regions in the west and southeast (1, 4) show a trend to more negative mass balances with larger exchange coefficients. Regions 3, 5, 6, 10, and to a lesser extent 2 and 7 show a distinct decrease in the width of the SMB distribution of the ensemble with increasing D_{SH} and a slight decrease in the mean (excluding region 6). The general negative trend for the SMB with D_{SH} is a result of higher air than snow surface temperatures. The negative trend is most pronounced at the lower regions of the west and south, where warm air advection is frequent, resulting in increased melt due to the heat supplied by the sensible heat flux. The regions are also quite moist, in particular in the southeast (region 4), leading to a positive turbulent latent heat flux (condensation), which in turn heats the surface too.

The northeast (region 2, 3, 6, 7) of Greenland is colder and drier, resulting in decreased turbulent fluxes, and therefore the effect of D_{SH} on the SMB and surface energy balance is lower. The ensemble spread is narrower at higher altitudes (7–11) due to a generally positive mass balance. An increased energy input due to any parameter will raise the snow temperature, but in the absence of melt the mass balance does not change strongly. Still, the snow temperature change alters sublimation, accounting for the remaining variability in SMB. This is pronounced in region 10: at low exchange coefficients melt is still possible if other parameters result in a strong positive energy input, leading to skewness towards negative SMB. At a large exchange coefficient the tight coupling with the heat reservoir of the atmosphere limits melt and the skewness towards negative SMBs vanishes, while the median stays almost constant. The SMB does not strongly vary with parameter D_{SH} in region 10; rather the parameter acts as a buffer of the SMB. With strong turbulent sensible heat exchange the surface temperature will be buffered by the air temperature heat reservoir, so the spread of the ensemble becomes narrow. The buffering effect is vis-

ible for most regions, where air temperatures are below the melting point for most of the year (2, 3, 5, 7–10).

The turbulent heat exchange coefficient D_{SH} also impacts the SMB via the turbulent latent heat flux (Q_L in Eq. (12), additional figure available in the "Additional information"). Q_L becomes more negative with an increasing exchange coefficient. Firstly, the higher surface water vapor pressure of the warmer snow/ice surface, as a result of the heating by the turbulent sensible heat flux Q_{SH}, increases sublimation. Secondly, the absolute vapor flux is also larger with a higher exchange coefficient. The annual average of the ensemble over Greenland is a negative turbulent latent heat flux, meaning sublimation occurs more often than condensation. At larger exchange rates more mass can be moved, and therefore the variation over the ensemble increases.

The average SMB increases at low elevations if the turbulent latent heat flux is switched on (χ_{QL-on} sub-ensemble); it decreases above 2000 m and is almost constant above 3000 m, where the annual average of the latent heat flux is almost zero. The first trend is a result of reduced melt due to a negative latent heat flux (sublimation), and the SMB increase is therefore most pronounced in the northeast. This is a region where melt only occurs for a few extreme ensemble members, so the sublimation is the only mass loss, and therefore the SMB decreases with increased sublimation.

Ensemble statistics of other parameters for the PD. The other parameter results are consistent with the GSA: an increase in ϵ_{atm} decreases the SMB, but melting increases disproportionally with higher emissivity. The high impact of ϵ_{atm} is mainly related to the all-year-around impact altering ice exposure and albedo decay. The snow albedos increase the SMB, with the fresh snow albedo being more important. The SMB ensemble plots do not show any dependency on ice albedo and liquid water content, and the mean is also unaffected by $r_{lh/sh}$. Additional figures are available in the "Additional information".

LGM. The general features are similar to those in the PD. Larger values of D_{SH} reduce the variability in or impact of the other parameters, resulting in slightly lower SMB. Similarly to for the GSA, a shift to lower elevations is seen. The impact of D_{SH} on the SMB is negligible above 2500 instead of above 3000 m for the PD and melt tails are limited to below 2000 m. ϵ_{atm}, as well as the snow-albedo-related parameters, has less influence during the colder period.

Sensitivity of the 10 m firn temperature. In addition to the SMB, the sensitivity of the 10 m firn temperature was assessed. This was not possible for the GSA due the limited sample size. We limited the analysis of the firn temperature to 13 locations in the interior of Greenland. The firn temperature at these mostly central locations is sensitive to three parameters: ϵ_{atm}, α_{fs}, and D_{SH}. The first two have a rather linear impact with increasing temperature with increasing emissivity and decreasing albedo. The turbulent heat exchange coefficient has a similar effect on the 10 m firn temperature to that shown for region 5. At small D_{SH} values the 10 m temperature has a larger variability depending on the other two sensitive parameters, while at large values the air temperature buffers the snow temperature, even down to 10 m. The sensitive parameters are the main drivers of the SEB, which determines the 10 m temperature in those areas as discussed previously for the SMB. The only difference to the SMB for regions at higher elevations is the insignificance of χ_{QL}. The turbulent latent heat flux has only a minor importance for the SEB, but in the absence of melt, the vapor flux is the only SMB change. Tuning the model for the 10 m firn temperature only provides information about the sensitive parameters, which are ϵ_{atm}, α_{fs}, and D_{SH}.

4 Discussion

In this study we assess the model sensitivity due to parametric uncertainties. Cloud cover and the associated atmospheric radiation are large uncertainties in both present-day and glacial climates. The uncertainty in cloud cover is represented by the large parameter uncertainty in the atmospheric emissivity ϵ_{atm}. The SMB is most sensitive to ϵ_{atm} under present-day (PD) conditions. The sensitivity of the SMB is not drastically different during the Last Glacial Maximum (LGM). However, lower atmospheric temperatures reduce the impact of the atmospheric emissivity while also leading to fewer areas where melt and runoff occur. The relative contribution of the mass flux associated with the turbulent latent heat flux to the SMB increases drastically during the LGM (4 % to 15 % of the total mass flux), making the turbulent latent heat flux switch the model's most sensitive parameter in large parts of the ice sheet. The increased importance of Q_L is due to the absence of melt, similarly to at the highest elevations during the PD climate. Additionally, SMB values have a smaller magnitude as precipitation is lower during the LGM and therefore the relative contribution of the vapor fluxes to the SMB is larger. For an accurate modeling of the SMB over the glacial cycle, an inclusion of the turbulent latent heat flux is necessary, which may not be as important for a warmer climate.

The sensitivity metric we applied is a relative measurement that depends on two components: the absolute strength of a particular flux and the chosen parameter uncertainty range of the parameter. The latter depends on the subjective choice. We based the parameter values on published common ranges (Table 1). The incoming longwave radiation is the largest single energy source for the surface energy balance during the PD, ranging from twice the incoming solar radiation around the margin to about one-third in the interior of Greenland in the annual average. Therefore, the impact of the atmospheric emissivity decreases from the coast inwards for multiple reasons: first, temperatures are higher around the margin leading to increased incoming thermal radiation. Second, cloud cover is higher and therefore solar radiation is reduced. Lastly, at negative SMB the rate of melting depends

greatly on the total energy flux and albedo decays faster for a warmer snowpack if more longwave radiation reaches the surface during winter.

It is important to differentiate between the sensitivity of the Greenland-wide integrated mass balance and the local SMB, as well as between the impact of the individual fluxes on the absolute SMB. The Greenland-wide surface mass balance is most sensitive to the atmospheric emissivity during the PD (Fig. 2). During the LGM the SMB shows additional increased sensitivity to the fresh snow albedo, the choice of albedo parameterization, and the turbulent latent heat flux. In the LGM, lower air temperatures and an ice sheet with less melt overall increases the importance of the vapor fluxes similarly to at high elevations in the PD. It is therefore not a necessity for models to include Q_L in a warm climate, though it is desirable. Conversely, the turbulent latent heat flux Q_L cannot be ignored during a colder and dryer climate. In addition, this means that although the cloud cover uncertainty may be similar during the colder period of the LGM, the sensitivity of our model towards the emissivity uncertainty is lower. Simple surface mass balance models like enhanced temperature index models are likely to create a bias as solar insolation changes are accounted for while the impact of the cloud cover on other components of the energy balance is neglected or implicitly included in the PDD factor; even under PD conditions PDD may result in bias as the impact of clouds on the SMB is highly variable (Van Tricht et al., 2016; Hofer et al., 2017).

At the local scale such as in the interior of Greenland, even in the PD climate, the vapor flux (Q_L) is up to one-third of the total SMB, despite its small impact on the Greenland-wide integrated scale. In addition, in the absence of melt the sublimation and condensation are the only changes to the SMB with a fixed precipitation forcing. Neglecting sublimation and condensation will result in fundamental biases over long-term simulations of the Greenland ice sheet, in particular in its interior. This needs to be considered when tuning surface mass balance models for long timescales. Tuning for the Greenland-wide SMB will mainly constrain the most sensitive parameters, which constrain certain key regions of high mass turnover but not for the bulk surface. Furthermore, the temporal differences in the sensitivities on the local scale indicate that models of reduced complexity may fail drastically for other time periods (absence of Q_L for example).

The sensitivity analysis shows that the uncertainty in the longwave radiation has a larger impact on the SMB uncertainty than the uncertainty in the incoming solar radiation, but as it is not defined relative to the absolute flux, this does not necessarily tell us that the SMB is most sensitive to the longwave radiation energy component. The impact each energy flux has on the absolute SMB has to be analyzed separately. The longwave radiation dominates, followed by the solar radiation. The larger sensitivity of the χ_{QL} switch in the LGM is mainly due to χ_{QL}'s increased contribution to the absolute SMB. In the absence of melt and with reduced precipitation, sublimation accounts for a larger portion of the absolute SMB.

It is beyond the scope of BESSI to resolve all the physical processes. We use a simple parameterization for the incoming longwave radiation which does not accurately represent reality. The atmospheric emissivity is constant in neither space nor time. Area-distributed values may work during the observational period, but differences in the atmospheric circulation alter these patterns over the glacial cycle. We conclude that the overall model uncertainty can effectively be improved by changing the simplified representation of the longwave radiation flux as a function of atmospheric temperature and emissivity either for a more sophisticated parameterization or to use longwave radiation as climate model input. If the model were to be tuned for the Greenland-wide SMB, it would be biased towards the melt regions around the margin and therefore the atmospheric emissivity. Where possible, parameters should be calibrated via quantities which they are sensitive to. None of our parameters are to be assumed constant in space, as albedo for example strongly depends on impurities and snow temperature, but unless the uncertainty in the incoming longwave radiation is reduced, it is justifiable to work with optimized values from the PD. The current model version does not use wind fields, although they impact the SEB via the turbulent fluxes. The strength of the turbulent exchange does not have a large impact on the SMB, and the approach to neglect wind speed variability is therefore justified in the context of more uncertain parameters. The model sensitivity towards the parameters that has been found is to be set into context with the assumed forcing (climate) uncertainty.

5 Summary and conclusions

The surface mass and energy balance model BESSI has been improved by accounting for turbulent latent heat flux and snow aging. The sensitivity of the model to the new implementations and uncertain model parameters was assessed with a variance-based sensitivity method based on two ensembles with a total of 16 500 simulations. The warm present-day and the cold Last Glacial Maximum climate were used to study the differences in the model response under different present-day and Last Glacial Maximum boundary conditions. The sensitivity analysis reveals that the inclusion of the turbulent latent heat flux is a necessity to simulate the local SMB and the integrated SMB over the entire Greenland ice sheet. The relative importance of sublimation and condensation is larger in the dry and cold climate of the LGM as air temperature and precipitation are lower.

The uncertainty associated with cloud cover and atmospheric emissivity dominates the SMB model uncertainty. With the different circulation during the Last Glacial Maximum due to the presence of the Laurentide ice sheet, a changing energy input from the atmosphere to the surface will re-

sult in an SMB response. The sensitivity study further reveals that the uncertainty in the SMB as a result of the atmospheric radiation decreases in a colder climate.

We find that uncertainties in the ice albedo and liquid water content and differences in the turbulent fluxes are of minor importance for our and likely also similar models. In order to reduce model uncertainty most effectively, the larger energy sources of shortwave and longwave radiation need to be constrained first via the snow albedo and the atmospheric emissivity.

Appendix A: Additional plots

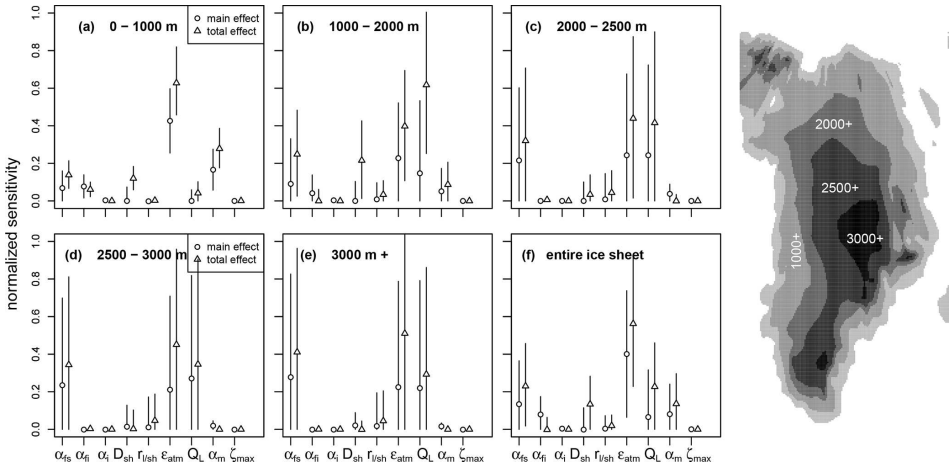

Figure A1. The global sensitivity analysis of the LGM SMB provides the main-order effect (circle) and the total effect (triangle). The two indices are displayed for all nine parameters over the different elevation bands ranging from 0–1000, 1000–2000, 2000–2500, and 2500–3000 to above 3000 m and for the entire ice sheet. The symbol represents the mean value of the sensitivity index with the bars as $\pm 1\sigma$. The elevation bands of the LGM topography over Greenland are displayed on the right; the analysis is only performed for cells where ice is present. The uncertainty in the sensitivity indices is larger than for the PD due to the smaller ensemble size.

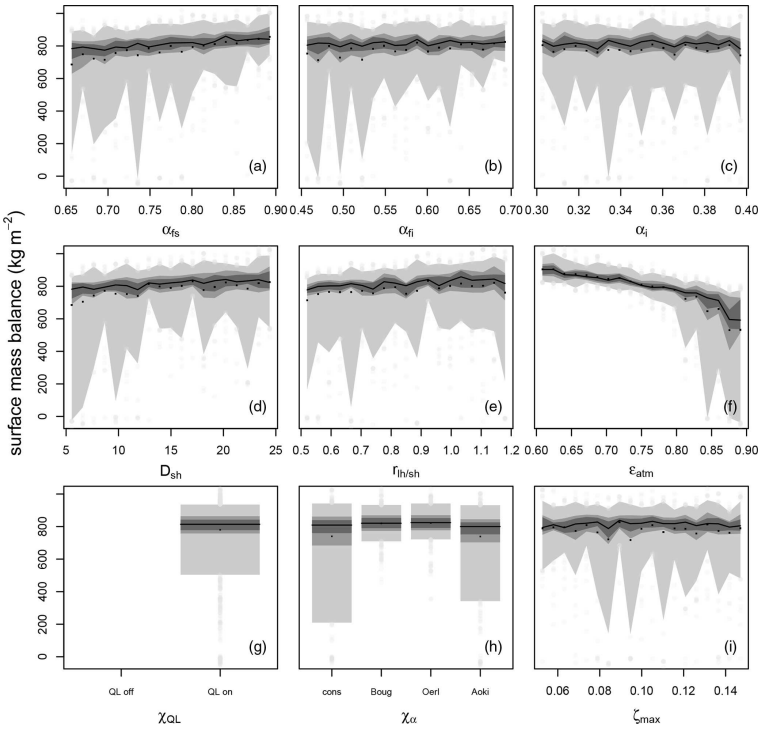

Figure A2. The ensemble statistics for the surface mass balance for the entire ensemble at region 5 (west 1000–2000 m) in the LGM, showing the 5th and 95th, 25th and 75th, 33rd and 66th, and 50th quantiles in progressively darker shading. Black points represent the ensemble mean, and the grey points correspond to the rest of the ensemble, apart from outliers (max five per bin allowed), which are removed to improve readability. Each plot represents the range of one parameter with α_{fs}, α_{fi}, and α_i in the top row; D_{SH}, $r_{lh/sh}$, and ϵ_{atm} in the middle; and $Q_{Lon/off}$, χ_α, and ζ_{max} at the bottom. As $Q_{Lon/off}$ and χ_α have two and four discrete values, respectively, the parameter range is not split into 20 intervals.

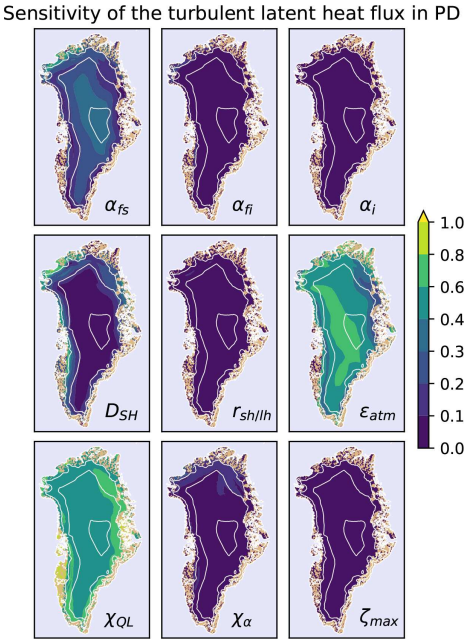

Figure A3. Global sensitivity of the turbulent latent heat flux in the PD. The total sensitivity index of Q_L of every parameter for the PD is displayed for every ice-covered grid cell. The ice-free land is in brown; the ocean is in blue.

Code and data availability. The BESSI model code is available on GitHub (https://github.com/TobiasZo/BESSI/tree/TobiasZo---GSA-model-version, last access: 3 June 2020). Additionally, the GitHub branch also contains the analysis and plotting scripts.

Additional information. The additional information including the plots of model output variables not shown here is available at https://doi.org/10.5281/zenodo.4310369 (Zolles and Born, 2020).

Author contributions. TZ implemented the model changes; conducted the ensemble simulations, the sensitivity studies, and the data analysis; and wrote the main part of the manuscript. AB contributed to all aspects of this study.

Competing interests. The authors declare that they have no conflict of interest.

Review statement. This paper was edited by Louise Sandberg Sørensen and reviewed by Andy Aschwanden and two anonymous referees.

References

Amante, C. and Eakins, B.: ETOPO1 1 Arc-Minute Global Relief Model: Procedures, Data Sources and Analysis [data], https://doi.org/10.7289/V5C8276M, 2009.

Aoki, T., Hachikubo, A., and Mashiro, H.: Effects of snow physical parameters on shortwave broadband albedos, J. Geophys. Res., 108, 1–12, https://doi.org/10.1029/2003JD003506, 2003.

Aschwanden, A., Fahnestock, M. A., Truffer, M., Brinkerhoff, D. J., Hock, R., Khroulev, C., Mottram, R., and Khan, S. A.: Contribution of the Greenland Ice Sheet to sea-level over the next millennium, Science Advances, 5, 12 pp., https://doi.org/10.1126/sciadv.aav9396, 2019.

Beven, K.: Changing ideas in hydrology – The case of physically-based models, J. Hydrol., 105, 157–172, https://doi.org/10.1016/0022-1694(89)90101-7, 1989.

Bintanja, R., Van de Wal, R., and Oerlemans, J.: Global ice volume variations through the last glacial cycle simulated by a 3-D ice-dynamical model, Quatern. Int., 95, 11–23, https://doi.org/10.1016/S1040-6182(02)00023-X, 2002.

Born, A., Imhof, M. A., and Stocker, T. F.: An efficient surface energy–mass balance model for snow and ice, The Cryosphere, 13, 1529–1546, https://doi.org/10.5194/tc-13-1529-2019, 2019.

Bougamont, M., Bamber, J. L., and Greuell, W.: A surface mass balance model for the Greenland Ice Sheet, J. Geophys. Res.-Earth, 110, 1–13, https://doi.org/10.1029/2005JF000348, 2005.

Box, J. E. and Steffen, K.: Sublimation on the Greenland ice sheet from automated station observations, J. Geophys. Res., 106, 965–981, https://doi.org/10.1029/2001JD900219, 2001.

Box, J. E., Bromwich, D. H., and Bai, L. S.: Greenland ice sheet surface mass balance 1991–2000: Application of Polar MM5 mesoscale model and in situ data, J. Geophys. Res.-Atmos., 109, 1–21, https://doi.org/10.1029/2003JD004451, 2004.

Brady, E. C., Otto-Bliesner, B. L., Kay, J. E., and Rosenbloom, N.: Sensitivity to glacial forcing in the CCSM4, J. Climate, 26, 1901–1925, https://doi.org/10.1175/JCLI-D-11-00416.1, 2013.

Braithwaite, R. J.: Calculation of sensible-heat flux over a melting ice surface using simple climate data and daily measurements of ablation, Ann. Glaciol., 50, 9–15, https://doi.org/10.3189/172756409787769726, 2009.

Bulthuis, K., Arnst, M., Sun, S., and Pattyn, F.: Uncertainty quantification of the multi-centennial response of the Antarctic ice sheet to climate change, The Cryosphere, 13, 1349–1380, https://doi.org/10.5194/tc-13-1349-2019, 2019.

Busetto, M., Lanconelli, C., Mazzola, M., Lupi, A., Petkov, B., Vitale, V., Tomasi, C., Grigioni, P., and Pellegrini, A.: Parameterization of clear sky effective emissivity under surface-based temperature inversion at Dome C and South Pole, Antarctica, Antarct. Sci., 25, 697–710, https://doi.org/10.1017/S0954102013000096, 2013.

Cuffey, K. M. and Paterson, W. S. B.: The physics of glaciers, Fourth edition, Elsevier, ISBN: 978-0-12-369461-4, 2010.

Cullen, N. J., Mölg, T., Conway, J. P., and Steffen, K.: Assessing the role of sublimation in the dry snow zone of the Greenland ice sheet in a warming world, J. Geophys. Res.-Atmos., 119, 1–15, https://doi.org/10.1002/2014JD021557, 2014.

Fettweis, X.: Reconstruction of the 1979–2006 Greenland ice sheet surface mass balance using the regional climate model MAR, The Cryosphere, 1, 21–40, https://doi.org/10.5194/tc-1-21-2007, 2007.

Fettweis, X., Hofer, S., Krebs-Kanzow, U., Amory, C., Aoki, T., Berends, C. J., Born, A., Box, J. E., Delhasse, A., Fujita, K., Gierz, P., Goelzer, H., Hanna, E., Hashimoto, A., Huybrechts, P., Kapsch, M.-L., King, M. D., Kittel, C., Lang, C., Langen, P. L., Lenaerts, J. T. M., Liston, G. E., Lohmann, G., Mernild, S. H., Mikolajewicz, U., Modali, K., Mottram, R. H., Niwano, M., Noël, B., Ryan, J. C., Smith, A., Streffing, J., Tedesco, M., van de Berg, W. J., van den Broeke, M., van de Wal, R. S. W., van Kampenhout, L., Wilton, D., Wouters, B., Ziemen, F., and Zolles, T.: GrSMBMIP: intercomparison of the modelled 1980–2012 surface mass balance over the Greenland Ice Sheet, The Cryosphere, 14, 3935–3958, https://doi.org/10.5194/tc-14-3935-2020, 2020.

Gallet, J.-C., Domine, F., Savarino, J., Dumont, M., and Brun, E.: The growth of sublimation crystals and surface hoar on the Antarctic plateau, The Cryosphere, 8, 1205–1215, https://doi.org/10.5194/tc-8-1205-2014, 2014.

Greuell, W.: Numerical modelling of the energy balance and the englacial temperature of the ETH Camp, West Greenland, Verlag d. Fachvereine, Zürcher Geografische Schriften, 51, p. 82, 1992.

Greuell, W. and Konzelmann, T.: Numerical modelling of the energy balance and the englacial temperature of the Greenland Ice Sheet. Calculations for the ETH-Camp location (West Greenland, 1155 m a.s.l.), Global Planet. Change, 9, 91–114, https://doi.org/10.1016/0921-8181(94)90010-8, 1994.

Greuell, W. and Smeets, P.: Variations with elevation in the surface energy balance on the Pasterze (Austria), J. Geophys. Res., 106, 31717, https://doi.org/10.1029/2001JD900127, 2001.

Hofer, S., Tedstone, A. J., Fettweis, X., and Bamber, J. L.: Decreasing cloud cover drives the recent mass loss on

the Greenland Ice Sheet, Science Advances, 3, e1700584, https://doi.org/10.1126/sciadv.1700584, 2017.

Klok, E. J. and Oerlemans, J.: Modelled climate sensitivity of the mass balance of Morteratschgletscher and its dependence on albedo parameterization, Int. J. Climatol., 24, 231–245, https://doi.org/10.1002/joc.994, 2004.

Krapp, M., Robinson, A., and Ganopolski, A.: SEMIC: an efficient surface energy and mass balance model applied to the Greenland ice sheet, The Cryosphere, 11, 1519–1535, https://doi.org/10.5194/tc-11-1519-2017, 2017.

Krebs-Kanzow, U., Gierz, P., and Lohmann, G.: Brief communication: An ice surface melt scheme including the diurnal cycle of solar radiation, The Cryosphere, 12, 3923–3930, https://doi.org/10.5194/tc-12-3923-2018, 2018.

Lehning, M., Bartelt, P., Brown, B., and Fierz, C.: A physical SNOWPACK model for the Swiss avalanche warning: Part III: Meteorological forcing, thin layer formation and evaluation, Cold Reg. Sci. Technol., 35, 169–184, https://doi.org/10.1016/S0165-232X(02)00072-1, 2002.

Listion, G. E. and Elder, K.: A Meteorological Distribution System for High-Resolution Terrestrial Modeling (MicroMet), J. Hydrometeorol., 7, 217–234, https://doi.org/10.1175/JHM486.1, 2006.

Noël, B., van de Berg, W. J., van Wessem, J. M., van Meijgaard, E., van As, D., Lenaerts, J. T. M., Lhermitte, S., Kuipers Munneke, P., Smeets, C. J. P. P., van Ulft, L. H., van de Wal, R. S. W., and van den Broeke, M. R.: Modelling the climate and surface mass balance of polar ice sheets using RACMO2 – Part 1: Greenland (1958–2016), The Cryosphere, 12, 811–831, https://doi.org/10.5194/tc-12-811-2018, 2018.

Oerlemans, J. and Knapp, W. H.: A 1-year record of global radiation and albedo in the ablation zone of Marteratschgletscher, Switzerland, J. Glaciol., 44, 231–238, https://doi.org/10.3189/S0022143000002574, 1998.

Ohmura, A.: Physical Basis for the Temperature-Based Melt-Index Method, J. Appl. Meteorol., 40, 753–761, https://doi.org/10.1175/1520-0450(2001)040<0753:PBFTTB>2.0.CO;2, 2001.

Peltier, W., Argus, D., and Drummond, R.: Space geodesy constrains ice-age terminal deglaciation: The global ICE-6G_C (VM5a) model., J. Geophys. Res.-Sol. Ea., 120, 450–487, https://doi.org/10.1002/2014JB011176, 2015.

Plach, A., Nisancioglu, K. H., Langebroek, P. M., Born, A., and Le clec'h, S.: Eemian Greenland ice sheet simulated with a higher-order model shows strong sensitivity to surface mass balance forcing, The Cryosphere, 13, 2133–2148, https://doi.org/10.5194/tc-13-2133-2019, 2019.

Robinson, A., Calov, R., and Ganopolski, A.: Greenland ice sheet model parameters constrained using simulations of the Eemian Interglacial, Clim. Past, 7, 381–396, https://doi.org/10.5194/cp-7-381-2011, 2011.

Rolstad, C. and Oerlemans, J.: The residual method for determination of the turbulent exchange coefficient applied to automatic weather station data from Iceland, Switzerland and West Greenland, Ann. Glaciol., 42, 367–372, https://doi.org/10.3189/172756405781813041, 2005.

Saltelli, A., Campolongo, F., and Tarantola, S.: Sensitivity Anaysis as an Ingredient of Modeling, Stat. Sci., 15, 377–395, https://doi.org/10.1214/ss/1009213004, 2000.

Saltelli, A., Ratto, M., Tarantola, S., and Campolongo, F.: Sensitivity analysis practices: Strategies for model-based inference, Reliab. Eng. Syst. Safe., 91, 1109–1125, https://doi.org/10.1016/j.ress.2005.11.014, 2006.

Saltelli, A., Annoni, P., Azzini, I., Campolongo, F., Ratto, M., and Tarantola, S.: Variance based sensitivity analysis of model output. Design and estimator for the total sensitivity index, Comput. Phys. Commun., 181, 259–270, https://doi.org/10.1016/j.cpc.2009.09.018, 2010.

Sauter, T. and Obleitner, F.: Assessing the uncertainty of glacier mass-balance simulations in the European Arctic based on variance decomposition, Geosci. Model Dev., 8, 3911–3928, https://doi.org/10.5194/gmd-8-3911-2015, 2015.

Sobol, I., Tarantola, S., Gatelli, D., Kucherenko, S., and Mauntz, W.: Estimating the approximation error when fixing unessential factors in global sensitivity analysis, Reliab. Eng. Syst. Safe., 92, 957–960, https://doi.org/10.1016/j.ress.2006.07.001, 2007.

Uppala, S. M., Healy, S. B., Balmaseda, M. A., de Rosnay, P., Isaksen, L., van de Berg, L., Geer, A. J., McNally, A. P., Matricardi, M., Haimberger, L., Dee, D. P., Dragani, R., Bormann, N., Hersbach, H., Vitart, F., Kobayashi, S., Andrae, U., Beljaars, A. C. M., Poli, P., Monge-Sanz, B. M., Peubey, C., Thépaut, J.-N., Delsol, C., Hólm, E. V., Simmons, A. J., Köhler, M., Bechtold, P., Berrisford, P., Balsamo, G., Park, B.-K., Fuentes, M., Bidlot, J., Bauer, P., Tavolato, C., Kållberg, P., and Morcrette, J.-J.: The ERA-Interim reanalysis: configuration and performance of the data assimilation system, Q. J. Roy. Meteor. Soc., 137, 553–597, https://doi.org/10.1002/qj.828, 2011.

van de Berg, W. J., van den Broeke, M., Ettema, J., van Meijgaard, E., and Kaspar, F.: Significant contribution of insolation to Eemian melting of the Greenland ice sheet, Nat. Geosci., 4, 679–683, https://doi.org/10.1038/ngeo1245, 2011.

Van Den Berg, J., van de Wal, R., and Oerlemans, H.: A mass balance model for the Eurasian Ice Sheet for the last 120,000 years, Global Planet. Change, 61, 194–208, https://doi.org/10.1016/j.gloplacha.2007.08.015, 2008.

van den Broeke, M., Smeets, P., Ettema, J., van der Veen, C., van de Wal, R., and Oerlemans, J.: Partitioning of melt energy and meltwater fluxes in the ablation zone of the west Greenland ice sheet, The Cryosphere, 2, 179–189, https://doi.org/10.5194/tc-2-179-2008, 2008.

Van Tricht, K., Lhermitte, S., Lenaerts, J. T., Gorodetskaya, I. V., L'Ecuyer, T. S., Noël, B., van den Broeke, M. R., Turner, D. D., and van Lipzig, N. P.: Clouds enhance Greenland ice sheet meltwater runoff, Nat. Commun., 7, 10266, https://doi.org/10.1038/ncomms10266, 2016.

van Wessem, J. M., van de Berg, W. J., Noël, B. P. Y., van Meijgaard, E., Amory, C., Birnbaum, G., Jakobs, C. L., Krüger, K., Lenaerts, J. T. M., Lhermitte, S., Ligtenberg, S. R. M., Medley, B., Reijmer, C. H., van Tricht, K., Trusel, L. D., van Ulft, L. H., Wouters, B., Wuite, J., and van den Broeke, M. R.: Modelling the climate and surface mass balance of polar ice sheets using RACMO2 – Part 2: Antarctica (1979–2016), The Cryosphere, 12, 1479–1498, https://doi.org/10.5194/tc-12-1479-2018, 2018.

Zemp, M., Huss, M., Thibert, E., Eckert, N., McNabb, R., Huber, J., Barandun, M., Machguth, H., Nussbaumer, S., Gärtner-Roer, I., Thomson, L., Paul, F., Maussion, F., Kutuzov, S., and Cogley, J. G.: Global glacier mass changes and their contribu-

tions to sea-level rise from 1961 to 2016, Nature, 568, 382–386, https://doi.org/10.1038/s41586-019-1071-0, 2019.

Zolles, T. and Born, A.: Sensitivity of the Greenland surface mass and energy balance to uncertainties in key model parameters: Supplement and Model code, Zenodo [code], https://doi.org/10.5281/zenodo.4310370, 2020.

Zolles, T., Maussion, F., Galos, S. P., Gurgiser, W., and Nicholson, L.: Robust uncertainty assessment of the spatio-temporal transferability of glacier mass and energy balance models, The Cryosphere, 13, 469–489, https://doi.org/10.5194/tc-13-469-2019, 2019.

How does a change in climate variability impact the Greenland ice-sheet surface mass balance?

Tobias Zolles and Andreas Born
Department of Earth Science, University of Bergen, Bergen, Norway.
Bjerknes Centre of Climate Research, Bergen, Norway.

The Cryosphere Discussion
doi: doi.org/10.5194/tc-2021-379

II

https://doi.org/10.5194/tc-2021-379
Preprint. Discussion started: 18 January 2022

The Cryosphere Discussions

How does a change in climate variability impact the Greenland ice-sheet surface mass balance?

Tobias Zolles[1,2] and Andreas Born[1,2]

[1]Department for Earth science, University of Bergen, Bergen, Norway
[2]Bjerknes Centre for Climate Research, Bergen, Norway

Correspondence: Tobias Zolles (tobias.zolles@uib.no)

Abstract. The future of the Greenland ice-sheet largely depends on the changing climate. When ice-sheet models are run for time periods that extend far beyond the observational record they are often forced by climatology instead of a transient climate. We investigate how this simplification impacts the surface mass balance using the Bergen Snow Simulator. The model was run for up to 500 years using the same atmospheric climatology, but different variability, as forcing. We achieve this by re-arranging the years in the ERA-interim reanalysis while leaving the intra-annual variations unchanged. This changes the surface mass balance by less than 5 % over the entire Greenland ice sheet.

However, using daily averages as forcing introduces large changes in intra-annual variability and thereby overestimates the Greenland-wide surface mass balance by 40 %. The biggest contributor is precipitation followed by temperature. The most important process is that small amounts of snow fall from the daily climatology overestimate the albedo, leading to an increased SMB. We propose a correction that distributes the monthly precipitation over a realistic intra-monthly variability. This approach reduces the SMB overestimation to 15-25 %. We conclude that simulations of the Greenland surface mass and energy balance should be forced with a transient climate. Particular care must be taken if only climatological data is available for simulations with a model that was calibrated with transient data. If daily transient data cannot be used, at least the precipitation should follow a natural daily distribution.

1 Introduction

The Greenland ice sheet is one of the main contributors to sea level rise. Ice-sheet models are run to project the future of the ice-sheet. Future projections show that uncertainty associated with the atmospheric climate forcing becomes the dominant component within the next century (Aschwanden et al., 2019). The climate forcing itself is inherently uncertain due the used boundary conditions (like an emission scenario) (O'Neill et al., 2016) but also depends on the used climate model, which remains a major source of uncertainty until the end of the century (Holube et al., 2021). Furthermore, ice-sheet models may be forced with a multiyear climatology, monthly or daily data with unclear consequences due to the non-linearity, increased melt at warmer temperatures, of the SMB.

Paleo simulations of ice-sheets are often based on proxy temperature reconstructions (Van de Berg et al., 2008; Robinson et al., 2011). Because proxy data has a limited temporal resolution, it is often impossible to accurately reconstruct inter- and

https://doi.org/10.5194/tc-2021-379
Preprint. Discussion started: 18 January 2022

The Cryosphere Discussions

intra-annual variability. While it is common practice to use a constant temperature index to interpolate between the coldest (Last Glacial Maximum) and the warmest (Present Day) state (e.q. Forsström and Greve, 2004; Alvarez Solas et al., 2018), it has not been studied what impact additional variability on short time scales would have. The effect of additional non-resolved variability may be an even larger issue as the most common temperature proxies used are ice cores, which in turn rather reflect the precipitation events than only climatological temperatures (Madsen et al., 2019). Proxies vary greatly in their temporal resolution, so we investigate the variability on multiple time scales (50 - 500 years). Although the initial question arises from proxy and climate reconstruction it is equally applicable to projections of the distant future of the Greenland ice sheet.

In this study, we perform simulations using the latest version of the BErgen Snow SImulator (BESSI) (Zolles and Born, 2021). Prior model parameter tuning was performed relative to the GRACE satellite data set and RACMO simulations (Noël et al., 2018; Fettweis et al., 2020a; Holube et al., 2021). The model is designed for the simulations of long time scales, leading to a trade off between complexity and computational efficiency. Therefore, we need a representative climate forcing for longer time periods.

Input data to force BESSI is derived from the ERA-interim reanalysis data set, instead of using an artificial inter-annual variability or internal climate model variability (Semenov, 2008; Verdin et al., 2018) based on a climatology. Firstly, the rapidly increasing temperature over the last 50 years is a good example of a non-representative climatological average. Secondly, ERA-interim provides a reasonable natural variability and daily data is available over the entire Greenland Ice-sheet at a sufficiently high spatial resolution (Berrisford et al., 2011). Potential climate model data for climate reconstructions and projections will be of a similar or lower resolution. Climate variability of different time scales is achieved by a reordering the individual years. The ultimate test is weather a re-arranged forcing mimics reality by simulating the same SMB as the transient - real - forcing. For a longer simulation duration the ERA-interim period is copied multiple times. We use ERA-interim as its resolution is of the same order of magnitude as most Global Circulation climate Models (GCM) and refrain from higher resolution models like MAR (Fettweis et al., 2017) or RACMO (van Meijgaard et al., 2008) as those will not be available for the most of the past (last glacial) and are computationally demanding. We choose the current rapid climate change as it provides an upper uncertainty estimate for the entire glacial. Furthermore, the model sensitivity of the surface mass balance model has been evaluated prior for this time period (Zolles and Born, 2021).

This leaves us with three goals of the study:

- Quantify the uncertainty associated with inter-annual variability and climatological forcing
- Identify the reasons for and potentially reduce this uncertainty
- Find a procedure to create a representative climate forcing for the past based on temperature proxies

In section 2 we will give a brief description of the surface mass balance model and the set-up of the climate ensemble used in this study. The results in section 3 are split into the uncertainty of inter-annual variability, individual forcing variables, and precipitation and associated albedo impact. After that, we discuss our findings in section 4 and conclude in section 5.

https://doi.org/10.5194/tc-2021-379
Preprint. Discussion started: 18 January 2022

The Cryosphere Discussions

2 Model setup

2.1 Snow model - BESSI

The study uses the Bergen Snow SImulator (BESSI), which calculates the mass and energy balance with a daily time step (Born et al., 2019). It compares well to other surface mass balance models over Greenland with a slight positive bias for melt regions (Fettweis et al., 2020a). The latest model version is described in detail in Zolles and Born (2021) so that we will only provide an abridged description here. The model domain is based on a stereo-graphic projection of Greenland and uses an equidistant grid with a resolution of 10 km. The model uses a mass based vertical grid of 15 layers, with up to 500 kgm^{-2}. The model uses five input fields with a daily resolution: surface temperature, total precipitation, dew point, and down-welling long- and shortwave radiation. A full energy balance is calculated at the surface including diffusion of heat in the snow pack and latent contributions from freezing and melting of water and liquid precipitation. Liquid water in the snow is explicitly represented. Mass changes due to melting, precipitation, or sublimation processes. The model parameters have been tuned using a multi-variate calibration towards RACMO (Noël et al., 2018) and the GRACE data set.

2.2 Atmospheric climate forcing

We use the daily ERA-interim reanalysis data from 1979-2017 (Uppala et al., 2011). The input variables of atmospheric temperature, precipitation, dew point, and short and long-wave radiation are bi-linearly interpolated to a 10x10 km grid over Greenland. This initial forcing data of 39 years is then taken 12 times to represent longer time periods. We define the natural transient forcing as the ERA-interim forcing in the true historical order and then looping forward and backward (F-BWD). This means the following order 1979-2017-1979-2017-1979-.. .

We arrange the original transient forcing in four different ways: repeating the ERA-interim forcing in its original order multiple times (forward, FWD), repeating the same data in reverse order (backward, BWD), alternating between FWD and BWD to avoid the abrupt transition between the forcing years 2017 and 1979 (forward-backward, F-BWD), and again the same in reverse (backward-forward, B-FWD). This already creates synthetic time series with different frequencies (Fig. 1). However, to achieve even lower frequencies with the same data we also re-arrange the original transient forcing based on the Greenland ice-sheet wide average annual air temperature. This changes the order of the 39 years in the record. Note that this does not break the consistency between the atmospheric variables, or add energy or mass to the atmospheric system relative to the original natural forcing. Temporal continuity is only broken at the year break with arguably negligible consequences.

The other time series are the temperature ordered forcing with different frequencies (rows) and sequential arrangement (columns, similar to the first row). All these time series have the same average forcing values, respectively the daily same climatology, but different temporal variability. They are obtained by ordering the 12 cycles of 39 years by the Greenland wide temperature from the coldest of the series to the warmest. Afterwards depending on the chosen frequency we sample every n-th member of this series starting at the coldest/warmest year, where n is the frequency and once the end of the series is reached we start over at the 2nd member sampling every n^{th} member thereafter, this is repeated in total n times for one time series.

https://doi.org/10.5194/tc-2021-379
Preprint. Discussion started: 18 January 2022

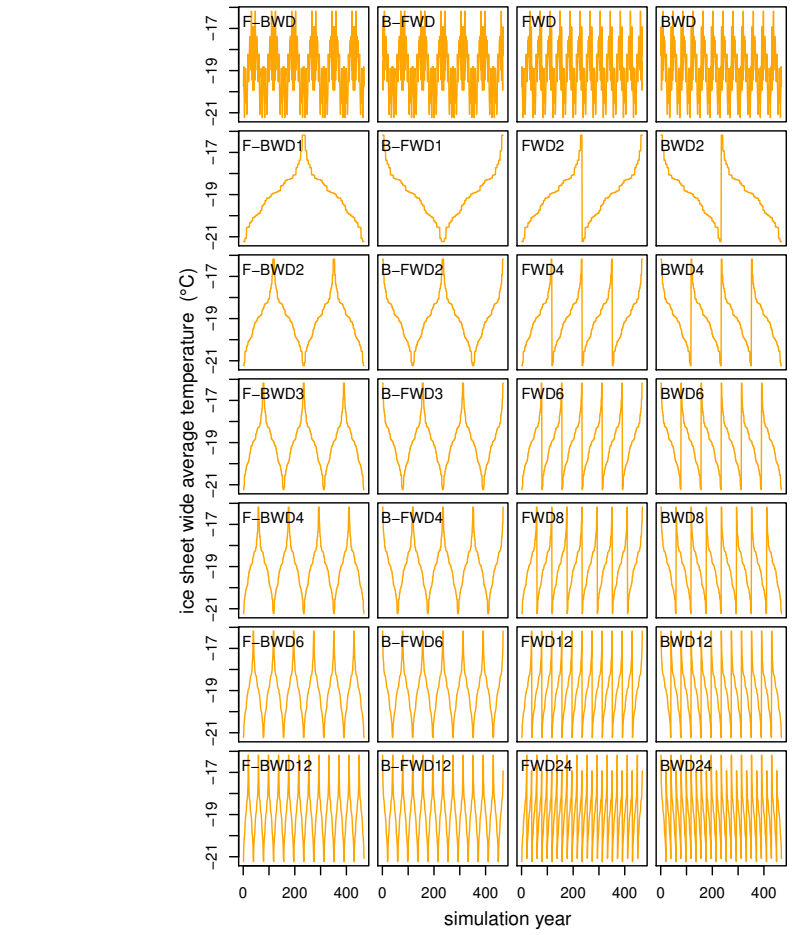

Figure 1. 28 different temperature time series based on 12 cycles of ERA-interim forcing. Each of them consist of the 12x39 years of ERA-interim which are ordered by temperature with different reoccurring frequencies. The first row shows the normal ERA-interim sequence (1979-2017) with different reoccurring patterns (2017-1979-2017x6,1979-2017-1979x6,1979-2017x12,2017-1979x12). Rows three to six show the temperature ordered sequence with increasing frequencies, with row one starting cold (F-BWD) and row two starting warm (B-FWD). Instead of looping back and forth from cold to warm the last two rows (orange) only increase/decrease in temperature and once the maximum/minimum is reached it starts over with the coldest/warmest forcing year again.

https://doi.org/10.5194/tc-2021-379
Preprint. Discussion started: 18 January 2022

The Cryosphere Discussions

These individual forcings allow us to investigate the sensitivity and feedback of the SMB to different inter-annual variability and, for example, extended warm periods.

2.3 Simulations

All simulations are spun up with 500 years of ERA-interim F-BWD to reach a stable firn cover. We then simulate the surface mass balance with the different forcing time series (sec. 2.2). The surface mass balance is calculated for five different total simulations with a duration of 78, 117, 156, 234 and 468 years, to mimic different temperature proxy resolutions

The first set of simulations use the unaltered transient climate forcing only reordered in time (FWD/BWD/F-BWD/F-BWD 1-12). The second set of simulations mixes climatological and transient forcing. Lastly, we investigate the impact of the temporal precipitation distribution by simulating 468 years with the same monthly precipitation average but different sub-monthly frequency.

3 Results

Inter-annual variability - ordering The average surface mass balance of the Greenland ice sheet is around 200 $\mathrm{kg\ m^{-2}\ yr^{-1}}$ independent of the ordering of the forcing years (fig. 2). The lowest SMB occurs if multiple warm years happen after each other, corresponding to a low frequency (second row FWD/BWD/F-BWD/F-BWD 1). The memory effect of the firn cover to extended warm periods is rather low on an integrated level, though in the extreme case of only one cycle the SMB is slightly lower on the second cooling branch than the warming one. Within each frequency BWD (last column) always shows the lowest SMB, because it starts with the warmest year and no protective firn cover can be built up first to reduce the amount of ice exposure. Note that we do not simulate changes in surface elevation, which could cause a significant positive feedback at multi-centennial time scales.

While the temporal order for the forcing years is of marginal influence (< 5% difference in SMB) over the entire ice-sheet, it is larger on a regional level. The variability mainly impacts the SMB around the equilibrium line, with a standard deviation of up to 500 $\mathrm{kg\ m^{-2}\ yr^{-1}}$ on the local scale (fig. 3). The standard deviation is also quite high in the northeast.

As proxy resolution is variable we also study additional simulation lengths of 78, 117, 156, and 234 years, corresponding to two, three, four, and six ERA-interim cycles. The general results are similar for shorter simulation periods (78, 117, 156, and 234 years instead of 468), though the difference between the simulations decreases, as with fewer ERA-interim cycles the duration of extended warm or cold periods decreases (not shown).

Climatological forcing / Intra-annual variability As the order of the inter-annual variability has a low impact, can we actually use daily climatologies? We study the impact of the daily climatology for every variable individually and only for the B-FWD case. Two mixed data sets are created, one where all but one variable are held at their climatological averages, and vice versa, where only one variable uses the climatology. Based on the results from the previous section we select the B-FWD member as a representative for the transient forcing, as the other reordered time series yieled similar SMB values.

https://doi.org/10.5194/tc-2021-379
Preprint. Discussion started: 18 January 2022

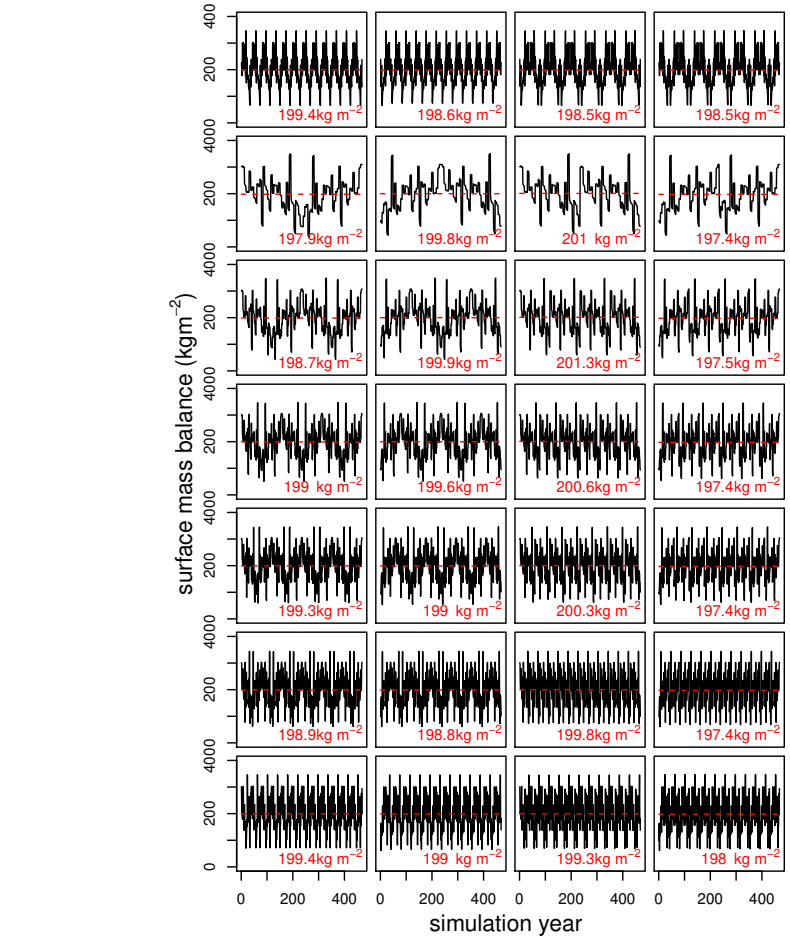

Figure 2. The SMB response of the Greenland ice-sheet to climate forcing with different inter-annual variability. Each box displays the annual surface mass balance over the entire simulation period of 468 years in black and the mean in red. The respective forcing is in the same order shown in figure 1, with F-BWD,B-FWD,FWD,BWD from left to right. The difference between the SMB with the different forcing is below 5 %.

https://doi.org/10.5194/tc-2021-379
Preprint. Discussion started: 18 January 2022

The Cryosphere Discussions
Open Access
EGU

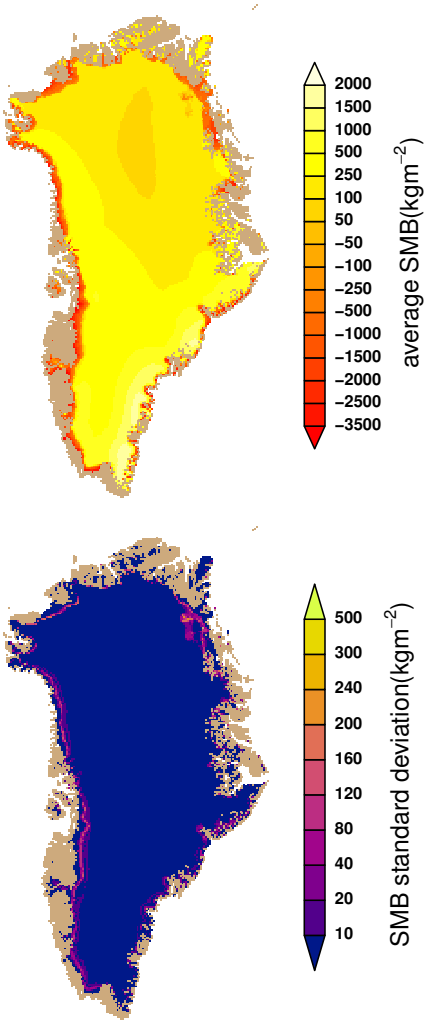

Figure 3. The average SMB and its standard deviation of the 28 simulations with different inter-annual variability order. The individual ensemble members all have the same climatology. The variation in the SMB is greatest around the equilibrium line and the northeast.

https://doi.org/10.5194/tc-2021-379
Preprint. Discussion started: 18 January 2022

The Cryosphere Discussions

The daily climatology leads to a drastic overestimation of the SMB by 40 % (274 $\mathrm{kg\,m^{-2}\,yr^{-1}}$ Fig. 4 a,b.). We further investigate this overestimation by studying the impact of the individual forcing variables: using a transient forcing for all but one variable, which comprises of daily climatological averages (right), and the climatological forcing is mixed with one transient variable (left) (fig. 4 c-l). The SMB of these simulations exceed the transient forcing (4 b), meaning that daily climatologies always lead to an SMB increase. This is no surprise due to the non-linearity of the SMB to energy input. There is a clear difference in the impact of the individual variables. While the climatological dew point only slightly changes the SMB (fig. 4 l), the radiation components increase the SMB by 5 % (fig. 4 h, j). Average temperatures increase the SMB by 15% (fig. 4 d) and daily averages of precipitation increase the SMB by 30% (fig. 4 f). Vice versa the complementary effect is true for climatological forcing (fig. 4 c, e, g, i, k), with climatological forcing with transient precipitation showing the lowest SMB (fig. 4 e).

The small effect and low variability of the radiation components shows that using climatologies is justified in this case (fig. 4 g-j), as the inter-annual variability of Greenland wide radiation is relatively low anyway. Though it is still connected to a slight bias of 5% in the current climate. The turbulent latent heat flux has a relatively low impact on the Greenland wide SMB (Zolles and Born, 2021), which is in line with the low effect the dew point change has (fig. 4 k, l). While the biggest differences between the previous simulations where found around the equilibrium line (fig. 3), the largest difference between climatological and transient forced SMB simulations is found in the melting region of Greenland (fig. 5). Temperature has the second highest influence, which can be attributed mainly to the non-linearity of the SMB. However, the overestimation by climatological precipitation cannot be explained by the non-linearity, but the albedo. Using a daily climatology leads to small amounts of mostly snowfall every day leading to a surface albedo increase. The annual average albedo increase is up to 0.1 in the melt region of Greenland. The drastic effect of daily climatologies of precipitation can be attributed to this albedo overestimation.

Can we emulate intra-annual variability of precipitation? We have shown that BESSI overestimates the SMB drastically if daily climatologies of precipitation are used. A daily climatology is unrealistic as it has small amounts of snow fall every day. This does not agree with observations of highly event-based precipitation in the Atlantic region (Sodemann et al., 2008). We therefore calculate alternative temporal precipitation distributions by taking monthly averages with a sub-monthly distribution instead. Regular precipitation frequencies of 2, 4, 8, 15, and 30 days are tested as well as the sub-monthly distributions from each of the 39 ERA-interim years. For the ERA-interim based distributions the original daily time series P_{day} is scaled to have the same monthly average:

$$P_{day} = P^t_{day} \cdot \frac{\overline{P_m}}{P^t_m} \quad \forall t \in [1979, 2017] \tag{1}$$

with P^t_m as the monthly mean of the year t, and $\overline{P_m}$ the monthly climatological precipitation amount. This correction can be compared to the Delta Method for precipitation (Beyer et al., 2019). We obtain 39 possible precipitation time series, each with a different sub-monthly distribution of the precipitation analogous to the true precipitation of the specific year. Though the monthly sum of precipitation is similar for all the simulations the resulting distributions are quite different. April 2014 was a

https://doi.org/10.5194/tc-2021-379
Preprint. Discussion started: 18 January 2022

The Cryosphere Discussions
Open Access
EGU

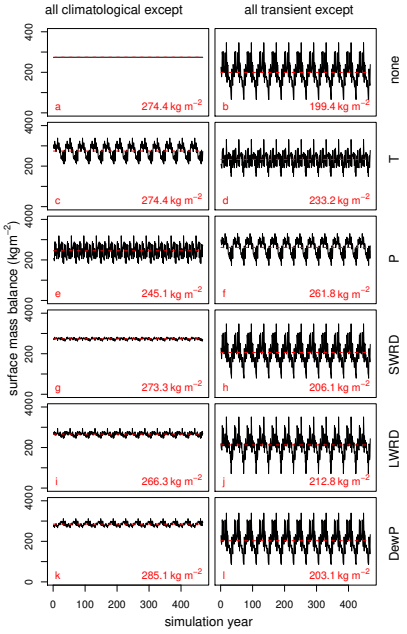

Figure 4. The Greenland wide integrated SMB with climatological and transient forcing. On the left side the model is forced with climatological (daily averages) forcing, with one transient variable in the rows 2-6. Transient forcing mixed with one climatological variable is shown on the right. The climatologically forced SMB model (a) overestimates the SMB relative to the fully transient case (b). If transient variables are taken individually the precipitation lowers the SMB the most (e). Vice versa climatological precipitation distorts the "true" transient SMB the most (f). Climatological dew point, short-wave and long-wave radiation lead to slightly increased SMB (h, j, l).

https://doi.org/10.5194/tc-2021-379
Preprint. Discussion started: 18 January 2022

The Cryosphere Discussions
Open Access
EGU

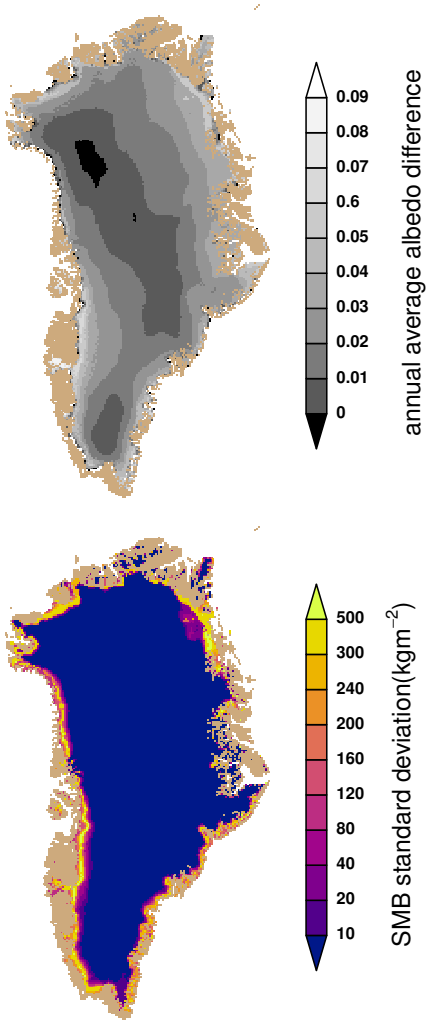

Figure 5. The standard deviation of the SMB for the transient and climatological mixed simulations (fig. 4) on the bottom, and the difference between the transient and the climatological forced surface albedo on the top. The largest standard deviation is in the melt region, due to an up to 0.1 larger annual average albedo.

https://doi.org/10.5194/tc-2021-379
Preprint. Discussion started: 18 January 2022

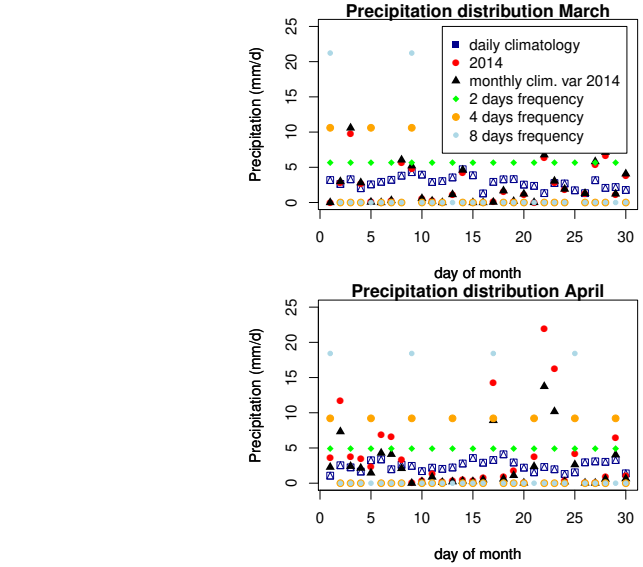

Figure 6. Sub-monthly precipitation distribution for March and April of different simulations. The same monthly precipitation is either distributed via daily climatologies (blue), monthly climatology with the sub-monthly distribution of, for example, 2014 (black) or with regular frequencies (green, orange, light blue). The red distribution is the true distribution for 2014 which is then adjusted to the climatological average (black, eq. 1), as can be seen April 2014 was wetter than the average April of the ERA-interim period.

wet month, so for the resulting forcing it is adjusted to be less but still has four days with precipitation of up and above 10 $kg\ m^{-2}$ (fig. 6).

The simulated SMB depends on the chosen sub-monthly precipitation distribution (fig. 7). For regular precipitation the SMB decreases with precipitation frequency (255/233/200/154 and 87 $\mathrm{kg\ m^{-2}\ yr^{-1}}$ at precipitation every $2^{nd}/4^{th}/6^{th}/15^{th}$ and 30^{th} day). Independent of the forcing type of the other variables introducing a lower frequency than precipitation every day (daily climatology) decreases the SMB, this is also true for the sub-monthly distribution from the individual 39 ERA-interim years (fig. 7c, d). The precipitation heavy years of the unaltered forcing are now showing lower SMBs than in the B-FWD simulation. The monthly climatology (fig. 7d) instead of the daily climatology (fig. 7b) reduces the mass balance by

https://doi.org/10.5194/tc-2021-379
Preprint. Discussion started: 18 January 2022

The Cryosphere Discussions

30 $\mathrm{kg\ m^{-2}\ yr^{-1}}$, which is much closer to the "true" value of the transient forcing (fig. 7a). The amplitude of this simulations SMB time series is rather low as the same amount of precipitation falls every year, it was investigated further. Instead of using different sub-monthly frequencies every year the distribution from each year ERA-interim year is taken as the forcing for the entire simulation period (as example 2009: fig. 7 f,g; the entire range is given in fig. 8). It spans from 224-253 $\mathrm{kg\ m^{-2}\ yr^{-1}}$. Using the sub-monthly precipitation distribution for the climatology reduces the SMB overestimation from 40% to 10-25%. A Greenland wide regular frequency may by chance show similar values as the transient simulation (8 days in this case), and 2-8 days give SMB values comparable to natural distributions.

The decrease in SMB is due to the non-linearity effect of the SMB, as in dry years earlier ice exposure triggers a feedback. Due to the non-linearity of the mass balance and albedo feedback, the range of these simulations is larger than the amplitude of the single simulation (fig.7 d).

4 Discussion

We study the impact of inter-annual variability by a simple reordering. The SMB shows a low dependency of 5% over 468 years on the order of the forcing. In case of unknown inter-annual variability the use of a climatological forcing over estimates the SMB by 40 % due to the non-linearity of the SMB and albedo overestimation. We try to reduce this effect by instead using only monthly precipitation averages with a sub-monthly distribution. The overestimation is reduced but an uncertainty of 15% based on the chosen distribution is introduced.

Climate model simulations of the same time period vary in their inter-annual variability, they can very well represent the climatology, but not the order. We show that the effect of the order of the inter-annual variability is less than 5 %. This indicates that the memory effect of the Greenland wide integrated SMB to multiple warm or cold years is low enough to be modeled with climate forcing which may not have a realistic temporal variability. Even multiple warmer years over Greenland after each other do not significantly lead to strong feedback. The used ERA-interim period with its temperature trend (Hanna et al., 2021) as the study period can be considered an upper boundary for steady state climate. The simulation lengths were 78,117, 156, 234 and 468 years, and even the extreme case of 12 consecutive years with the warmest temperature the average SMB only decreased by 3.5 %. If the climatology is known and the amplitude of the variability of the forcing data, the order does not really matter, despite the high inter annual variability observed in line with Van den Broeke et al. (2011). In case of climate simulations based on climatologies derived from proxies or other boundary conditions they likely are applicable for SMB simulations as long as the amplitude of the variability is good, even if there is a sub-resolution trend not visible in the proxy data. However, the effect is larger on a regional basis and around the equilibrium line the sensitivity towards this inter-annual variability increases. For the ERA-interim climate the northeast of Greenland with its sparse precipitation and large inter-annual variability in particular shows a standard deviation of up to 300 $\mathrm{kgm^{-2}yr^{-1}}$.

If the inter-annual variability is not known as is most often the case for the distant past or future, the forcing has to be based on climatologies. BESSI uses daily forcing data and is sensitive to daily precipitation. A small amount of snow-fall every day leads to an albedo overestimation as BESSI resolves albedo adjustments on a daily bases. A possible solution is to

https://doi.org/10.5194/tc-2021-379
Preprint. Discussion started: 18 January 2022

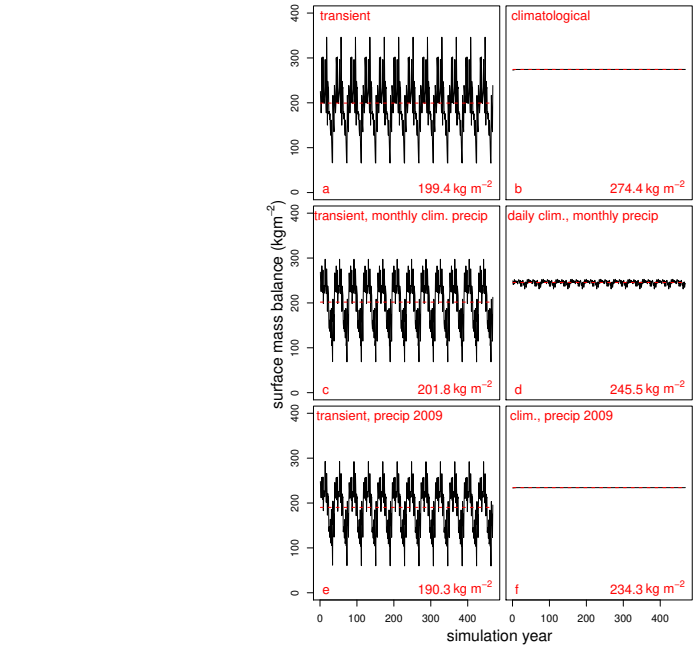

Figure 7. The Greenland-wide integrated SMB forced with different precipitation variability. The SMB time series is shown in black, with the average SMB as a red line. The SMB average value is shown in each panel. The transient B-FWD (a) and the full daily climatology (b) are shown again for direct comparison and are identical to Figure 4. The transient precipitation was scaled to have the same monthly average every year, with the sub-monthly frequency of the individual years, which is combined with either transient forcing (c) or daily climatological forcing (d) of the other variables. Similarly, we combine the sub-monthly precipitation distribution of one year, 2009, with transient (e) and the daily climatological (f) forcing of the other variables. 2009 was chosen as its monthly precipitation distribution is closed to the climatological average.

https://doi.org/10.5194/tc-2021-379
Preprint. Discussion started: 18 January 2022

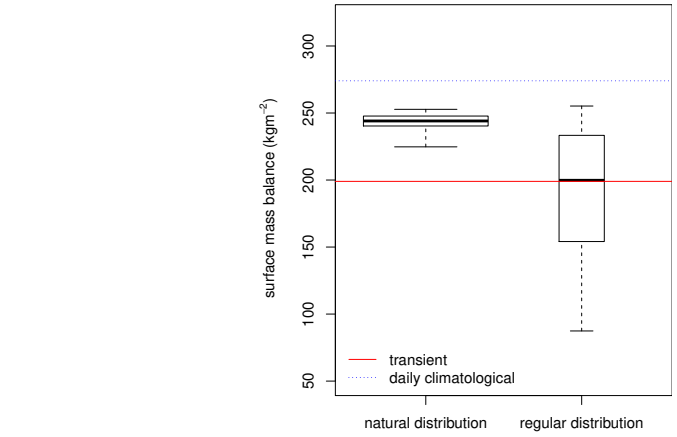

Figure 8. SMB averages for climate forcing with different precipitation variability based on the ERA-interim ensemble. In total 39 different sub-monthly natural precipitation distributions are shown on the left based on monthly averages distributed by the 39×12 sub-monthly distributions of each year 1979-2017. The SMB response to regular precipitation on the 2/4/6/15/30th day is on the right. The simulations are forced with the daily climatology of temperature, short and long-wave radiation, and dew point. The width of the boxes is relative to the size of the ensemble (39/5).

parameterize the albedo routine differently for climatology and transient data. Alternatively, the precipitation climatology has to be calculated in a physical more reasonable way which we explore here. We show that monthly climatologies with a natural sub-monthly distribution reduce the SMB overestimation. In practice, there are multiple ways how to define such a distribution: regular or stochastic frequencies for a region using normalized precipitation from reanalysis or climate simulation data. Either approach, may be prone to the sampling period and not invariant in time, and multiple solution may exist. The redistributing of the same precipitation amount at each grid point within a month can change the SMB by 15% (fig. 8). This is to be considered when selecting the fields for projections or reconstructions, purely based on scalar temperature and/or precipitation anomalies of a given field. The precipitation is quite variable in Greenland (Mosley-Thompson et al., 2005), but not only the total amount is important but also its temporal distribution, in particular in the melt region. There is no clear best representative of the precipitation variability among the individual years of the ERA-interim period.

Based on our findings we suggest that in the absence of full climate simulations with natural variability, temperature and precipitation anomalies are applied to a related climatology with sub-monthly frequency in precipitation. Still using climatological forcing may be overestimating SMB, as it does for BESSI, due to the non-linearity of mass balance, which is in line with (Mikkelsen et al., 2018) who found a 13 % overestimation of the SMB if inter-annual temperature fluctuation is not

https://doi.org/10.5194/tc-2021-379
Preprint. Discussion started: 18 January 2022

The Cryosphere Discussions

considered. The choice of the representative precipitation distribution which is scaled may be accompanied by an uncertainty of up to 15%.

BESSI does not use sub-daily parameterizations for the daily cycle, which could reduce the effect of small amounts of snow falling every day and the accompanied albedo overestimation while using climatological forcing if considered. Though small amounts of precipitation every day are physical not reasonable for the region and it has to be considered in the snow models. BESSI showed a positive SMB bias in general relative to other snow-models, we cannot state how big the mentioned effects are for the other SMB models (Fettweis et al., 2020b).

We did not try to adjust climatological fields for temperature, or the other forcing variables. Due to the event based nature of the precipitation this has the biggest impact, but daily climatologies overestimate the SMB also due to the other variables too. The effect of the non-linearity alone has been previously studied with the model (Born et al., 2019). We furthermore did not study the impact of precipitation distributions on the point scale.

5 Conclusions

A surface mass and energy balance model was run for up to 500 years with different climate forcing. They all share the same climatology in the five forcing variables, atmospheric temperature, precipitation, long and short-wave radiation, and humidity. While different frequencies of climate variability have very little impact (< 5 %), using an average climate leads to a drastic overestimation (40 %) of the surface mass balance. This is mainly observed around the melt region of the Greenland ice sheet. The biggest contribution to this overestimation is the precipitation forcing (≈30 %), due to the resulting albedo increase. Averaging multiple years to obtain a climatology produces a data set with frequent light precipitation, and a high surface albedo due to the continuous presence of fresh snow. Small amounts of snowfall are not physically reasonable for a region with event based precipitation like Greenland.

To overcome the problem we calculated alternative precipitation climatologies to be used together with daily climatologies of the other variables. Monthly averages following a natural sub-monthly distribution lead to the smallest errors. Though, there is a dependency on the chosen distribution. Using a regular frequency is not feasible as there is a large spatial dependency and empirical relations may change through time periods. We conclude that the surface mass balance model is best forced with transient climate. If daily climatologies with an altered precipitation forcing are used an overestimation of 15-25 % of the SMB should be assumed.

Code availability. The BESSI model code is available on git-hub (https://github.com/TobiasZo/BESSI)

Author contributions. TZ conducted the model tuning and ensemble simulations, the data analysis and wrote the main part of the manuscript. AB contributed to the study design, and the manuscript.

https://doi.org/10.5194/tc-2021-379
Preprint. Discussion started: 18 January 2022

The Cryosphere Discussions
Open Access
EGU

Table A1. The simulations done for this study.

	Years	78 y	156 y	234 y	468 y	# of simulations
ERA-interim	B-FWD	1	1	1	1	4
	F-BWD	1	1	1	1	4
	FWD	1	1	1	1	4
	BWD	1	1	1	1	4
temperature ordered, 6 frequencies	B-FWD	6	6	6	6	24
	F-BWD	6	6	6	6	24
	FWD	6	6	6	6	24
	BWD	6	6	6	6	24
Point wise temperature ordered, 6 frequencies	B-FWD				6	6
	F-BWD				6	6
	FWD				6	6
	BWD				6	6
Daily climatological forcing		1	1	1	1	4
Mixed forcing, 1 climatological variable	T, P, SW, LW, DewP				5	5
Mixed forcing, 1 transient variable	T, P, SW, LW, DewP				5	5
Other precipitation climatologies	Sub-monthly natural				39	39
	Regular 2,4,8,15,30				5	5
	mixed				3	3
						197

Competing interests. The authors declare that they have no conflict of interest.

https://doi.org/10.5194/tc-2021-379
Preprint. Discussion started: 18 January 2022

The Cryosphere Discussions
Open Access
EGU

References

Alvarez Solas, J., Banderas, R., Robinson, A., and Montoya, M.: A new approach for simulating the paleo-evolution of the Northern Hemisphere ice sheets, Geoscientific model development, 11, 2299–2314, 2018.

Aschwanden, A., Fahnestock, M. A., Truffer, M., Brinkerhoff, D. J., Hock, R., Khroulev, C., Mottram, R., and Khan, S. A.: Contribution of the Greenland Ice Sheet to sea-level over the next millennium, Science Advances, https://doi.org/10.1126/sciadv.aav9396, 2019.

Berrisford, P., Dee, D., Poli, P., Brugge, R., Fielding, K., Fuentes, M., Kallberg, P., Kobayashi, S., Uppala, S., and Simmons, A.: The ERA-Interim archive, version 2.0, 2011.

Beyer, R., Krapp, M., and Manica, A.: A systematic comparison of bias correction methods for paleoclimate simulations, Clim. Past Discuss, 11, 1–23, 2019.

Born, A., Imhof, M. A., and Stocker, T. F.: An efficient surface energy–mass balance model for snow and ice, The Cryosphere, 13, 1529–1546, https://doi.org/10.5194/tc-13-1529-2019, https://tc.copernicus.org/articles/13/1529/2019/, 2019.

Fettweis, X., Box, J. E., Agosta, C., Amory, C., Kittel, C., Lang, C., van As, D., Machguth, H., and Gallée, H.: Reconstructions of the 1900–2015 Greenland ice sheet surface mass balance using the regional climate MAR model, The Cryosphere, 11, 1015–1033, 2017.

Fettweis, X., Hofer, S., Krebs-Kanzow, U., Amory, C., Aoki, T., Berends, C. J., Born, A., Box, J. E., Delhasse, A., Fujita, K., Gierz, P., Goelzer, H., Hanna, E., Hashimoto, A., Huybrechts, P., Kapsch, M.-L., King, M. D., Kittel, C., Lang, C., Langen, P. L., Lenaerts, J. T. M., Liston, G. E., Lohmann, G., Mernild, S. H., Mikolajewicz, U., Modali, K., Mottram, R. H., Niwano, M., Noël, B., Ryan, J. C., Smith, A., Streffing, J., Tedesco, M., van de Berg, W. J., van den Broeke, M., van de Wal, R. S. W., van Kampenhout, L., Wilton, D., Wouters, B., Ziemen, F., and Zolles, T.: GrSMBMIP: intercomparison of the modelled 1980–2012 surface mass balance over the Greenland Ice Sheet, The Cryosphere, 14, 3935–3958, https://doi.org/10.5194/tc-14-3935-2020, https://tc.copernicus.org/articles/14/3935/2020/, 2020a.

Fettweis, X., Hofer, S., Krebs-Kanzow, U., Amory, C., Aoki, T., Berends, C. J., Born, A., Box, J. E., Delhasse, A., Fujita, K., et al.: GrSMBMIP: Intercomparison of the modelled 1980–2012 surface mass balance over the Greenland Ice sheet, The Cryosphere, 14, 3935–3958, 2020b.

Forsström, P.-L. and Greve, R.: Simulation of the Eurasian ice sheet dynamics during the last glaciation, Global and Planetary Change, 42, 59–81, 2004.

Hanna, E., Cappelen, J., Fettweis, X., Mernild, S. H., Mote, T. L., Mottram, R., Steffen, K., Ballinger, T. J., and Hall, R. J.: Greenland surface air temperature changes from 1981 to 2019 and implications for ice-sheet melt and mass-balance change, International Journal of Climatology, 41, E1336–E1352, 2021.

Holube, K. M., Zolles, T., and Born, A.: Sources of Uncertainty in Greenland Surface Mass Balance in the 21 st century, The Cryosphere Discussions, pp. 1–27, 2021.

Madsen, M. V., Steen-Larsen, H. C., Hörhold, M., Box, J., Berben, S. M. P., Capron, E., Faber, A.-K., Hubbard, A., Jensen, M. F., Jones, T., et al.: Evidence of isotopic fractionation during vapor exchange between the atmosphere and the snow surface in Greenland, Journal of Geophysical Research: Atmospheres, 124, 2932–2945, 2019.

Mikkelsen, T. B., Grinsted, A., and Ditlevsen, P.: Influence of temperature fluctuations on equilibrium ice sheet volume, The Cryosphere, 12, 39–47, https://doi.org/10.5194/tc-12-39-2018, https://tc.copernicus.org/articles/12/39/2018/, 2018.

Mosley-Thompson, E., Readinger, C., Craigmile, P., Thompson, L., and Calder, C.: Regional sensitivity of Greenland precipitation to NAO variability, Geophysical Research Letters, 32, 2005.

https://doi.org/10.5194/tc-2021-379
Preprint. Discussion started: 18 January 2022

The Cryosphere Discussions
Open Access
EGU

Noël, B., Berg, W. J. v. d., Wessem, J., Meijgaard, E. v., As, D. v., Lenaerts, J., Lhermitte, S., Kuipers Munneke, P., Smeets, C., Ulft, L. H. v., et al.: Modelling the climate and surface mass balance of polar ice sheets using RACMO2–Part 1: Greenland (1958–2016), The Cryosphere, 12, 811–831, 2018.

O'Neill, B. C., Tebaldi, C., Vuuren, D. P. v., Eyring, V., Friedlingstein, P., Hurtt, G., Knutti, R., Kriegler, E., Lamarque, J.-F., Lowe, J., et al.: The scenario model intercomparison project (ScenarioMIP) for CMIP6, Geoscientific Model Development, 9, 3461–3482, 2016.

Robinson, A., Calov, R., and Ganopolski, A.: Greenland ice sheet model parameters constrained using simulations of the Eemian Interglacial, Climate of the Past, 7, 381–396, https://doi.org/10.5194/cp-7-381-2011, 2011.

Semenov, M. A.: Simulation of extreme weather events by a stochastic weather generator, Climate Research, 35, 203–212, 2008.

Sodemann, H., Schwierz, C., and Wernli, H.: Interannual variability of Greenland winter precipitation sources: Lagrangian moisture diagnostic and North Atlantic Oscillation influence, Journal of Geophysical Research: Atmospheres, 113, 2008.

Uppala, S. M., Healy, S. B., Balmaseda, M. A., de Rosnay, P., Isaksen, L., van de Berg, L., Geer, A. J., McNally, A. P., Matricardi, M., Haimberger, L., Dee, D. P., Dragani, R., Bormann, N., Hersbach, H., Vitart, F., Kobayashi, S., Andrae, U., Beljaars, A. C. M., Poli, P., Monge-Sanz, B. M., Peubey, C., Thépaut, J.-N., Delsol, C., Hólm, E. V., Simmons, A. J., Köhler, M., Bechtold, P., Berrisford, P., Balsamo, G., Park, B.-K., Fuentes, M., Bidlot, J., Bauer, P., Tavolato, C., Kållberg, P., and Morcrette, J.-J.: The ERA-Interim reanalysis: configuration and performance of the data assimilation system, Quarterly Journal of the Royal Meteorological Society, 137, 553–597, https://doi.org/10.1002/qj.828, 2011.

Van de Berg, J., van de Wal, R., and Oerlemans, H.: A mass balance model for the Eurasian Ice Sheet for the last 120,000 years, Global and Planetary Change, 61, 194–208, https://doi.org/10.1016/j.gloplacha.2007.08.015, 2008.

Van den Broeke, M., Smeets, C., and Van de Wal, R.: The seasonal cycle and interannual variability of surface energy balance and melt in the ablation zone of the west Greenland ice sheet, The Cryosphere, 5, 377–390, 2011.

van Meijgaard, E., Van Ulft, L., Van de Berg, W., Bosveld, F., Van den Hurk, B., Lenderink, G., and Siebesma, A.: The KNMI regional atmospheric climate model RACMO, version 2.1, KNMI De Bilt, Netherlands, 2008.

Verdin, A., Rajagopalan, B., Kleiber, W., Podestá, G., and Bert, F.: A conditional stochastic weather generator for seasonal to multi-decadal simulations, Journal of Hydrology, 556, 835–846, 2018.

Zolles, T. and Born, A.: Sensitivity of the Greenland surface mass and energy balance to uncertainties in key model parameters, The Cryosphere, 15, 2917–2938, 2021.

Sources of uncertainty in Greenland surface mass balance in the 21st century

Katharina M. Holube, Tobias Zolles and Andreas Born
Department of Earth Science, University of Bergen, Bergen, Norway.
Bjerknes Centre of Climate Research, Bergen, Norway.
The Cryosphere, 16, 315–331, 2022
doi: doi.org/10.5194/tc-16-315-2022

III

The Cryosphere, 16, 315–331, 2022
https://doi.org/10.5194/tc-16-315-2022

The Cryosphere Open Access EGU

Sources of uncertainty in Greenland surface mass balance in the 21st century

Katharina M. Holube[1,a], **Tobias Zolles**[1,2], **and Andreas Born**[1,2]

[1]Department of Earth Science, University of Bergen, Bergen, Norway
[2]Bjerknes Centre for Climate Research, University of Bergen, Bergen, Norway
[a]now at: Meteorological Institute, Universität Hamburg, Hamburg, Germany

Correspondence: Andreas Born (andreas.born@uib.no)

Received: 26 April 2021 – Discussion started: 18 May 2021
Revised: 1 November 2021 – Accepted: 10 November 2021 – Published: 25 January 2022

Abstract. The surface mass balance (SMB) of the Greenland ice sheet is subject to considerable uncertainties that complicate predictions of sea level rise caused by climate change. We examine the SMB of the Greenland ice sheet in the 21st century with the Ber*g*e*n* Snow Simulator (BESSI) surface energy and mass balance model. To estimate the uncertainty of the SMB, we conduct simulations for four greenhouse gas emission scenarios using the output of a wide range of Earth system models (ESMs) from the sixth phase of the Coupled Model Intercomparison Project (CMIP6) to force BESSI. In addition, the uncertainty of the SMB simulation is estimated by using 16 different parameter sets in our SMB model. The median SMB across ESMs and parameter sets, integrated over the ice sheet, decreases over time for every emission scenario. As expected, the decrease in SMB is stronger for higher greenhouse gas emissions. The regional distribution of the resulting SMB shows the most substantial SMB decrease in western Greenland for all ESMs, whereas the differences between the ESMs are most pronounced in the north and around the equilibrium line. Temperature and precipitation are the input variables of the snow model that have the largest influence on the SMB and the largest differences between ESMs. In our ensemble, the range of uncertainty in the SMB is greater than in previous studies that used fewer ESMs as forcing. An analysis of the different sources of uncertainty shows that the uncertainty caused by the different ESMs for a given scenario is larger than the uncertainty caused by the climate scenarios. In comparison, the uncertainty caused by the snow model parameters is negligible, leaving the uncertainty of the ESMs as the main reason for SMB uncertainty.

1 Introduction

The Greenland ice sheet (GrIS) currently experiences a net mass loss through changes in surface mass balance (SMB) and dynamical processes such as solid ice discharge. In 2005–2017, the GrIS contributed almost as much to sea level rise as all glaciers worldwide (Sasgen et al., 2020). There is substantial uncertainty in the magnitude of sea level rise that will be caused by the GrIS in the future (Goelzer et al., 2020). According to Slater et al. (2020), the contribution of melt to sea level rise in 2007–2017 exceeded the highest estimates of the IPCC Fifth Assessment Report sea level predictions, whereas for dynamic ice loss the lower or middle estimates were met. The influence of SMB on the total mass loss becomes more important in the future because outlet glaciers will retreat above sea level (Fettweis et al., 2013). The uncertainty in ice discharge is not as substantial as the uncertainties of climate projections and in SMB (Aschwanden et al., 2019).

SMB simulations are subject to uncertainty from multiple sources, such as the spatial resolution of the ice sheet model, the parametrization of processes like melt–albedo feedback and the forcing of the SMB model (Goelzer et al., 2013). The latter can be separated into the uncertainty about the radiative forcing pathway (hereafter, climate scenario), and the climate projection uncertainty, which can be assessed with projections of different Earth system models (ESMs), although their similarities limit the validity of this approach (Knutti et al., 2013). The influence of climate projection uncertainty on the SMB of the GrIS has been simulated with SMB models of different complexities. Positive degree-day

(PDD) models apply an empirical relationship between melt and temperature. Several ESMs from the third generation of the Coupled Model Intercomparison Project (CMIP3) have been used to force an ice sheet model in which the SMB is calculated by the PDD method (Graversen et al., 2011). Yan et al. (2014) employed another ice sheet model that also uses the PDD method for the SMB calculations and forced it with CMIP5 ESMs. However, PDD models are calibrated to match the present state of the climate and so their validity in a warming climate is limited (Vizcaino, 2014). This is less of a concern in regional climate models (RCMs) coupled with a snow model where many physical processes are resolved. These are used to downscale ESM simulations, which often do not have the spatial resolution needed to simulate the SMB with sufficient accuracy. However, RCMs are expensive, limiting their use to downscaling only a few ESMs (Fettweis et al., 2008; Franco et al., 2011; Fettweis et al., 2013; Hanna et al., 2020). Fettweis et al. (2008) utilized RCM simulations forced with a subset of CMIP3 simulations and performed a multilinear regression for the SMB changes as a function of temperature and precipitation to calculate the SMB changes for CMIP3 models not used as forcing. For CMIP6, Hanna et al. (2020) simulated the SMB of Greenland using the output of five ESMs. Hofer et al. (2020) showed that the predicted climate from these representatively selected ESMs leads to a larger GrIS SMB decrease in CMIP6 than in CMIP5. While their results already include some variability between ESMs, their selection from the CMIP6 model pool is necessarily incomplete, and the relative importance of climate simulation as compared with other sources of uncertainty remains unclear.

We address some of those open questions in this study with the surface energy and mass balance model Berg*e*n Snow Simulator (BESSI) (Born et al., 2019; Zolles and Born, 2021), which simulates energy exchange processes at the snow or ice surface and is therefore more physically correct than PDD models, while requiring fewer computational resources than RCMs. To assess the uncertainty of the radiative forcing, we consider four climate scenarios that lead to different extents of climate change. We simulate the SMB for these climate scenarios using the output of 26 ESMs from CMIP6 to take into account the uncertainty of climate projections. To estimate the uncertainty of the parametrization, we conduct all simulations with 16 sets of parameters for BESSI (Born et al., 2019; Zolles and Born, 2021). While this approach cannot substitute a comparison of different SMB models as in Fettweis et al. (2020), it enables us to assess the relative importance of climate- and snow-related parameters in a coherent framework. We compare the different uncertainties and study spatial variations in the simulated SMB and the importance of the different input variables in different parts of Greenland (Sect. 3) after a description of our methods (Sect. 2). Finally, we compare our results to previous studies (Sect. 4).

2 Methods

2.1 Snow model

The Berg*e*n Snow Simulator (BESSI) (Born et al., 2019; Zolles and Born, 2021) is a surface energy and mass balance model for glaciated regions with a flexible spatial domain. In this study, the domain is Greenland with an equidistant resolution of 10 km. The topography of the ice sheet is based on ETOPO1 (Amante and Eakins, 2009) and remains fixed throughout the simulations. The vertical dimension consists of up to 15 snow or firn layers that are adjusted by splitting or merging layers depending on the snow mass in each grid cell (Born et al., 2019; Zolles and Born, 2021). The five daily input variables are air temperature and dew point at 2 m above ground, the amount of precipitation, and surface downwelling shortwave and longwave radiation. The top layer changes its mass and energy according to the forcing of the input variables. Precipitation falls as snow when the air temperature is below 0 °C and as rain otherwise. Meltwater percolates down into deeper layers and refreezes. Horizontal exchanges of mass or energy are deemed negligible on the 10 km grid. When there is no more snow left to melt, the excess energy is used to melt ice. Corrections are made when the melt exceeds the existing amount of ice (Appendix A). For a detailed description of the snow model, see Born et al. (2019) and Zolles and Born (2021). The performance of BESSI has been compared with other SMB models in Fettweis et al. (2020). Although snowfall and runoff are lower in BESSI than in other SMB models, the SMB and its trend are consistent with most other studied models because both biases cancel each other out.

BESSI uses parameterizations of several physical processes. In this study, we vary the albedo and turbulent heat exchange parameters (Table C1), which contribute to the parameter uncertainty discussed below. The albedo changes caused by ageing of the snow are parameterized depending on temperature, whereas the ageing is accelerated at 0 °C depending on the liquid water content (Bougamont et al., 2005; Zolles and Born, 2021). Thus, the albedo of the snow can take values between the prescribed albedos of fresh snow and firn. Ice is assigned a separate albedo. The turbulent sensible heat flux depends on the difference between air and surface temperature, and on the turbulent heat exchange coefficient, which is a model parameter describing both changes in wind speed and efficiency of the turbulent exchange (Zolles and Born, 2021).

The model parameters of BESSI are calibrated to the RACMO SMB (Noël et al., 2016). Here, we use an ensemble of equally plausible model parameter settings based on a multivariate calibration (Zolles et al., 2019). For the calibration, BESSI was run for 500 years with ERA-Interim (Dee et al., 2011) as forcing data using different parameter combinations. The performance of the simulation is compared to the RACMO SMB over the period 1979–2017 on an annual ba-

sis. We are using seven measures of goodness of fit, based on the bias, the mean absolute deviation (MAD), and the root-mean-square error (RMSE) of the SMB. The bias is the difference between the ice-sheet-wide integrated SMB between RACMO and BESSI, while we calculate three representations of RMSE and MAD. The first calculates the Greenland-wide SMB and its temporal MAD over the years, the second calculates a temporal MAD for each grid point and averages them over all grid points, with the third and final being the MAD over all points in space and time. A similar approach is used for the RMSE. In total we are using seven objective functions for the multivariate optimization. We evaluate the performance of BESSI relative to all the objective functions. In a non-ideal world not all objectives can be minimized simultaneously. This yields multiple equally plausible optimal solutions, where one objective function can not be improved without compromising another. The ensemble of these optimal solutions is referred to as Pareto optimal set. Similar to the method used by Zolles et al. (2019), we calculate the Pareto optimal set. This yields a total of 16 different solutions whose parameter ranges are given in Table C1.

2.2 Earth system models

We use ESM output of CMIP6 for the period of 2015–2100 (Eyring et al., 2016). The Tier 1 scenarios (with increasing radiative forcing: SSP126, SSP245, SSP370, and SSP585) from ScenarioMIP are selected for this study because they encompass a wide range of future forcing possibilities (O'Neill et al., 2016) and are available for many different ESMs. We selected 26 ESMs that provide all of BESSI's input variables for at least two scenarios (Appendix Table B1), with the exception of the dew point, which is calculated from the relative humidity if necessary.

The input variables are interpolated linearly to the 10 km BESSI grid. ESM biases are calculated based on the delta method (Beyer et al., 2020) by comparing the daily mean of the historical simulation and the daily mean of the ERA-Interim reanalysis in the period of 1979–2014, in which both datasets are available. For all input variables except precipitation, the differences between the daily means are subtracted from the future projection. These differences also include discrepancies in topography, so the dependence of, for example, temperature on elevation is accounted for in the additive bias correction. As mentioned in Sect. 2.1, BESSI uses ETOPO1 and accounts for the differences with the ERA-Interim topography by performing a correction with a constant moist adiabatic lapse rate. Precipitation is bias corrected by the ratio of ERA-Interim and historical mean precipitation because its high variability would lead to negative values if the difference was used. During the winter, shortwave radiation may be very weak so that the bias correction can lead to localized, small negative values. These values are set to zero. The daily means of precipitation are affected by individual intense precipitation events due to the short length of

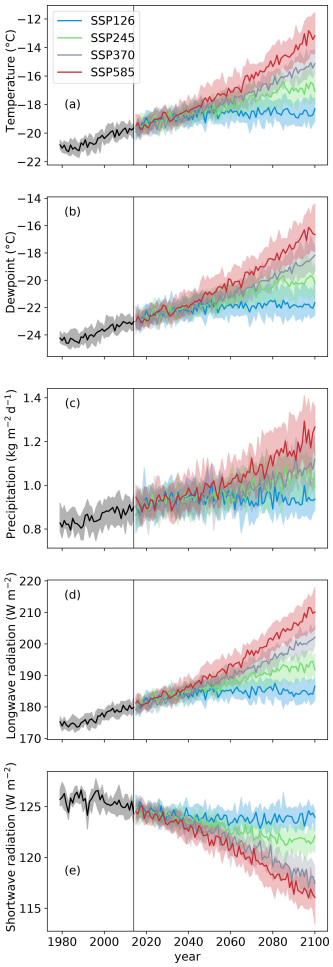

Figure 1. Input variables for BESSI, which are interpolated and bias-corrected ESM data, for different scenarios, averaged over the Greenland ice sheet. The solid line is the median over all ESMs for one scenario, and the shaded area between the 25 % and 75 % percentiles represents half of the ESMs. **(a)** Temperature at 2 m above ground. **(b)** Dew point at 2 m above ground. **(c)** Amount of precipitation. **(d)** Surface downwelling longwave radiation. **(e)** Surface downwelling shortwave radiation. The vertical line indicates the boundary between the common time period of the historical ESM simulations and ERA-Interim (1979–2014) and the future projection time period (from 2015). Please note that the precipitation unit, 1 kg m^{-2} d^{-1}, equals 1 mm (w.e.) per day; w.e. stands for water equivalent.

the historical period. The monthly biases are less affected by these events, and therefore we multiply the projected precipitation with the ratio of the monthly mean precipitation of the historical reference and the reanalysis data to perform bias correction instead of the daily means.

Throughout the 21st century, the median air temperature over all ESMs rises in every scenario except in the scenario with the smallest increase in greenhouse gases (SSP126), where it remains almost constant during the second half of the century (Fig. 1a). While shortwave radiation decreases slightly, precipitation, longwave radiation, and dew point increase over the course of the century (Fig. 1b–e). The stronger the greenhouse gas forcing, the larger the change in these variables. For each variable except precipitation, there are distinct differences in ESM medians between all scenarios at the end of the century, and the differences between scenarios are of similar magnitude to the interquartile ranges. The trends in precipitation are weaker compared to the ranges of values between the ESMs.

2.3 Simulations and ensemble design

We conduct two different kinds of SMB simulations. (i) In the main ensemble, the forcing data for four climate scenarios are taken from different ESMs, and the snow model parameters are varied. It illustrates the temporal and spatial behaviour of the SMB and it enables us to separate the different uncertainty components. (ii) The "single-forcing" ensemble shows the influence of the individual input variables.

The main ensemble uses 96 selected ESM–scenario combinations (Table B1). In addition, we conduct 26 simulations for the historical reference period (1979–2014), i.e. one for each ESM. Each of the simulations is conducted with 16 different snow model parameter sets, resulting in 1952 simulations. The selection process of the parameter combinations is described in Sect. 2.1. The firn cover is initialized by forcing BESSI with ERA-Interim reanalysis data for 540 years, to reach a dynamically and thermodynamically stable firn cover at the year 2014. The long response time of the firn cover requires an initialization period of several hundred years, which is realized by forcing the model with the ERA-Interim data 15 times back and forth (Zolles and Born, 2021). For the historical time period, the initialization ends in 1979 after 14 ERA-Interim cycles back and forth. For every parameter set, the same initialized firn cover is used to save computation time, but the bias caused by this inconsistency is generally overcompensated after a few years of climate forcing.

In the single-forcing simulations, the transient ESM simulations are used as input for only one variable, and the daily ERA-Interim climatology is used for the others to assess the influence of each variable on the SMB. The scenario SSP585 is chosen because it is available for all 26 ESMs, and we used the snow model parameter set that produces the best results in the calibration with RACMO (Sect. 2.1). For precipitation, the daily ERA-Interim climatology cannot be used as it overestimates the surface albedo due to unrealistic small amounts of snowfall every day (Sodemann et al., 2008). This leads to an overestimation of the mass balance of up to 40 % (Zolles and Born, 2022). Instead we use the monthly precipitation climatology and distribute the ERA-Interim monthly average $P^{\mathrm{m}}_{\mathrm{ERAi}}$ following the temporal distribution of precipitation in the ESM simulation:

$$P^{\mathrm{d}}_{\mathrm{year,\,clim}} = \frac{P^{\mathrm{d}}_{\mathrm{year}} \cdot P^{\mathrm{m}}_{\mathrm{ERAi}}}{P^{\mathrm{m}}_{\mathrm{year,\,model}}}, \tag{1}$$

where P stands for precipitation, "m" stands for monthly mean, "d" stands for daily mean, and year stands for the point in time of the simulation. Therefore, the climatological daily precipitation distribution differs for each ESM, but the monthly averages are identical. For each of the 26 ESMs, we conducted six simulations for the SMB: a reference simulation with the historical climatology and five simulations with different transient variables (air and dew point temperature, precipitation, shortwave and longwave radiation). We need a separate reference simulation for each ESM because the precipitation distribution differs for each ESM according to Eq. (1).

3 Results

3.1 Scenario surface mass balance simulations

In this section, we show temporal and spatial differences between the ESMs and climate scenarios of the median SMB over all parameter combinations. The median SMB at the end of the century over the ESMs and snow model parameters is shown for the different climate scenarios in Table 1. The surface mass balance decreases relative to the historical simulations in all scenarios (Fig. 2). In the moderate scenario SSP126, the SMB is relatively stable to the end of the century. Higher emissions of greenhouse gases (stronger forcing) lead to a lower SMB (SSP245, SSP370, SSP585). With stronger warming, the range in simulated SMB for different ESMs increases, although the range in input variables except precipitation does not seem to depend on the scenario (Fig. 1). For precipitation, the interquartile range between the ESMs increases only slightly with stronger greenhouse gas forcing. Precipitation variability alone cannot explain the larger interquartile range in SMB in the warmer scenarios. The reason for the increasingly dissimilar SMBs with stronger greenhouse gas forcing is that larger changes in the input variables have a larger cumulative effect on the SMB (Sect. 3.3).

When BESSI is forced with ERA-Interim data (Fig. 2, orange), a relatively low SMB in the early 21st century is apparent. This correlates with more frequent Greenland blocking (Sasgen et al., 2020). A similar reduction in SMB is not observed when forcing BESSI with historical ESM data

Table 1. Median and quartiles over all ESM and snow model parameter combinations of the 2091–2100 SMB mean value for different scenarios.

Scenario	Historical	SSP126	SSP245	SSP370	SSP585
Median SMB (1979–2014 or 2091–2100)/Gt yr^{-1}	399	318	254	42	−226
75 % quantile SMB/Gt yr^{-1}	415	384	308	194	−1
25 % quantile SMB/Gt yr^{-1}	378	257	104	−308	−623

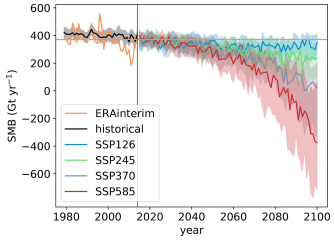

Figure 2. Surface mass balance simulations forced with ERA-Interim reanalysis data, historical ESM simulations, and scenario climate simulations, given as the median over the SMB for all snow model parameter combinations. The solid line is the median of all ESMs, and the shading shows the 25 % and 75 % percentiles. Orange represents SMB forced with ERA-Interim, and the horizontal line is its mean value.

(Fig. 2, black) because the coarse horizontal resolution hampers the representation of the observed blocking and its increased activity (Davini and D'Andrea, 2020).

Spatial anomalies for the last decade of the SMB in the low-emission scenario SSP126 and the high-emission scenario SSP585 are shown in Fig. 3. In the west of Greenland, the SMB in the 2090s is lower than in ERA-Interim (1979–2014), independent of the scenario (Fig. 3a and b). In this region, higher temperatures lead to increased melt. In the centre of the ice sheet, the SMB is slightly higher than in ERA-Interim, especially in the southeast. There, heavier precipitation occurs under a warmer climate. However, the SMB increase in the centre is outweighed by the SMB decrease at the margin of the ice sheet. These SMB changes are much more pronounced in the high-end scenario SSP585 because of the enhanced change in the input variables. Currently observed SMB changes are dominated by amplified melting in the west and by snowfall in the east (Sasgen et al., 2020). In the north, the temperatures are too low for much melt at the present day, but with an average increase of temperature over the ice sheet of approximately 6 K in SSP585 (Fig. 1a), melt increases considerably there.

At the margin of the ice sheet, the standard deviation of the SMB between the ESMs is largest (Fig. 3c and d). The relative standard deviation of the SMB reaches the highest values near the equilibrium line (Fig. 3e and f), and thus the choice of ESM is decisive for the SMB in this region. In the high-emission scenario SSP585, the equilibrium line is subject to substantial uncertainty, which is greater than in the moderate scenario SSP126 (Fig. 4). Equilibrium line changes show that the differences between ESMs driven by the same scenario increase with stronger greenhouse gas forcing (Fig. 2).

3.2 Estimation of uncertainties

Having examined the spatial variations between ESMs, we next study the variance of the full ensemble containing ESMs, emission scenarios and snow model parameters. We split the variance in spatially integrated SMB over all simulations into four different components using a method based on Hawkins and Sutton (2009) and described in more detail in Appendix C: a fourth degree polynomial fit is applied to the decadal running mean of spatially integrated SMB for each individual simulation to separate trends from variations on small timescales. The residuals of the fits are considered the internal variability of the system, for example fluctuations in SMB caused by alternating dry and wet periods. The law of total variance is applied to the whole ensemble of polynomials to split the total variance into three independent components for each year. These components are the variances caused by ESMs, climate scenarios, and BESSI parameters (albedo of fresh snow and firn, turbulent heat exchange coefficient). These variances quantify three relevant sources of uncertainty, with internal variability being the fourth.

The sum of the different uncertainty components increases strongly over the course of the century (Fig. 5a). The relative contributions of the different uncertainty components are shown in Fig. 5b by normalizing with the sum of all components. In the first years of the simulations, the internal variability is the largest source of uncertainty, showing that it is most important in the absence of external forcing. While the scenario uncertainty has the smallest contribution in the beginning, its importance increases in the second half of the century, as decarbonization measures and the adaption of the climate system take time (Davy and Outten, 2020). The parameter uncertainty is slightly larger than the scenario uncertainty at first, but its relative importance decreases over time. Its overall small contribution to uncertainty indicates that the results of our SMB simulations are almost independent of the specific parameter combination of BESSI. The parameter uncertainty does not depict the total snow model uncertainty because the approach to calculate the SMB is the same re-

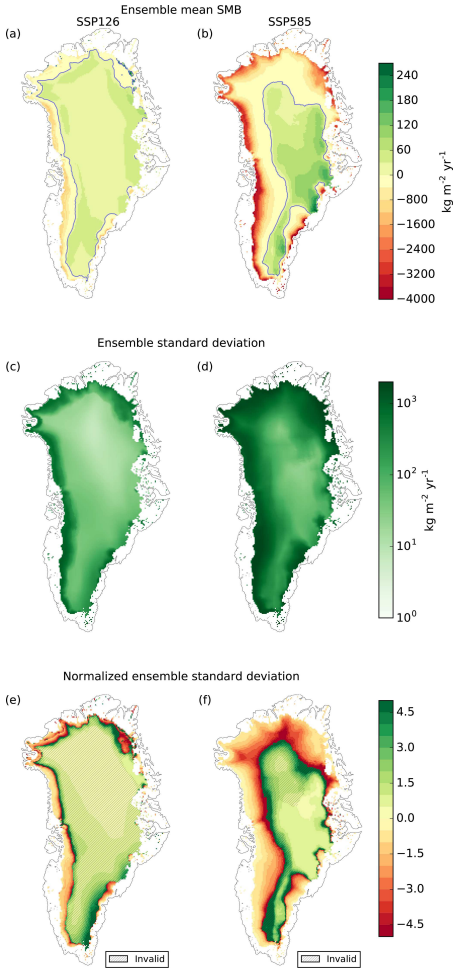

Figure 3. Anomaly of the median SMB over all parameter combinations (2090–2099 mean) with respect to ERA-Interim (1979–2014 mean) **(a, b)** with standard deviation **(c, d)** and relative standard deviation **(e, f)** for the scenarios SSP126 **(a, c, e)** and SSP585 **(b, d, f)**. **(a, b)** The contour line indicates a mass balance of zero. Note the different scales for positive and negative values. **(e, f)** In the shaded area, the absolute value of the surface mass balance is smaller than $50\,\mathrm{kg\,m^{-2}}$, which is considered to be close to zero, and thus the relative standard deviations are invalid.

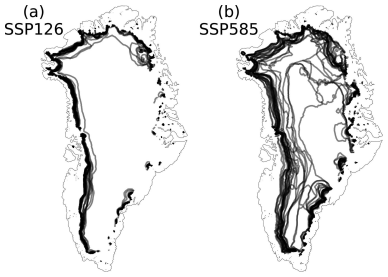

Figure 4. Equilibrium lines of the median SMB over all parameter combinations (temporal mean for the period of 2090–2099) for different ESMs and the scenarios SSP126 **(a)** and SSP585 **(b)**.

gardless of the parameter combination, whereas differences in the ESMs are caused by different ways of simulating the processes. The spatial resolution necessarily contributes to the uncertainty in SMB modelling because elevation and associated temperature differences on the sub-grid scale can lead to unrealistically high temperatures prescribed above the ablation zone, reducing the SMB (Goelzer et al., 2013). Furthermore, the calculation of precipitation and runoff is less accurate in BESSI compared to other snow models, and these biases could increase in a warming climate (Fettweis et al., 2020), which is not represented in the parameter uncertainty either.

A few years into the simulation, the ESM uncertainty becomes the largest contributor to the uncertainty and the share of the internal variability decreases rapidly. However, our uncertainty quantification may erroneously attribute a part of the internal variability of the climate simulations to ESM uncertainty (Lehner et al., 2020). In order to estimate this error, we forced BESSI with 10 different realizations of the ESM ACCESS-ESM1-5 (Table B1) and applied the method of Hawkins and Sutton (2009) by replacing the different ESMs with the different realizations of a single ESM. This shows a non-negligible bias in the attribution of the uncertainty in the first decades, up to 35 %, adding a caveat to the relative uncertainties in Fig. 5b for this time period. Note, however, that multiple realizations are available for only about half of the ESMs, and thus we cannot systematically investigate this effect. More importantly for the results of this study, the method bias is small at the end of the century, which means that the ESM uncertainty is robustly shown to be greater than the scenario uncertainty. In other words, in the scenarios with strong forcing, there are some ESMs that induce only small SMB changes, while other ESMs lead to a much stronger SMB decrease. This pronounced uncertainty is larger than the differences between the medians over the ESMs for each scenario. At the end of the century, the ESM uncertainty is about 62 % and the scenario uncertainty is about 35 % of

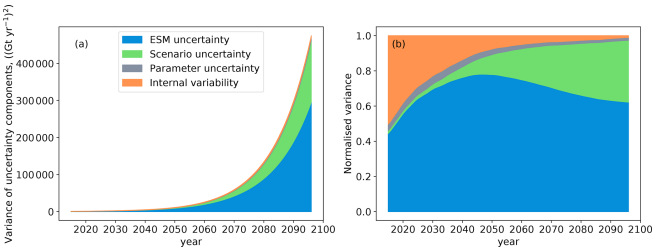

Figure 5. (a) Total and **(b)** relative variances of the different uncertainty components: choice of ESM (blue), different emission scenarios (green), different snow model parameters (grey), and internal variability (orange). The time period does not extend to 2100 because the variance splitting approach is applied to the decadal running means of the yearly SMB.

the total variance, whereas the snow model parameter uncertainty and the internal variability represent about 3 % combined.

The separation of variances can be generalized to every grid cell of the GrIS. The total variance of the 1952 simulations is largest at the margin of the ice sheet, where the SMB changes considerably (Fig. 6a and b). The total variance increases by several orders of magnitude from the middle to the end of the century. At the middle of the century, the ESM uncertainty is the most important component at the margin and in the centre of the ice sheet (Fig. 6c). Only in the north and at higher altitudes in the west is the internal variability at its largest. Compared to the other components, the scenario uncertainty is insignificant at the middle of the century (Fig. 6e). At the end of the century, the scenario uncertainty becomes more pronounced, especially at the western margin, where the amount of melt differs considerably between the scenarios (Fig. 6d). The area where the ESM uncertainty has the largest share increases even more at the end of the century, mainly at the expense of the regions where the internal variability is important at the middle of the century. The scenario uncertainty is of similar magnitude as the ESM uncertainty only at the margins of the ice sheet and in the area where the total variance is low.

3.3 Single-forcing and regional analysis

In the single-forcing simulations, we run the snow model using only one input variable from each CMIP model simulation. This variable is hereafter called the transient variable. For the other variables, daily means of the historical period of ERA-Interim data are used in the simulation, except for precipitation, whose temporal distribution is again adapted as described in Sect. 2.3. We study the influence of the different input variables on the SMB across the entire GrIS and show three regions previously used by Zolles and Born (2021) (Fig. 7). These regions are selected because they illustrate the spatial differences in the behaviour of the SMB.

The SMB increases when precipitation is the transient variable due to an increase in snowfall (Fig. 1c). In the simulation with transient dew point, the SMB also increases through an increase in desublimation, but the effect is smaller. When the downwelling longwave radiation increases, the snow temperature rises, which leads to more melt. The effect of melting caused by increased air temperature is stronger than that of increased longwave radiation except for the east where the SMB change is dominated by precipitation changes. The interquartile range is largest when temperature or precipitation are the transient variables, except for the east where the dew point has a larger interquartile range than the temperature. Consequently, these variables dominate the uncertainty of the SMB simulations. Shortwave radiation alone has a negligible influence on the SMB in the idealized experiments performed. This does not agree with Hofer et al. (2017), who found a link between amplified melt and recent increases in shortwave radiation through shifts in North Atlantic Oscillation and Greenland blocking. However, the ESMs used in this study predict a decrease in shortwave radiation, which could explain the disagreement. In addition, Greenland blocking is not well represented in ESMs (Davini and D'Andrea, 2020).

The sum of all individual changes does not equal the fully transient simulation driven by the SSP585 scenario (Fig. 7). This highlights non-linearities that amplify the SMB reduction. For example, air temperature and precipitation often covary so that the increased precipitation compensates the increased melt only partly. If heavier precipitation delivers more rain, the energy required to refreeze the additional rain in the snowpack increases its heat. We conclude that when air temperature and longwave radiation rise together in a warmer and cloudier future and more energy is available at the surface and due to the non-linearity of the SMB, increased melt is detected than from each of these forcing components individually. The impact of the increasing amount of longwave radiation decreases with rising surface temperature because the net flow of sensible heat depends on the temperature dif-

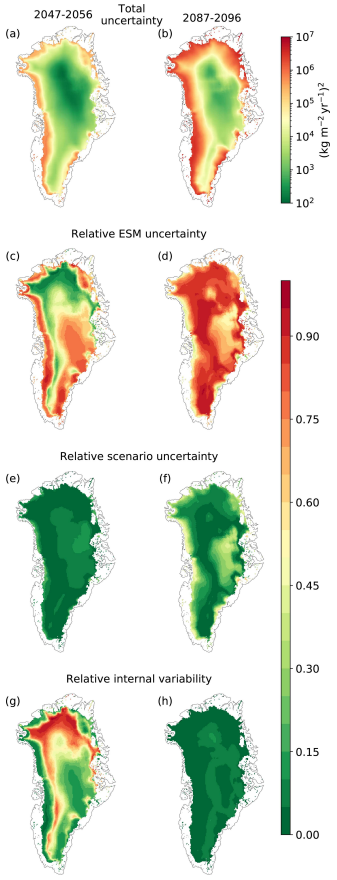

Figure 6. (a, b) Total variance, consisting of ESM uncertainty, scenario uncertainty, snow model parameter uncertainty, and internal variability. **(c, d)** Ratio of ESM uncertainty and sum of the uncertainties. **(e, f)** Ratio of scenario uncertainty and sum of the uncertainties. **(g, h)** Ratio of internal variability and sum of the uncertainties. Panels **(a, c, e, g)** show the mean over the years 2047–2056, panels **(b, d, f, h)** show the mean over the years 2087–2096. The latter is the last decade that the variance splitting approach is valid for because it is applied to the decadal running mean of the yearly SMB. The years 2047–2056 are chosen as a decade in the middle of the 21st century.

ference between air and snow surface. Since the sublimation is driven by the saturation pressure difference between the lower atmosphere and the surface, sublimation increases for a warmer surface and decreases for a higher dew point temperature. In the different ESMs, the SMB reduction is amplified to different extents by the described non-linear effects. Therefore, the interquartile range in the fully transient simulation is larger than the interquartile range in each of the single-forcing simulations.

In the western region, the SMB and its different components follow a similar course as for the entire GrIS, except for the amount of SMB decrease per area, which is in the fully transient simulation about 5 times as high (Fig. 7). Additionally, the internal variability is not as important as in the total GrIS, and the scenario uncertainty is slightly higher (Fig. 8a). This shows a high dependence of surface melt on the climate scenario in this region.

In the northern region, the SMB increases with transient precipitation and transient dew point to the same extent (Fig. 7c). Desublimation and sublimation are important contributors to the SMB in this dry region. This is in line with Box and Steffen (2001), who show that 28 % of the accumulation is caused by desublimation at one station in the northeast at 2113 m above sea level. Even the precipitation increase will not dominate in the north by the end of the century. In the fully transient simulation and in the simulation with transient temperature, the SMB decreases strongly and non-linearly at the end of the century (Fig. 7c, orange line). The decrease in SMB is rather late because of the low temperatures in the north at present day. However, when the temperatures rise high enough, ice can be exposed at the surface, which is not always covered by the scarce snowfall and thus triggers a strong albedo feedback. The uncertainty associated with the choice of ESM has a larger share in the north than across all of Greenland because the temperature differences between ESMs are more pronounced, which suggests discrepancies in the simulated sea ice cover. As a consequence, the scenario uncertainty is reduced (Fig. 8b).

In the east, the SMB with transient precipitation follows the SMB with all variables transient closely, showing that the main cause for SMB changes is the precipitation (Fig. 7d). Fettweis et al. (2013) also found increased precipitation in the east because the reduced sea ice cover leads to a moister atmosphere. The uncertainty ranges between ESMs for transient precipitation and the fully transient simulation are also very similar; therefore, the ESM uncertainty is mostly a precipitation uncertainty. The internal variability has a large contribution to uncertainty (Fig. 8c) because the total uncertainty of all other components is small (not shown). The ESM uncertainty is still the largest component, showing an increase at the end of the century (Fig. 8c) when the fully transient SMB stagnates (Fig. 7d).

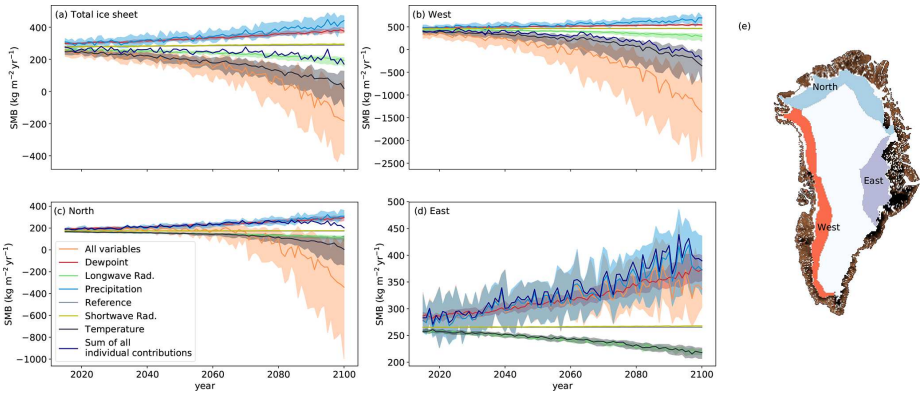

Figure 7. SMB for single-forcing simulations for the entire GrIS **(a)** and selected regions **(b–d)**. The variable named in the legend is transient for scenario SSP585, while all other variables are the ERA-Interim mean. "All variables" indicates that all variables are transient (the same as Fig. 2). "Reference" shows the historical climatology for all variables with precipitation distribution as in CMIP. **(e)** Positions of the selected regions. Regions "north" and "west" are at elevations of 1000–2000 m. The southeast is precipitation driven and the change in SMB with altitude is less developed; therefore, the region "east" is at elevations of 1000–3000 m.

4 Summary and discussion

We simulated the SMB of the GrIS with the snow model BESSI for most of the available climate simulations in the CMIP6 database, using four different climate scenarios and 16 parameter configurations of our snow model. In the high-emission scenario (SSP585), the surface mass loss accelerates and the integrated SMB is about $-230\,\mathrm{Gt\,yr^{-1}}$ at the end of the 21st century, whereas in the low-emission scenario SSP126 the integrated SMB is only slightly lower than in the historical time period and is approximately constant (Table 1, Fig. 2). Taking into account the ice discharge, which amounts to almost $500\,\mathrm{Gt\,yr^{-1}}$ between 2005 and 2019 (Mankoff et al., 2020), our historical simulations result in a negative total mass balance. Assuming an approximately unchanged discharge, the median SMB in all scenarios implies more substantial mass loss in the future.

The regions with the most pronounced changes in SMB are the west and the north of Greenland. In the west, the SMB is already dominated by melt, and in the north additional melt is not fully compensated by the scarce precipitation. In the east, we simulate a higher SMB than at present day because of a warmer and moister climate in future projections. We find that the choice of ESM has the largest overall influence on the uncertainty in SMB projection, exceeding even the variance between climate scenarios. This effect is localized mostly near the equilibrium line and can be primarily attributed to differences in simulated surface air temperature, followed by differences in the simulated precipitation. Note that we did correct the bias for all ESM simulations based on their performance in the period that overlaps with ERA-Interim (1979–2014) but that no further quality control was performed on the CMIP6 simulations. We speculate that a narrower selection of ESMs, e.g. based on their ability to simulate precipitation patterns and frequencies, could lead to a significant reduction in ESM uncertainty.

The results presented here are in good agreement with previous studies. All ice sheet models in Goelzer et al. (2020) simulated an accelerated mass loss with stronger greenhouse forcing. They used the high-end scenario in CMIP5 with a representative concentration pathway (RCP) that leads to a radiative forcing of $8.5\,\mathrm{W\,m^{-2}}$ at the end of the 21st century (RCP8.5), comparable to the SSP585 pathway we used here. Detailed SMB estimates are also available from the regional climate model MAR forced by a selection of CMIP6 ESMs (Hanna et al., 2020). This study also finds the familiar acceleration in mass loss. However, four of the five ESMs used to force MAR have an above-average equilibrium climate sensitivity (ECS, Meehl et al., 2020), and thus temperature changes are probably exacerbated. Comparing our simulations with those of MAR that were forced by the same CMIP6 models, we find that in four out of five cases BESSI simulates a higher SMB than MAR (Fig. 9a). This is plausible because BESSI has a stronger bias to higher SMBs than MAR (Fettweis et al., 2020). Notwithstanding this small disagreement, the primary contribution of our study is not the comparison with more complex models, but the fact that the high numerical efficiency of BESSI enables a more comprehensive analysis of model uncertainty, for example by extending the ESM pool to 26. The difference between the

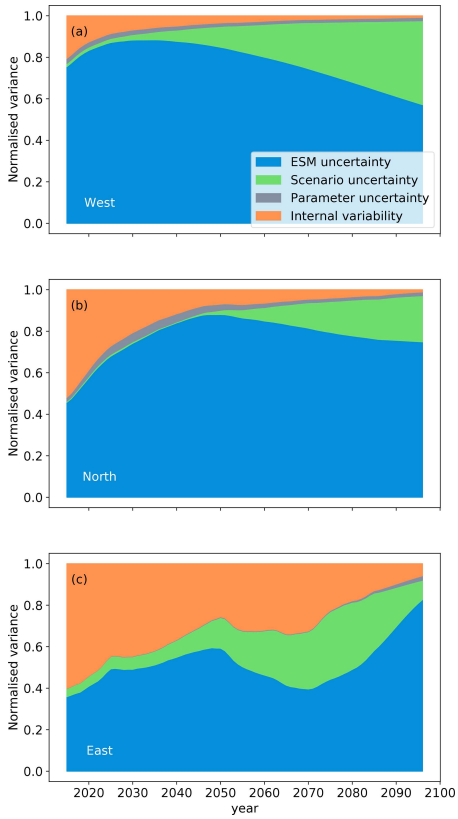

Figure 8. Relative variances of the different uncertainty components for three different regions of the GrIS: uncertainty associated with the choice of ESM (blue), uncertainty caused by different emission scenarios (green), uncertainty of different parameter combinations of the snow model (grey), and internal variability (orange), being the variance of the residues of a fourth-degree polynomial fit to the decadal mean integrated SMB. The calculations are described in Appendix C. The time period does not extend to 2100 because the variance splitting approach is applied to the decadal running means of the yearly SMB.

highest and lowest SMB in the last simulated years in our ensemble is more than 3 times as large as in Hanna et al. (2020) (Fig. 9a).

Similar to our high-emission scenario simulations with BESSI, Fettweis et al. (2013) also find a non-linear SMB decrease in simulations with MAR for the high-end scenario of CMIP5 (RCP8.5) (Fig. 9b). Likewise, the roughly linear trend in the MAR simulations forced by the moderate scenario RCP4.5 is qualitatively analogous to scenario SSP245. The differences between ESMs in the SMB simulations of Fettweis et al. (2013) are comparable to the interquartile range of our study. Another moderate scenario simulation with MAR was performed by Fettweis et al. (2008) for the CMIP3 A1B scenario (Fig. 9b), which is an intermediate scenario with greenhouse gas emissions between those in SSP245 and SSP370 (Fettweis et al., 2008; O'Neill et al., 2016). It also shows an approximately linear decrease in SMB but with a smaller uncertainty range than in our moderate SSP245 scenario simulation with BESSI. The multilinear regression performed in Fettweis et al. (2008), which approximates SMB changes as a linear combination of changes in temperature and precipitation, can reduce the uncertainty, as non-linear effects are not included there. Additionally, the smaller variations between ESMs in CMIP3 compared to CMIP6 can have an effect on the uncertainty of the snow model simulations because of the smaller variability in sensitivity to the carbon dioxide forcing (ECS) (Meehl et al., 2020).

The uncertainty in snow model parameters is negligibly small compared to the other uncertainty components, and thus our results hardly depend on the specific set of parameters in BESSI. However, this does not represent the total uncertainty of SMB modelling, as analysed in Fettweis et al. (2020). To address this question fully, our simulations would have to be repeated with every SMB model of that earlier study. This is not practicable because for some of the SMB models the computational requirements are too high to conduct several hundred simulations. Additionally, even RCMs fail in accurately predicting the snowline in years with much melt, leading to substantial biases in SMB prediction because of the albedo difference between snow and ice (Ryan et al., 2019). We expect a larger bias in BESSI because Fettweis et al. (2020) showed that BESSI underestimates the size of the bare ice area and the ablation zone already today. In addition, the total variance of our ensemble is a conservative approximation because our bias correction reduces the variations between the historical simulations of different ESMs and thus also the variability of the climate projections. Furthermore, our assumption of constant topography leads to a bias in SMB projections in 2100 of approximately 10 % (Vizcaino, 2014). Moreover, our simulations neglect the diurnal cycle, which could underestimate refreezing (Krebs-Kanzow et al., 2021). Finally, Greenland blocking leads to increased melt (Hanna et al., 2020), but ESMs do not seem to simulate the blocking correctly (Davini and D'Andrea, 2020). Therefore, our future SMB projections are conservative because the ESMs do not fully represent the expected increase of Greenland blocking in a warming climate. In spite of these caveats, the substantial difference between the ESM and snow model parameter uncertainties suggests that the ESM uncertainty is the largest source of error in the future projections of the GrIS SMB. This key result has two con-

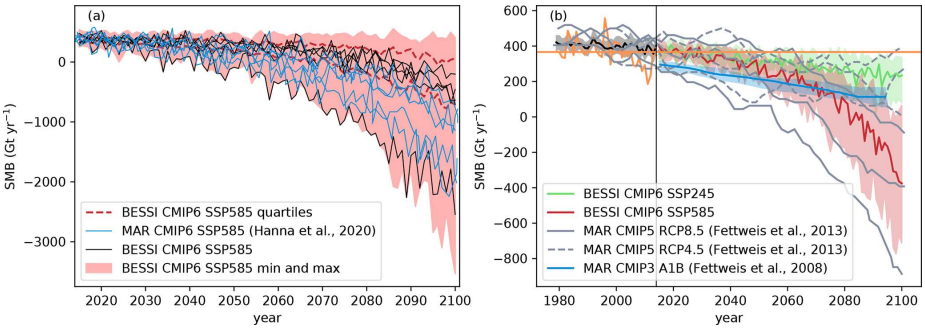

Figure 9. (a) SMB simulated by the regional climate model MAR (blue; Hanna et al., 2020, their Fig. 11) and the mean of our simulations (black), forced by the same CMIP6 models, scenario SSP585. The red shading illustrates the minimum and the maximum of SMB for our entire ensemble for this scenario, and the dashed lines are 25 % and 75 % percentiles. **(b)** Comparison of our simulations with BESSI, Fettweis et al. (2013), their Fig. 4a, and Fettweis et al. (2008), their Fig. 7a. Fettweis et al. (2013) use three different ESMs as input, and thus there are three grey lines for every scenario. The shading are 25 % and 75 % percentiles.

sequences. First, future SMB estimates based on multiple ESMs should explicitly address the quality of the individual simulations in the target region and consider using this skill metric to scale the weight of the individual ensemble members. Second, studies that only include a subset of the plausible climate projections and do not quantify the quality of these selected representations may produce an incomplete picture.

Appendix A: Treatment of melted ice in the snow model results

The snow model calculates the SMB for every grid cell on the land surface of Greenland. In the results, only grid cells that belong to the Greenland ice sheet should be considered. The snow model was tuned with the comprehensive RCM RACMO2.3; therefore, the RACMO-ice mask (Noël et al., 2016) is used to identify the grid cells with ice. In addition, we restrict the analysis to grid cells that have an ice thickness of at least 50 m according to the ice sheet topography used in BESSI, which is based on ETOPO1 (1 arcmin resolution) (Amante and Eakins, 2009). The 50 m threshold is chosen to exclude snow caps.

Because we do not simulate ice dynamics, the ice thickness stays constant throughout the simulations with the snow model. For each time step, BESSI calculates the ice that potentially melts at each grid box, regardless of whether ice is actually present or not. The combination of melt of ice, melt of snow, refreezing, snow, rain and runoff is the mass balance. Therefore, grid cells with thin ice cover can distort the mass balance when melt of ice that has already melted is added to the mass balance. This needs to be corrected.

To determine in which grid cells the ice has melted entirely, we subtract the melted ice from the initial ice topography and also consider the inflow by convergence of the lateral steady-state flux. If the result is negative, which means that more ice has melted than would be possible, the grid cell is not considered in the calculation of the mass balance. The ice thickness dh that is added to each grid cell by ice flux is calculated by the advection equation:

$$\mathrm{d}h = -\nabla \cdot (\boldsymbol{v} \cdot d)\,\mathrm{d}t, \tag{A1}$$

where d is the thickness of the ice in the initial topography and dt is the time step. We use the mean ice velocity $\boldsymbol{v}$ from Nagler et al. (2015) and assume that it is constant. Negative values of dh are treated as zero for this correction. In grid cells with thinner ice than a certain threshold, here 50 m, we cannot assume that the ice velocity is constant and therefore we do not take them into account in the SMB calculation.

This simplified calculation of the ice flow results in a lower SMB compared to neglecting the ice flow because it provides ice replenishment that may still melt. The difference amounts to less than 40 Gt yr^{-1} for all scenarios in the ESM and parameter median averaged over the last 10 years of the simulation. In a fully dynamical ice sheet model, the ice outflow from grid cells would be incorporated, which could cause the ice supply to empty more quickly, leading to a more positive SMB, as empty grid cells are not considered. Presumably, however, the lowering effect of melt–elevation feedback, which is not considered in this study, on the SMB is more substantial. The uncertainty related to the simplified representation of the ice flow is not addressed further.

Appendix B: Earth system models from CMIP6

Several ESMs show strong oversaturation of humidity in areas with very low temperatures, while only small oversaturation occurs in nature due to a lack of freezing nuclei. In ESMs, large oversaturations can be caused by, e.g. interpolation from the ESM levels to near-surface output. Some climate modelling groups truncate the relative humidity to 100 % before they make the data available (Ruosteenoja et al., 2017). To obtain physically realistic values, we truncated the relative humidity to 100 % in all ESMs used in this study. The ESMs HadGEM3-GC31-LL, HadGEM3-GC31-MM, and UKESM1-0-LL have a 360 d calendar, and thus 5 d (spread evenly over the year) are taken twice. We used only one ensemble member of each ESM.

Table B1. CMIP6-models (Eyring et al., 2016) used in this project. For each of the listed models, we use the scenarios SSP126, SSP245, SSP370, and SSP585 to force BESSI, except for some missing ESM–scenario combinations. FGOALS-g3 misses SSP126, GFDL-CM4 misses SSP126 and SSP370, GFDL-ESM4 misses SSP245, HadGEM3-GC31-LL misses SSP370, HadGEM3-GC31-MM misses SSP245 and SSP370, and NESM3 misses SSP370. Data were downloaded from https://esgf-node.llnl.gov/search/cmip6/ (last access: 9 December 2021).

Model	Institution	Grid	DOI
ACCESS-CM2	Collaboration for Australian Weather and Climate Research	144 × 192	https://doi.org/10.22033/ESGF/CMIP6.4271 https://doi.org/10.22033/ESGF/CMIP6.2285
ACCESS-ESM1-5	Collaboration for Australian Weather and Climate Research	145 × 192	https://doi.org/10.22033/ESGF/CMIP6.4272 https://doi.org/10.22033/ESGF/CMIP6.2291
BCC-CSM2-MR	Beijing Climate Center	160 × 320	https://doi.org/10.22033/ESGF/CMIP6.2948 https://doi.org/10.22033/ESGF/CMIP6.1732
CanESM5	Canadian Centre for Climate Modelling and Analysis	64 × 128	https://doi.org/10.22033/ESGF/CMIP6.3610 https://doi.org/10.22033/ESGF/CMIP6.1317
CESM2	National Center for Atmospheric Research	192 × 288	https://doi.org/10.22033/ESGF/CMIP6.7627 https://doi.org/10.22033/ESGF/CMIP6.2201
CESM2-WACCM	National Center for Atmospheric Research	192 × 288	https://doi.org/10.22033/ESGF/CMIP6.10071 https://doi.org/10.22033/ESGF/CMIP6.10026
CMCC-CM2-SR5	Euro-Mediterranean Centre on Climate Change	192 × 288	https://doi.org/10.22033/ESGF/CMIP6.3825 https://doi.org/10.22033/ESGF/CMIP6.1365
CNRM-CM6-1	Centre National de Recherches Météorologiques	128 × 256	https://doi.org/10.22033/ESGF/CMIP6.4066 https://doi.org/10.22033/ESGF/CMIP6.1384
CNRM-ESM2-1	Centre National de Recherches Météorologiques	128 × 256	https://doi.org/10.22033/ESGF/CMIP6.4068 https://doi.org/10.22033/ESGF/CMIP6.1395
EC-Earth3	EC-Earth consortium	256 × 512	https://doi.org/10.22033/ESGF/CMIP6.4700 https://doi.org/10.22033/ESGF/CMIP6.251
EC-Earth3-Veg	EC-Earth consortium	256 × 512	https://doi.org/10.22033/ESGF/CMIP6.4706 https://doi.org/10.22033/ESGF/CMIP6.727
FGOALS-g3	State Key Laboratory of Numerical Modelling for Atmospheric Sciences and Geophysical Fluid Dynamics, Institute of Atmospheric Physics	80 × 180	https://doi.org/10.22033/ESGF/CMIP6.3356 https://doi.org/10.22033/ESGF/CMIP6.2056
GFDL-CM4	Geophysical Fluid Dynamics Laboratory	180 × 288	https://doi.org/10.22033/ESGF/CMIP6.8594 https://doi.org/10.22033/ESGF/CMIP6.9242
GFDL-ESM4	Geophysical Fluid Dynamics Laboratory	180 × 288	https://doi.org/10.22033/ESGF/CMIP6.8597 https://doi.org/10.22033/ESGF/CMIP6.1414
HadGEM3-GC31-LL	Hadley Centre for Climate Prediction and Research	144 × 192	https://doi.org/10.22033/ESGF/CMIP6.6109 https://doi.org/10.22033/ESGF/CMIP6.10845
HadGEM3-GC31-MM	Hadley Centre for Climate Prediction and Research	324 × 432	https://doi.org/10.22033/ESGF/CMIP6.6112 https://doi.org/10.22033/ESGF/CMIP6.10846
IPSL-CM6A-LR	Institut Pierre Simon Laplace	143 × 144	https://doi.org/10.22033/ESGF/CMIP6.5195 https://doi.org/10.22033/ESGF/CMIP6.1532
MIROC6	University of Tokyo, Japan Agency for Marine-Earth Science and Technology	128 × 256	https://doi.org/10.22033/ESGF/CMIP6.5603 https://doi.org/10.22033/ESGF/CMIP6.898
MIROC-ES2L	University of Tokyo, Japan Agency for Marine-Earth Science and Technology	64 × 128	https://doi.org/10.22033/ESGF/CMIP6.5602 https://doi.org/10.22033/ESGF/CMIP6.936
MPI-ESM1-2-LR	Max Planck Institute for Meteorology	96 × 192	https://doi.org/10.22033/ESGF/CMIP6.6595 https://doi.org/10.22033/ESGF/CMIP6.793
MPI-ESM1-2-HR	Max Planck Institute for Meteorology	192 × 384	https://doi.org/10.22033/ESGF/CMIP6.6594 https://doi.org/10.22033/ESGF/CMIP6.2450
MRI-ESM2-0	Meteorological Research Institute, Japan Meteorological Agency	160 × 320	https://doi.org/10.22033/ESGF/CMIP6.6842 https://doi.org/10.22033/ESGF/CMIP6.638
NESM3	Nanjing University of Information Science and Technology	96 × 192	https://doi.org/10.22033/ESGF/CMIP6.8769 https://doi.org/10.22033/ESGF/CMIP6.2027
NorESM2-LM	Norwegian Climate Center	96 × 144	https://doi.org/10.22033/ESGF/CMIP6.8036 https://doi.org/10.22033/ESGF/CMIP6.604
NorESM2-MM	Norwegian Climate Center	192 × 288	https://doi.org/10.22033/ESGF/CMIP6.8040 https://doi.org/10.22033/ESGF/CMIP6.608
UKESM1-0-LL	UK Met Office, NERC research centres	144 × 192	https://doi.org/10.22033/ESGF/CMIP6.6113 https://doi.org/10.22033/ESGF/CMIP6.1567

Appendix C: Uncertainty estimation

To separate the different sources of uncertainty in our projections, we employ the approach of Hawkins and Sutton (2009). Between the different ESMs M, scenarios S, and perturbed snow model parameters in BESSI B, this analysis covers 1952 simulations. The snow model parameters varied in this study are shown in Table C1.

Assuming that the running average decadal mean of the simulated SMB $X_{B,M,S,t}$ can be expressed as the result of these uncertainty contributors and time t, as indicated by the subscripts, the snow model output can be divided into a smooth fit with a fourth-degree polynomial $P_{B,M,S,t}$ and a deviation $\varepsilon_{B,M,S,t}$ from that fit:

$$X_{B,M,S,t} = P_{B,M,S,t} + \varepsilon_{B,M,S,t}. \tag{C1}$$

We analyse the running average decadal means to facilitate the polynomial fit. The polynomial P can be further divided into a constant reference SMB i_M that only depends on the ESM, and a deviation $x_{B,M,S,t}$:

$$X_{B,M,S,t} = x_{B,M,S,t} + i_M + \varepsilon_{B,M,S,t}. \tag{C2}$$

We perform the analysis with $x_{B,M,S,t}$ so that we do not have to account for the constant ESM offset. The reference SMB i_M is the mean of the annual mean values from the time period 1979–2014, averaged over all BESSI configurations. The spread of the fit matches the spread of the SMB, and the deviations from the fit are only large for few simulations at the end of the simulated period (Fig. C1).

We give more weight to the ESMs that perform well in the historical period compared to ERA-Interim that we use as a reference. For the calculation of the weights, the average over the SMB of all different parameter combinations for the same ESM is determined first. The absolute deviation of the ESM simulation from ERA-Interim is the difference of the mean SMB over the historical period for all parameter combinations: $\overline{\mathrm{SMB}}_{\mathrm{M},79-14} - \overline{\mathrm{SMB}}_{\mathrm{E},79-14}$. Additionally, the performance of the ESMs is also measured by taking the difference in SMB change over the time period between the ESM and ERA-Interim. For every ESM, the total deviation d_M is obtained through the Euclidian distance of the absolute deviation and the deviation of the change:

$$d_M = \sqrt{\frac{(\overline{\mathrm{SMB}}_{\mathrm{M},79-14} - \overline{\mathrm{SMB}}_{\mathrm{E},79-14})^2 + ((\overline{\mathrm{SMB}}_{\mathrm{M},04-14} - \overline{\mathrm{SMB}}_{\mathrm{E},04-14}) - (\overline{\mathrm{SMB}}_{\mathrm{M},79-89} - \overline{\mathrm{SMB}}_{\mathrm{E},79-89}))^2}}. \tag{C3}$$

M stands for ESM, E for ERA-Interim, and the numbers for the years. The weights are obtained from the deviation as follows:

$$w_{\mathrm{M}} = \frac{1}{d_{\mathrm{M}}}. \tag{C4}$$

The weights are normalized through dividing by their sum, and the normalized weights are denoted W_{M}. The variance of the SMB can be split into components according to the law of total variance. There are six possibilities of how the split is performed exactly.

$$\begin{aligned}\mathrm{Var}(x) &= \mathrm{E}_{S,B}[\mathrm{Var}_M(x|S,B)] \\ &\quad + \mathrm{E}_S[\mathrm{Var}_B(\mathrm{E}_M[x|S,B]|S)] \\ &\quad + \mathrm{Var}_S(\mathrm{E}_{B,M}[x|S])\end{aligned} \tag{C5}$$

$$\begin{aligned}\mathrm{Var}(x) &= \mathrm{E}_{S,B}[\mathrm{Var}_M(x|S,B)] \\ &\quad + \mathrm{E}_B[\mathrm{Var}_S(\mathrm{E}_M[x|S,B]|B)] \\ &\quad + \mathrm{Var}_B(\mathrm{E}_{S,M}[x|B])\end{aligned} \tag{C6}$$

$$\begin{aligned}\mathrm{Var}(x) &= \mathrm{E}_{S,M}[\mathrm{Var}_B(x|S,M)] \\ &\quad + \mathrm{E}_S[\mathrm{Var}_M(\mathrm{E}_B[x|S,M]|S)] \\ &\quad + \mathrm{Var}_S(\mathrm{E}_{M,B}[x|S])\end{aligned} \tag{C7}$$

$$\begin{aligned}\mathrm{Var}(x) &= \mathrm{E}_{S,M}[\mathrm{Var}_B(x|S,M)] \\ &\quad + \mathrm{E}_M[\mathrm{Var}_S(\mathrm{E}_B[x|S,M]|M)] \\ &\quad + \mathrm{Var}_M(\mathrm{E}_{S,B}[x|M])\end{aligned} \tag{C8}$$

$$\begin{aligned}\mathrm{Var}(x) &= \mathrm{E}_{M,B}[\mathrm{Var}_S(x|M,B)] \\ &\quad + \mathrm{E}_M[\mathrm{Var}_B(\mathrm{E}_S[x|M,B]|M)] \\ &\quad + \mathrm{Var}_M(\mathrm{E}_{S,B}[x|M])\end{aligned} \tag{C9}$$

$$\begin{aligned}\mathrm{Var}(x) &= \mathrm{E}_{M,B}[\mathrm{Var}_S(x|M,B)] \\ &\quad + \mathrm{E}_B[\mathrm{Var}_M(\mathrm{E}_S[x|M,B]|B)] \\ &\quad + \mathrm{Var}_B(\mathrm{E}_{S,M}[x|B])\end{aligned} \tag{C10}$$

The possibilities (C8), (C9), and (C10) are discarded because expectation values of variances between scenarios are calculated. However, we assume that there should be differences between the scenarios because of their different extents of external forcing. We base our analysis on Eq. (C7), but the results of Eqs. (C5) and (C6) do not deviate much (Figs. 5 and C2).

The internal variability $V(t)$ is the variance of the residues of the polynomial fit. It is considered time dependent because the spread between the different simulations in Fig. C1c changes in time. Therefore, it is calculated for every point in time t over the 20 years around t ($t \pm 10a$) and over all scenarios and BESSI parameters. The weighted mean of this variance over all ESMs yields the internal variability:

$$V(t) = \sum_M W_{\mathrm{M}} \mathrm{Var}_{B,S,t\pm10a}(\varepsilon_{B,M,S,t\pm10a}). \tag{C11}$$

The total variance of the SMB $T(t)$ is the sum of the internal variability and the other uncertainty components that are considered as the ESM uncertainty $M(t)$, scenario uncertainty $S(t)$, and the snow model parameter uncertainty $B(t)$:

$$T(t) = V(t) + M(t) + S(t) + B(t). \tag{C12}$$

For the ESM uncertainty, the weighted variance $\mathrm{Var}^{\mathrm{w}}_{\mathrm{M}}$ of the ESMs over the mean parameter configuration is averaged

Table C1. Parameters in BESSI that are varied in this study. Standard stands for the simulations with only one parameter combination. All parameter combinations use the same albedo routine from Bougamont et al. (2005) and an ice albedo of 0.4.

Parameter	Standard	Minimum	Maximum
Fresh snow albedo	0.848	0.766	0.891
Firn albedo	0.554	0.480	0.696
Turbulent heat exchange coefficient/W m^{-2} K^{-1}	5.2	5.2	12.2

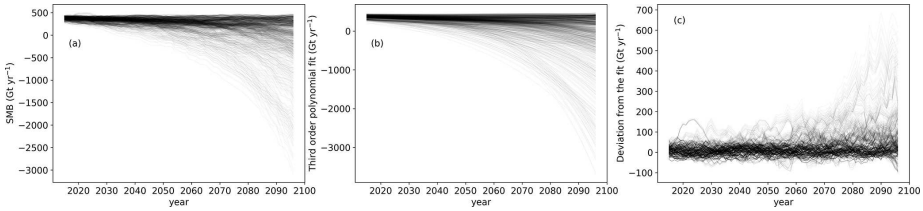

Figure C1. **(a)** Decadal running means of SMB for every parameter–scenario–ESM combination. **(b)** Fourth-degree polynomial fits of the curves in **(a)**. **(c)** Deviations of the curves in **(a)** from the fit in **(b)**.

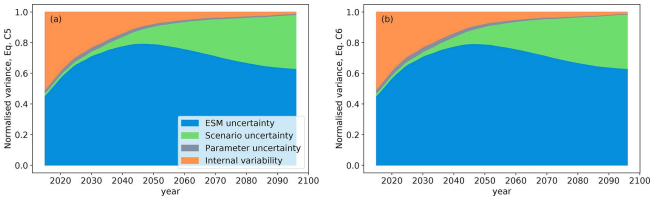

Figure C2. Variance components normalized with the total variance of the fit. **(a)** Calculated with Eq. (C5). **(b)** Calculated with Eq. (C6).

over the scenarios:

$$M(t) = \mathrm{E}_{S,B}[\mathrm{Var}^{\mathrm{w}}_{\mathrm{M}}(x|S,B)] = \frac{1}{N_{\mathrm{s}}}\sum_{\mathrm{s}}\mathrm{Var}^{\mathrm{w}}_{\mathrm{M}}\left(\frac{1}{N_B}\sum_{B}x_{B,M,S,t}\right). \quad \text{(C13)}$$

For the scenario uncertainty, the variance of the weighted multimodel mean of the mean parameter configuration is taken:

$$S(t) = \mathrm{E}_B[\mathrm{Var}_S(\mathrm{E}^{\mathrm{w}}_M[x|S,B]|B)] = \mathrm{Var}_S\left(\sum_M W_M\left(\frac{1}{N_B}\sum_B x_{B,M,S,t}\right)\right). \quad \text{(C14)}$$

The BESSI uncertainty is the mean uncertainty of all parameters:

$$B(t) = \mathrm{Var}_B(\mathrm{E}^{\mathrm{w}}_{S,M}[x|B]) = \frac{1}{N_S}\sum_S\sum_M W_M\mathrm{Var}_B(x_{B,M,S,t}). \quad \text{(C15)}$$

Code availability. The BESSI model code is available on GitHub: BESSI, created by Tobias Zolles, https://github.com/TobiasZo/BESSI/tree/TobiasZo---GSA-model-version (last access: 9 December 2021; Zolles, 2021).

Data availability. Simulation data of BESSI are available on request. CMIP6 data are available in the CMIP6 database, created by ESGF, https://esgf-node.llnl.gov/search/cmip6/ (last access: 12 September 2021). The surface topography ETOPO1 is available at https://doi.org/10.7289/V5C8276M (Amante and Eakins, 2009). ERA-Interim reanalysis data are available from ECMWF: ERA-Interim, https://www.ecmwf.int/en/forecasts/datasets/reanalysis-datasets/era-interim (last access: 2 July 2019).

Author contributions. KMH prepared the model input, conducted the experiments, analysed the results, and wrote the main part of the manuscript. TZ prepared the model experiments, applied the statistical methods, reviewed the analysis, and revised the manuscript. AB conceived the study, experimental design, and analysis and contributed to the writing of the manuscript.

Competing interests. The contact author has declared that neither they nor their co-authors have any competing interests.

Disclaimer. Publisher's note: Copernicus Publications remains neutral with regard to jurisdictional claims in published maps and institutional affiliations.

Acknowledgements. All authors acknowledge support by the Trond Mohn Foundation. Katharina M. Holube received financial support through an Erasmus+ traineeship. The authors are thankful for the constructive criticism by two anonymous referees.

Financial support. This research has been supported by the Trond Mohn Foundation (Modeling Englacial Layers and Tracers in Ice Sheets). Katharina M. Holube received financial support through an Erasmus+ traineeship.

Review statement. This paper was edited by Xavier Fettweis and reviewed by two anonymous referees.

References

Amante, C. and Eakins, B. W.: ETOPO1 1 Arc-Minute Global Relief Model: Procedures, Data Sources and Analysis, NOAA National Geophysical Data Center [data set], https://doi.org/10.7289/V5C8276M, 2009.

Aschwanden, A., Fahnestock, M. A., Truffer, M., Brinkerhoff, D. J., Hock, R., Khroulev, C., Mottram, R., and Khan, S. A.: Contribution of the Greenland Ice Sheet to sea level over the next millennium, Sci. Adv., 5, eeav9396, https://doi.org/10.1126/sciadv.aav9396, 2019.

Beyer, R., Krapp, M., and Manica, A.: An empirical evaluation of bias correction methods for palaeoclimate simulations, Clim. Past, 16, 1493–1508, https://doi.org/10.5194/cp-16-1493-2020, 2020.

Born, A., Imhof, M. A., and Stocker, T. F.: An efficient surface energy–mass balance model for snow and ice, The Cryosphere, 13, 1529–1546, https://doi.org/10.5194/tc-13-1529-2019, 2019.

Bougamont, M., Bamber, J. L., and Greuell, W.: A surface mass balance model for the Greenland Ice Sheet, J. Geophys. Res.-Earth, 110, F04018, https://doi.org/10.1029/2005JF000348, 2005.

Box, J. E. and Steffen, K.: Sublimation on the Greenland Ice Sheet from automated weather station observations, J. Geophys. Res.-Atmos., 106, 33965–33981, https://doi.org/10.1029/2001JD900219, 2001.

Davini, P. and D'Andrea, F.: From CMIP-3 to CMIP-6: Northern Hemisphere atmospheric blocking simulation in present and future climate, J. Climate, 33, 10021–10038, https://doi.org/10.1175/JCLI-D-19-0862.1, 2020.

Davy, R. and Outten, S.: The Arctic Surface Climate in CMIP6: Status and Developments since CMIP5, J. Climate, 33, 8047–8068, https://doi.org/10.1175/JCLI-D-19-0990.1, 2020.

Dee, D. P., Uppala, S. M., Simmons, A. J., Berrisford, P., Poli, P., Kobayashi, S., Andrae, U., Balmaseda, M. A., Balsamo, G., Bauer, P., Bechtold, P., Beljaars, A. C. M., Berg, L. v. d., Bidlot, J., Bormann, N., Delsol, C., Dragani, R., Fuentes, M., Geer, A. J., Haimberger, L., Healy, S. B., Hersbach, H., Hólm, E. V., Isaksen, L., Kållberg, P., Köhler, M., Matricardi, M., McNally, A. P., Monge-Sanz, B. M., Morcrette, J.-J., Park, B.-K., Peubey, C., Rosnay, P. D., Tavolato, C., Thépaut, J.-N., and Vitart, F.: The ERA-Interim reanalysis: configuration and performance of the data assimilation system, Q. J. Roy. Meteor. Soc., 137, 553–597, https://doi.org/10.1002/qj.828, 2011.

Eyring, V., Bony, S., Meehl, G. A., Senior, C. A., Stevens, B., Stouffer, R. J., and Taylor, K. E.: Overview of the Coupled Model Intercomparison Project Phase 6 (CMIP6) experimental design and organization, Geosci. Model Dev., 9, 1937–1958, https://doi.org/10.5194/gmd-9-1937-2016, 2016.

Fettweis, X., Hanna, E., Gallée, H., Huybrechts, P., and Erpicum, M.: Estimation of the Greenland ice sheet surface mass balance for the 20th and 21st centuries, The Cryosphere, 2, 117–129, https://doi.org/10.5194/tc-2-117-2008, 2008.

Fettweis, X., Franco, B., Tedesco, M., van Angelen, J. H., Lenaerts, J. T. M., van den Broeke, M. R., and Gallée, H.: Estimating the Greenland ice sheet surface mass balance contribution to future sea level rise using the regional atmospheric climate model MAR, The Cryosphere, 7, 469–489, https://doi.org/10.5194/tc-7-469-2013, 2013.

Fettweis, X., Hofer, S., Krebs-Kanzow, U., Amory, C., Aoki, T., Berends, C. J., Born, A., Box, J. E., Delhasse, A., Fujita, K., Gierz, P., Goelzer, H., Hanna, E., Hashimoto, A., Huybrechts, P., Kapsch, M.-L., King, M. D., Kittel, C., Lang, C., Langen, P. L., Lenaerts, J. T. M., Liston, G. E., Lohmann, G., Mernild, S. H., Mikolajewicz, U., Modali, K., Mottram, R. H., Niwano, M., Noël, B., Ryan, J. C., Smith, A., Streffing, J., Tedesco, M., van de Berg, W. J., van den Broeke, M., van de Wal, R. S. W., van Kampenhout, L., Wilton, D., Wouters, B., Ziemen, F., and Zolles, T.: GrSMBMIP: intercomparison of the modelled 1980–2012 surface mass balance over the Greenland Ice Sheet, The Cryosphere, 14, 3935–3958, https://doi.org/10.5194/tc-14-3935-2020, 2020.

Franco, B., Fettweis, X., Erpicum, M., and Nicolay, S.: Present and future climates of the Greenland ice sheet according to the IPCC AR4 models, Clim. Dynam., 36, 1897–1918, https://doi.org/10.1007/s00382-010-0779-1, 2011.

Goelzer, H., Huybrechts, P., Fürst, J. J., Nick, F. M., Andersen, M. L., Edwards, T. L., Fettweis, X., Payne, A. J., and Shannon, S.: Sensitivity of Greenland Ice Sheet Projections to Model Formulations, J. Glaciol., 59, 733–749, https://doi.org/10.3189/2013JoG12J182, 2013.

Goelzer, H., Nowicki, S., Payne, A., Larour, E., Seroussi, H., Lipscomb, W. H., Gregory, J., Abe-Ouchi, A., Shepherd, A., Simon, E., Agosta, C., Alexander, P., Aschwanden, A., Barthel, A., Calov, R., Chambers, C., Choi, Y., Cuzzone, J., Dumas, C., Edwards, T., Felikson, D., Fettweis, X., Golledge, N. R., Greve, R., Humbert, A., Huybrechts, P., Le clec'h, S., Lee, V., Leguy, G., Little, C., Lowry, D. P., Morlighem, M., Nias, I., Quiquet, A., Rückamp, M., Schlegel, N.-J., Slater, D. A., Smith, R. S., Straneo, F., Tarasov, L., van de Wal, R., and van den Broeke, M.: The future sea-level contribution of the Greenland ice sheet: a multi-

model ensemble study of ISMIP6, The Cryosphere, 14, 3071–3096, https://doi.org/10.5194/tc-14-3071-2020, 2020.

Graversen, R. G., Drijfhout, S., Hazeleger, W., van de Wal, R., Bintanja, R., and Helsen, M.: Greenland's contribution to global sea-level rise by the end of the 21st century, Clim. Dynam., 37, 1427–1442, https://doi.org/10.1007/s00382-010-0918-8, 2011.

Hanna, E., Cappelen, J., Fettweis, X., Mernild, S. H., Mote, T. L., Mottram, R., Steffen, K., Ballinger, T. J., and Hall, R. J.: Greenland surface air temperature changes from 1981 to 2019 and implications for ice-sheet melt and mass-balance change, Int. J. Climatol., 41, E1336–E1352, https://doi.org/10.1002/joc.6771, 2020.

Hawkins, E. and Sutton, R.: The Potential to Narrow Uncertainty in Regional Climate Predictions, B. Am. Meteorol. Soc., 90, 1095–1108, https://doi.org/10.1175/2009BAMS2607.1, 2009.

Hofer, S., Tedstone, A. J., Fettweis, X., and Bamber, J. L.: Decreasing cloud cover drives the recent mass loss on the Greenland Ice Sheet, Sci. Adv., 3, e1700584, https://doi.org/10.1126/sciadv.1700584, 2017.

Hofer, S., Lang, C., Amory, C., Kittel, C., Delhasse, A., Tedstone, A., and Fettweis, X.: Greater Greenland Ice Sheet contribution to global sea level rise in CMIP6, Nat. Commun., 11, 6289, https://doi.org/10.1038/s41467-020-20011-8, 2020.

Knutti, R., Masson, D., and Gettelman, A.: Climate model genealogy: Generation CMIP5 and how we got there, Geophys. Res. Lett., 40, 1194–1199, https://doi.org/10.1002/grl.50256, 2013.

Krebs-Kanzow, U., Gierz, P., Rodehacke, C. B., Xu, S., Yang, H., and Lohmann, G.: The diurnal Energy Balance Model (dEBM): a convenient surface mass balance solution for ice sheets in Earth system modeling, The Cryosphere, 15, 2295–2313, https://doi.org/10.5194/tc-15-2295-2021, 2021.

Lehner, F., Deser, C., Maher, N., Marotzke, J., Fischer, E. M., Brunner, L., Knutti, R., and Hawkins, E.: Partitioning climate projection uncertainty with multiple large ensembles and CMIP5/6, Earth Syst. Dynam., 11, 491–508, https://doi.org/10.5194/esd-11-491-2020, 2020.

Mankoff, K. D., Solgaard, A., Colgan, W., Ahlstrøm, A. P., Khan, S. A., and Fausto, R. S.: Greenland Ice Sheet solid ice discharge from 1986 through March 2020, Earth Syst. Sci. Data, 12, 1367–1383, https://doi.org/10.5194/essd-12-1367-2020, 2020.

Meehl, G. A., Senior, C. A., Eyring, V., Flato, G., Lamarque, J.-F., Stouffer, R. J., Taylor, K. E., and Schlund, M.: Context for interpreting equilibrium climate sensitivity and transient climate response from the CMIP6 Earth system models, Sci. Adv., 6, eaba1981, https://doi.org/10.1126/sciadv.aba1981, 2020.

Nagler, T., Rott, H., Hetzenecker, M., Wuite, J., and Potin, P.: The Sentinel-1 Mission: New Opportunities for Ice Sheet Observations, Remote Sens., 7, 9371–9389, https://doi.org/10.3390/rs70709371, 2015.

Noël, B., van de Berg, W. J., Machguth, H., Lhermitte, S., Howat, I., Fettweis, X., and van den Broeke, M. R.: A daily, 1 km resolution data set of downscaled Greenland ice sheet surface mass balance (1958–2015), The Cryosphere, 10, 2361–2377, https://doi.org/10.5194/tc-10-2361-2016, 2016.

O'Neill, B. C., Tebaldi, C., van Vuuren, D. P., Eyring, V., Friedlingstein, P., Hurtt, G., Knutti, R., Kriegler, E., Lamarque, J.-F., Lowe, J., Meehl, G. A., Moss, R., Riahi, K., and Sanderson, B. M.: The Scenario Model Intercomparison Project (ScenarioMIP) for CMIP6, Geosci. Model Dev., 9, 3461–3482, https://doi.org/10.5194/gmd-9-3461-2016, 2016.

Ruosteenoja, K., Jylhä, K., Räisänen, J., and Mäkelä, A.: Surface air relative humidities spuriously exceeding 100 % in CMIP5 model output and their impact on future projections, J. Geophys. Res.-Atmos., 122, 9557–9568, https://doi.org/10.1002/2017JD026909, 2017.

Ryan, J. C., Smith, L. C., van As, D., Cooley, S. W., Cooper, M. G., Pitcher, L. H., and Hubbard, A.: Greenland Ice Sheet surface melt amplified by snowline migration and bare ice exposure, Sci. Adv., 5, eaav3738, https://doi.org/10.1126/sciadv.aav3738, 2019.

Sasgen, I., Wouters, B., Gardner, A. S., King, M. D., Tedesco, M., Landerer, F. W., Dahle, C., Save, H., and Fettweis, X.: Return to rapid ice loss in Greenland and record loss in 2019 detected by the GRACE-FO satellites, Commun. Earth Environ., 1, 8, https://doi.org/10.1038/s43247-020-0010-1, 2020.

Slater, T., Hogg, A. E., and Mottram, R.: Ice-sheet losses track high-end sea-level rise projections, Nat. Clim. Chang., 10, 879–881, https://doi.org/10.1038/s41558-020-0893-y, 2020.

Sodemann, H., Schwierz, C., and Wernli, H.: Interannual variability of Greenland winter precipitation sources: Lagrangian moisture diagnostic and North Atlantic Oscillation influence, J. Geophys. Res.-Atmos., 113, D03107, https://doi.org/10.1029/2007JD008503, 2008.

Vizcaino, M.: Ice sheets as interactive components of Earth System Models: progress and challenges: Ice sheets as interactive components of Earth System Models, WIREs Clim Change, 5, 557–568, https://doi.org/10.1002/wcc.285, 2014.

Yan, Q., Wang, H., Johannessen, O. M., and Zhang, Z.: Greenland ice sheet contribution to future global sea level rise based on CMIP5 models, Adv. Atmos. Sci., 31, 8–16, https://doi.org/10.1007/s00376-013-3002-6, 2014.

Zolles, T.: BESSI, available at: https://github.com/TobiasZo/BESSI/tree/TobiasZo---GSA-model-version (last access: 9 December 2021), Github [code], 2021.

Zolles, T. and Born, A.: Sensitivity of the Greenland surface mass and energy balance to uncertainties in key model parameters, The Cryosphere, 15, 2917–2938, https://doi.org/10.5194/tc-15-2917-2021, 2021.

Zolles, T. and Born, A.: How does a change in climate variability impact the Greenland ice-sheet surface mass balance?, The Cryosphere Discuss. [preprint], https://doi.org/10.5194/tc-2021-379, in review, 2022.

Zolles, T., Maussion, F., Galos, S. P., Gurgiser, W., and Nicholson, L.: Robust uncertainty assessment of the spatio-temporal transferability of glacier mass and energy balance models, The Cryosphere, 13, 469–489, https://doi.org/10.5194/tc-13-469-2019, 2019.

3 Synthesis

3.1 Main findings

BESSI was developed to simulate the surface mass and energy balance. The model has undergone an extensive sensitivity analysis to identify the key free model parameters. The sensitivity of the SMB is different during the cold LGM and during PD conditions. Additionally, substantial spatial variations were found. During present day conditions over the entire Greenland ice sheet the model is most sensitive to the long-wave radiation and the parameterization thereof. Areas above the equilibrium line show an almost equal importance of the snow albedo parameterization and the turbulent latent heat flux. Despite its low importance on the Greenland-wide SMB today the turbulent latent heat flux is the dominant component during the last glacial maximum. Surface mass balance modeling during the glacial has to include the turbulent latent heat flux.

The order of the interannual-variability on the Greenland-wide SMB only has a marginal influence, but the simulated SMB is overestimated by more 40% if daily climatology is used as a forcing. BESSI is sensitive to the small amounts of snowfall occurring every day for daily averages, due to the albedo increase with fresh snow. Daily snowfall is physically unreasonable, but with the low resolution of proxies only a climatology may be available as a forcing. We provide a solution to overcome this. Instead of having daily averages, it is possible to reduce the overestimation by using monthly averages and distribute them following a natural distribution. We apply a sub-monthly precipitation distribution for example in Paper III to bias correct the precipitation.

The surface mass balance of Greenland over the next century is quite uncertain due to two main factors: the socio economic pathway/emission scenario and the uncertainty of the climate models. The SMB was simulated until 2100 using 26 different climate models. In the majority of the cases the SMB over Greenland will turn drastically negative by the end of the century. Though the impact of the scenario is a strong one, it is overshadowed by the SMB variability due to the choice of climate model input, which accounts for around 60% of the total SMB uncertainty at 2100. The uncertainty of the climate forcing is the main difficulty energy balance models will have to cope with.

3.2 Limitations and Discussion

BESSI was developed to be used for long time scales of up to a glacial cycle. With the thorough sensitivity and uncertainty analysis of the model it can now be used for its intended application. As an energy balance model of modest complexity, BESSI still relies on the quality of the forcing data. The uncertainties associated with the free model parameters are modest in comparison to the uncertainty of the GCM data around Greenland, and probably other ice sheets. It is expected that the uncertainty of the climate model even increases for the glacial (*Brady et al.*, 2013; *Hargreaves et al.*, 2013). BESSI participated in SMBMIP, which compared the SMB over Greenland modeled by 13 SMB models of varying complexity (*Fettweis et al.*, 2020). The models range from PDD models to full regional climate models. The SMB simulated by BESSI is

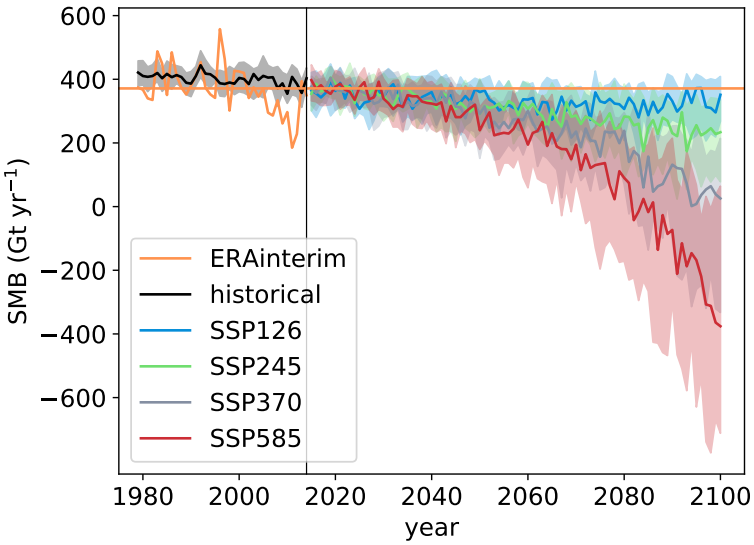

Figure 3.1: SMB simulations forced with ERA-Interim reanalysis data, historical GCM simulations and scenario climate simulations, median over the SMB for all snow model parameter combinations. The solid line is the median of all GCMs, the shading the 25 % and 75 % percentiles. Orange: SMB forced with ERA-Interim with mean value.

comparable to the other models, with a positive bias, mainly over the melt region of the west. There are a few reasons: The region is sensitive to topographic down-scaling and the atmospheric lapse rate, given the difference in ERA-interim model topography and the real topography. Furthermore, BESSI does not account for enhanced ice darkening due to dust/algae late in the melt season. Additionally, in the current setup BESSI uses a fixed wind speed for the turbulent fluxes. Neither of these parts were investigated, due to the assumption that such data (like high resolution wind speed) will be difficult to get for the intended use of BESSI. We do not want to compromise on the numerical efficiency.

Using CMIP6 to simulate the SMB over Greenland lead to a wide range of SMB values. The results are discouraging, given the large spread of potential SMB values for all scenarios. *Hanna et al.* (2020) used only a subset of CMIP6 with a regional climate model, MAR, (*Fettweis et al.*, 2005) resulting in a smaller range of SMB values. The same subset in BESSI disagrees in one simulation, showing a much larger SMB with BESSI than MAR. As BESSI already fails to reproduce the SMB decrease in the early 2000 for the historic period (Fig. 3.1) using the CMIP6 data, an RCM may be better suited as they can reproduce it for some GCMs *Noël et al.* (2020) . The disagreement may be due to the lack of enhanced Greenland blocking in the climate models (*Hanna et al.*, 2018). Simulating the SMB with BESSI cannot compensate for such deficiencies in the GCM data. In comparison *Noël et al.* (2020) managed to reproduce the SMB from reanalysis data using GCM data (CESM2) with the RCM RACMO. Similarly, MAR also reproduces the SMB over Greenland for the last 20 years using some GCM models. RCMs are likely providing better SMB data for biased GCM forcing, though this may be not happening

for drastic different climate state. Nevertheless, the advantage of BESSI is its efficiency. With BESSI the SMB using the entire CMIP6 ensemble could be simulated, without prior pre-selection of GCMs with strong/low climate sensitivity and/or performance over Greenland. A similar procedure was done for ISMIP, which compared ice sheet models over Greenland and Antarctica using CMIP5 and CMIP6 data (*Payne et al.*, 2021), but had to compromise on the choice of GCM. All SMB models need a boundary climate forcing. With the complexity of the model also the amount of required input increases. The advantage of RCMs like MAR (*Fettweis et al.*, 2005) and RACMO (*Noël et al.*, 2018) is that to a certain degree they can compensate for deficiencies of the boundary climate models over Greenland. Other models may compensate through a tuning procedure, which has the inherent problem of over-fitting and transferability of the parameterizations to other climate states (*Fettweis et al.*, 2020). Even for the RCMs it is unclear how well it does for past climate states, but most likely provide the best SMB estimates. Given the large uncertainty in climate models (over Greenland) forcing the SMB model with multiple climate models is beneficial. The uncertainty associated with the climate forcing may be the dominant factor over the choice of SMB model for most time periods. It would be very beneficial to do a sensitivity analysis including multiple SMB models together with multiple climate models to quantify the relative importance. Based on these findings it is likely easier to identify the right SMB model for a particular research question. At the current state, based on SMBMIP and the Papers I-III, using multiple models is a good choice. For example, an RCM is forced with 1-3 GCMs to provide a good SMB estimate and a surface energy balance model, like BESSI, could be run with many more GCMs to provide an uncertainty estimate.

The boundary climate conditions determine the SMB response in all SMB models. It is likely that this dependency decreases with the complexity of the SMB model. Given that the SMB uncertainty becomes the dominant factor of the ice sheet uncertainty by the end of the century over Greenland (*Goelzer et al.*, 2017; *Aschwanden et al.*, 2019), the largest uncertainty for the evolution of the ice sheet is the uncertainty of the climate (model). Similar results are to be expected for paleoclimate where proxy based reconstructions feed into the climate reconstructions/models with their increased uncertainty. Though in a deep glacial state with shelves forming around Greenland, the marine processes increase in importance (*Tabone et al.*, 2018; *Blasco et al.*, 2019). A big factor in all cases is probably the uncertainty in precipitation and the storm tracks, which in turn are impacted by the size of the Laurantide ice sheet on North-America. Additionally, the influence of the local ice sheet topography on the precipitation pattern is substantial (*Merz et al.*, 2014a,b), showing the need for maybe a coupled climate model or a clever down-scaling method. Obtaining a representative climate forcing for the glacial cycle is challenging. Based on the findings about inter-annual variability it could be possible to create a climate forcing using proxy data for the average climate and superimposing climate variability. Glacier index or climate reconstructions based on an analog method are potential candidates (*Forsström et al.*, 2003; *Jensen et al.*, 2018). Though an uncertainty of around 20% in the mass balance is to be expected due to the forcing.

BESSI does not resolve the daily cycle, following the conclusions from the inter-annual variability, a similar effect is likely occurring for the daily cycle. In the absence of a daily cycle, the mass balance is larger for a tuned model than with it. It is not feasible to run BESSI at a sub-daily resolution, due to the computational efficiency constraints, though

the effect should be studied in the future. Given the uncertainty of the boundary climate forcing this is not of priority. Additionally, the thick snow layers of BESSI (50-100 cm) will dampen any signal anyway. The thick surface layer also reduces melt and refreezing relative to other models (*Plach et al.*, 2019; *Fettweis et al.*, 2020). While this does not impact the absolute SMB, it does the internal layering and furthermore the behavior on the surface. The albedo parameterization in BESSI depends on the snow temperature, which is less sensitive to the surface energy balance at thick layers than thin ones. Due to the numerical stability layer thickness was not tested in any study, even though it may be interesting. As the sensitivity towards the snow albedo parameterization was less than towards the long-wave radiation and the climate uncertainty this is likely also of minor importance in comparison.

BESSI compares well with other SMB models including more complex ones (*Fettweis et al.*, 2020). The snow albedo can be compared to MODIS satellite data (*Justice et al.*, 2002), it reproduces perennial firn aquifers over Greenland (*Imhof*, 2016; *Born et al.*, 2019), and 10 m firn temperatures were also checked. As mentioned previously processes and effects close to the surface may be under-captured as the snow layers in BESSI are large. For example the absolute amount of refreezing and melting during the Emian found by *Plach et al.* (2019) vary by around 200 Gt between MAR and BESSI, with both having a similar SMB. The large snow layers in BESSI just buffer the melt-refreezing cycle and in the absence of a daily forcing cycle the entire daily melt-refreezing cycle is lacking. BESSI is an efficient SMB model, which also provides a rough firn structure. High resolution vertical data is better obtained from snow models rather than energy balance models for long term simulations (*Bartelt and Lehning*, 2002; *Vionnet et al.*, 2012). BESSI has no horizontal transport of mass and energy and runoff occurs instantly once the bottom of the snow pack is reached. Given a horizontal grid size of 10×10 km it is not expected that the firn becomes impermeable to melt water from the cells above even with ice layers present. Additionally, recent studies revealed that firn pore volume can also be build up in a melting state ice sheet (*Rennermalm et al.*, 2021) enabling runoff. Ongoing research indicates that BESSI as well as MAR overestimate the turbulent latent heat flux in winter at least in the north-east of Greenland at the EASTgrip ice core drilling site, the prevailing catabatic winds could be a reason for it (*Dietrich et al.*, 2021). The authors also highlight that this could furthermore increase the relative importance of the vapor flux on the total SMB.

During the previous discussion the SMB model was seen as the link between the atmospheric forcing from a climate model to the SMB. Within BESSI there is only topographic down-scaling for the atmospheric temperature and the related long-wave radiation. All prior adjustment of the climate model data, like bias correction, is seen as being not part of the SMB model. This may not be similar for other models. The sensitivity towards the climate model furthermore translates to a sensitivity to the used bias correction and down-scaling method. With the studies on the influence of the inter-annual variability, daily precipitation and SMB projections, we hope to be able to bias correct and downscale in a scientifically sound way. Though the uncertainties will increase for large difference between climate model and real topography.

3.3 Outlook

BESSI is a ready to use model written in Fortran and online available at github (https://github.com/TobiasZo/BESSI). With its focus on efficiency by accounting for all important surface processes it fills the gap between regional climate and temperature index based models. The model has recently been parallelized in our working group and more than 100 simulation years can now be run on a relatively small (24 cores) machine in one minute. BESSI is now coupled to the ice sheet model YELMO (*Robinson et al.*, 2020; *Born and Robinson*, 2021), and my working group started modeling the evolution of the Greenland ice sheet over the last glacial cycle. Initial results show that the main source of uncertainty is not related to BESSI, but rather the ocean-ice interaction. Furthermore, the same model setup is used to simulate the retreat of the Scandinavian ice sheet over the Barents sea.

BESSI had been used at the IceFinse course of the University of Bergen during a student project to simulate a small Norwegian ice cap, Hardangerjøkulen. Since autumn 2021 a new PhD-student in our working group studies the Folgefonna ice cap with BESSI.

Bibliography

Agosta, C., C. Amory, C. Kittel, A. Orsi, V. Favier, H. Gallée, M. R. van den Broeke, J. Lenaerts, J. M. van Wessem, W. J. van de Berg, et al. (2019), Estimation of the Antarctic surface mass balance using the regional climate model MAR (1979–2015) and identification of dominant processes, *The Cryosphere*, *13*(1), 281–296, doi:10.5194/tc-13-281-2019. 2

Aschwanden, A., M. A. Fahnestock, M. Truffer, D. J. Brinkerhoff, R. Hock, C. Khroulev, R. Mottram, and S. A. Khan (2019), Contribution of the Greenland Ice Sheet to sea-level over the next millennium, *Science Advances*, doi:10.1126/sciadv.aav9396. 75

Augustin, L., C. Barbante, P. R. Barnes, J. M. Barnola, M. Bigler, E. Castellano, O. Cattani, J. Chappellaz, D. Dahl-Jensen, B. Delmonte, et al. (2004), Eight glacial cycles from an Antarctic ice core, *Nature*, *429*, 623–628, doi:10.1038/nature02599. 1

Bartelt, P., and M. Lehning (2002), A physical SNOWPACK model for the Swiss avalanche warning: Part I: numerical model, *Cold Regions Science and Technology*, *35*(3), 123–145, doi:10.1016/S0165-232X(02)00074-5. 1, 76

Bauer, E., and A. Ganopolski (2017), Comparison of surface mass balance of ice sheets simulated by positive-degree-day method and energy balance approach, *Climate of the Past*, *13*(7), 819–832, doi:10.5194/cp-13-819-2017. 2, 3

Beven, K. (1989), Changing ideas in hydrology - The case of physically-based models, *Journal of Hydrology*, *105*(1-2), 157–172, doi:10.1016/0022-1694(89)90101-7. 2

Beven, K., and A. Binley (1992), The Future of Distributed Models: Model Calibration and Uncertainity Prediction, *Hydrol. Process.*, *6*(May 1991), 279–298, doi:10.1002/hyp.3360060305. 2

Blasco, J., I. Tabone, J. Alvarez-Solas, A. Robinson, and M. Montoya (2019), The antarctic ice sheet response to glacial millennial-scale variability, *Climate of the Past*, *15*(1), 121–133, doi:10.5194/cp-15-121-2019. 75

Born, A., and A. Robinson (2021), Modeling the Greenland englacial stratigraphy, *The Cryosphere*, *15*(9), 4539–4556, doi:10.5194/tc-15-4539-2021. 77

Born, A., M. A. Imhof, and T. F. Stocker (2019), An efficient surface energy–mass balance model for snow and ice, *The Cryosphere*, *13*(5), 1529–1546, doi:10.5194/tc-13-1529-2019. 2, 5, 76

Bougamont, M., J. L. Bamber, and W. Greuell (2005), A surface mass balance model for the Greenland Ice Sheet, *Journal of Geophysical Research: Earth Surface*, *110*(4), 1–13, doi:10.1029/2005JF000348. 1, 3

Box, J. E., X. Fettweis, J. C. Stroeve, M. Tedesco, D. K. Hall, and K. Steffen (2012), Greenland ice sheet albedo feedback : thermodynamics and atmospheric drivers, *The Cryosphere*, *6*, 821–839, doi:10.5194/tc-6-821-2012. 1

Brady, E. C., B. L. Otto-Bliesner, J. E. Kay, and N. Rosenbloom (2013), Sensitivity to glacial forcing in the CCSM4, *Journal of Climate*, *26*(6), 1901–1925, doi:10.1175/JCLI-D-11-00416.1. 5, 73

Braithwaite, R. J. (1995), Aerodynamic stability and turbulent sensible-heat flux over a melting ice surface, the Greenland ice sheet, *Journal of Glaciology*, *41*(139), 562–571, doi:10.1017/S0022143000034882. 1

Brock, B. W., I. C. Willis, and M. J. Sharp (2000), Measurement and parameterisation of albedo variations at Haut Glacier d ' Arolla , Switzerland, *Journal of Glaciology*, *46*(155), 675–688, doi:10.3189/172756506781828746. 1

Cai, Z., Q. You, F. Wu, H. W. Chen, D. Chen, and J. Cohen (2021), Arctic warming revealed by multiple CMIP6 models: evaluation of historical simulations and quantification of future projection uncertainties, *Journal of Climate*, *34*(12), 4871–4892, doi:10.1175/JCLI-D-20-0791.1. 3

Cuffey, K. M., and S. J. Marshall (2000), Substantial contribution to sea-level rise during the last interglacial from the Greenland ice sheet, *Nature*, *404*(6778), 591–594, doi:10.1038/35007053. 1

Dansgaard, W., S. J. Johnsen, J. Møller, and C. C. Langway Jr (1969), One thousand centuries of climatic record from Camp Century on the Greenland ice sheet, *Science*, *166*(3903), 377–381, doi:10.1126/science.166.3903.377. 1

Dietrich, L., H. C. Steen-Larsen, C. Agosta, X. Fettweis, A.-K. Faber, and S. Wahl (2021), The Role of Sublimation on the Surface Mass Balance of the Interior Greenland Ice Sheet, in *EGU General Assembly Conference Abstracts*, pp. EGU21–16,503, doi:10.5194/egusphere-egu21-16503. 76

Donat-Magnin, M., N. C. Jourdain, H. Gallée, C. Amory, C. Kittel, X. Fettweis, J. D. Wille, V. Favier, A. Drira, and C. Agosta (2020), Interannual variability of summer surface mass balance and surface melting in the Amundsen sector, West Antarctica, *The Cryosphere*, *14*(1), 229–249, doi:10.5194/tc-14-229-2020. 3

Eyring, V., S. Bony, G. A. Meehl, C. A. Senior, B. Stevens, R. J. Stouffer, and K. E. Taylor (2016), Overview of the Coupled Model Intercomparison Project Phase 6 (CMIP6) experimental design and organization, *Geoscientific Model Development*, *9*(5), 1937–1958, doi:10.5194/gmd-9-1937-2016. 5

Fettweis, X., H. Gallée, F. Lefebre, and J.-P. van Ypersele (2005), Greenland surface mass balance simulated by a regional climate model and comparison with satellite-derived data in 1990–1991, *Climate Dynamics*, *24*(6), 623–640, doi:10.1007/s00382-005-0010-y. 1, 74, 75

Fettweis, X., S. Hofer, U. Krebs-Kanzow, C. Amory, T. Aoki, C. J. Berends, A. Born, J. E. Box, A. Delhasse, K. Fujita, P. Gierz, H. Goelzer, E. Hanna, A. Hashimoto, P. Huybrechts, M.-L. Kapsch, M. D. King, C. Kittel, C. Lang, P. L. Langen, J. T. M. Lenaerts, G. E. Liston, G. Lohmann, S. H. Mernild, U. Mikolajewicz, K. Modali, R. H. Mottram, M. Niwano, B. Noël, J. C. Ryan, A. Smith, J. Streffing, M. Tedesco, W. J. van de Berg, M. van den Broeke, R. S. W. van de Wal, L. van Kampenhout, D. Wilton, B. Wouters, F. Ziemen, and T. Zolles (2020), GrSMBMIP: intercomparison of the modelled 1980–2012 surface mass balance over the Greenland Ice Sheet, *The Cryosphere*, *14*(11), 3935–3958, doi:10.5194/tc-14-3935-2020. 73, 75, 76

Forsström, P.-L., O. Sallasmaa, R. Greve, and T. Zwinger (2003), Simulation of fast-flow features of the Fennoscandian ice sheet during the Last Glacial Maximum, *Annals of Glaciology*, *37*, 383–389, doi:10.3189/172756403781815500. 3, 75

Fürst, J. J., H. Goelzer, and P. Huybrechts (2015), Ice-dynamic projections of the Greenland ice sheet in response to atmospheric and oceanic warming, *The Cryosphere*, *9*(3), 1039–1062, doi:10.5194/tc-9-1039-2015. 1

Goelzer, H., P. Huybrechts, M.-F. Loutre, and T. Fichefet (2016), Last Interglacial climate and sea-level evolution from a coupled ice sheet–climate model, *Climate of the Past*, *12*(12), 2195–2213, doi:10.5194/cp-12-2195-2016. 1

Goelzer, H., A. Robinson, H. Seroussi, and R. S. Van De Wal (2017), Recent progress in Greenland ice sheet modelling, *Current climate change reports*, *3*(4), 291–302, doi:10.1007/s40641-017-0073-y. 75

Greuell, W., and P. Smeets (2001), Variations with elevation in the surface energy balance on the Pasterze (Austria), *Journal of Geophysical Research*, *106*(D23), 31,717, doi:10.1029/2001JD900127. 1

Greve, R., K.-H. Wyrwoll, and A. Eisenhauer (1999), Deglaciation of the Northern Hemisphere at the onset of the Eemian and Holocene, *Annals of Glaciology*, *28*, 1–8, doi:doi:10.3189/172756499781821643. 1, 3

Gurgiser, W., B. Marzeion, L. Nicholson, M. Ortner, and G. Kaser (2013), Modeling energy and mass balance of shallap glacier, Peru, *The Cryosphere*, *7*(6), 1787–1802, doi:10.5194/tc-7-1787-2013. 3

Hanna, E., X. Fettweis, and R. J. Hall (2018), Brief communication: Recent changes in summer greenland blocking captured by none of the cmip5 models, *The Cryosphere*, *12*(10), 3287–3292, doi:10.5194/tc-12-3287-2018. 74

Hanna, E., J. Cappelen, X. Fettweis, S. H. Mernild, T. L. Mote, R. Mottram, K. Steffen, T. J. Ballinger, and R. J. Hall (2020), Greenland surface air temperature changes from 1981 to 2019 and implications for ice-sheet melt and mass-balance change, *International Journal of Climatology*, (November 2019), 1–17, doi:10.1002/joc.6771. 74

Hargreaves, J. C., J. D. Annan, R. Ohgaito, A. Paul, and A. Abe-Ouchi (2013), Skill and reliability of climate model ensembles at the last glacial maximum and mid-holocene, *Climate of the Past*, *9*(2), 811–823, doi:10.5194/cp-9-811-2013. 3, 73

Hock, R. (2003), Temperature index melt modelling in mountain areas, *Journal of Hydrology*, *282*(1-4), 104–115, doi:10.1016/S0022-1694(03)00257-9. 1

Hock, R. (2005), Glacier melt: a review of processes and their modelling, *Progress in Physical Geography*, *29*(3), 362–391, doi:10.1191/0309133305pp453ra. 1

Hock, R., and B. Holmgren (2005), A distributed surface energy-balance model for complex topography and its application to Storglaciären, Sweden, *Journal of Glaciology*, *51*(172), 25–36, doi:10.3189/172756505781829566. 1

Imhof, M. (2016), An Energy and Mass Balance Firn Model coupled to the Ice Sheets of the Northern Hemisphere, Master's thesis, University of Bern. 4, 76

IPCC 2021: Climate Change 2021: The Physical Science Basis. Contribution of Working Group I to the Sixth Assessment Report of the Intergovernmental Panel on Climate Change, IPCC, V. Delmotte, P. Zhai, A. Pirani, S. Connors, C. Péan, S. Berger, Y. C. N. Caud, L. Goldfarb, M. Gomis, M. Huang, K. Leitzell, E. Lonnoy, J. Matthews, T. Maycock, T. Waterfield, O. Yelekçi, R. Yu, and B. Zhou, Cambridge University Press. In Press. 1, 6

Jensen, M. F., A. Nummelin, S. B. Nielsen, H. Sadatzki, E. Sessford, B. Risebrobakken, C. Andersson, A. Voelker, W. H. G. Roberts, J. Pedro, and A. Born (2018), A spatiotemporal reconstruction of sea-surface temperatures in the north atlantic during dansgaard–oeschger events 5–8, *Climate of the Past*, *14*(6), 901–922, doi:10.5194/cp-14-901-2018. 75

Justice, C., J. Townshend, E. Vermote, E. Masuoka, R. Wolfe, N. Saleous, D. Roy, and J. Morisette (2002), An overview of modis land data processing and product status, *Remote sensing of Environment*, *83*(1-2), 3–15, doi:10.1016/S0034-4257(02)00084-6. 76

Klok, E. J., and J. Oerlemans (2004), Modelled climate sensitivity of the mass balance of Morteratschgletscher and its dependence on albedo parameterization, *International Journal of Climatology*, *24*(2), 231–245, doi:10.1002/joc.994. 1

Klok, E. J. L., and J. Oerlemans (2002), Model study of the spatial distribution of the energy and mass balance of Morteratschgletscher , Switzerland, *Journal of Glaciology*, *48*(163), 505–518, doi:10.3189/172756502781831133. 1

Krapp, M., A. Robinson, and A. Ganopolski (2017), SEMIC: an efficient surface energy and mass balance model applied to the Greenland ice sheet, *The Cryosphere*, *11*(4), 1519–1535, doi:10.5194/tc-11-1519-2017. 2

Krebs-Kanzow, U., P. Gierz, and G. Lohmann (2018), Brief communication: An ice surface melt scheme including the diurnal cycle of solar radiation, *The Cryosphere*, *12*(12), 3923–3930, doi:10.5194/tc-12-3923-2018. 2

Krebs-Kanzow, U., P. Gierz, C. B. Rodehacke, S. Xu, H. Yang, and G. Lohmann (2021), The diurnal Energy Balance Model (dEBM): a convenient surface mass balance solution for ice sheets in Earth system modeling, *The Cryosphere*, *15*(5), 2295–2313, doi:10.5194/tc-15-2295-2021. 2

Lefebre, F. (2003), Modeling of snow and ice melt at ETH Camp (West Greenland): A study of surface albedo, *Journal of Geophysical Research*, *108*(D8), 4231, doi:10.1029/2001JD001160. 1

Li, H. (2020), Spatial and temporal transferability of degree-day model and simplified energy balance model: a case study, *Sciences in Cold and Arid Regions*, *12*(2), 95–103, doi:10.3724/SP.J.1226.2020.00095. 2

Lucas-Picher, P., M. Wulff-Nielsen, J. H. Christensen, G. Aoalgeirsdóttir, R. Mottram, and S. B. Simonsen (2012), Very high resolution regional climate model simulations over Greenland: Identifying added value, *Journal of Geophysical Research Atmospheres*, *117*(2), 1–16, doi:10.1029/2011JD016267. 1

MacDougall, A. H., B. A. Wheler, and G. E. Flowers (2011), A preliminary assessment of glacier melt-model parameter sensitivity and transferability in a dry subarctic environment, *The Cryosphere*, *5*(4), 1011–1028, doi:10.5194/tc-5-1011-2011. 2

MacGregor, J. A., M. A. Fahnestock, G. A. Catania, J. D. Paden, S. P. Gogineni, S. K. Young, S. C. Rybarski, A. N. Mabrey, B. M. Wagman, and M. Morlighem (2015), Radiostratigraphy and age structure of the Greenland Ice Sheet, *Journal of Geophysical Research: Earth Surface*, *120*(2), 212–241, doi:10.1002/2014JF003215. 4

Masson-Delmotte, V., H. C. Steen-Larsen, P. Ortega, D. Swingedouw, T. Popp, B. Vinther, H. Oerter, A. Sveinbjornsdottir, H. Gudlaugsdottir, J. Box, et al. (2015), Recent changes in north-west Greenland climate documented by NEEM shallow ice core data and simulations, and implications for past-temperature reconstructions, *The Cryosphere*, *9*(4), 1481–1504, doi:10.5194/tc-9-1481-2015. 1

Merz, N., A. Born, C. C. Raible, H. Fischer, and T. F. Stocker (2014a), Dependence of Eemian Greenland temperature reconstructions on the ice sheet topography, *Climate of the Past*, *10*(3), 1221–1238, doi:10.5194/cp-10-1221-2014. 75

Merz, N., G. Gfeller, A. Born, C. C. Raible, T. F. Stocker, and H. Fischer (2014b), Influence of ice sheet topography on Greenland precipitation during the Eemian interglacial, *Journal of Geophysical Research*, *119*(18), 10.749–10.768, doi:10.1002/2014JD021940. 75

Neff, B., A. Born, and T. F. Stocker (2016), An ice sheet model of reduced complexity for paleoclimate studies, *Earth System Dynamics*, *7*(2), 397–418, doi:10.5194/esd-7-397-2016. 4

Niu, L., G. Lohmann, S. Hinck, E. J. Gowan, and U. Krebs-Kanzow (2019), The sensitivity of Northern Hemisphere ice sheets to atmospheric forcing during the last glacial cycle using PMIP3 models, *Journal of Glaciology*, *65*(252), 645–661, doi:10.1017/jog.2019.42. 3

Noël, B., W. Van De Berg, J. Van Wessem, E. Van Meijgaard, D. Van As, J. T. M. Lenaerts, S. Lhermitte, P. Munneke, C. Smeets, L. Van Ulft, R. Van De Wal, and M. Van Den Broeke (2018), Modelling the climate and surface mass balance of polar ice sheets using RACMO2 - Part 1: Greenland (1958-2016), *The Cryosphere*, *12*(3), 811–831, doi:10.5194/tc-12-811-2018. 1, 75

Noël, B., L. van Kampenhout, W. J. van de Berg, J. T. M. Lenaerts, B. Wouters, and M. R. van den Broeke (2020), Brief communication: CESM2 climate forcing (1950–2014) yields realistic Greenland ice sheet surface mass balance, *The Cryosphere*, *14*(4), 1425–1435, doi:10.5194/tc-14-1425-2020. 74

Ohmura, A. (2001), Physical Basis for the Temperature-Based Melt-Index Method, *Journal of Applied Meteorology*, *40*(4), 753–761, doi:10.1175/1520-0450(2001)040<0753:PBFTTB>2.0.CO;2. 1

Payne, A. J., S. Nowicki, A. Abe-Ouchi, C. Agosta, P. Alexander, T. Albrecht, X. Asay-Davis, A. Aschwanden, A. Barthel, T. J. Bracegirdle, R. Calov, C. Chambers, Y. Choi, R. Cullather, J. Cuzzone, C. Dumas, T. L. Edwards, D. Felikson, X. Fettweis, B. K. Galton-Fenzi, H. Goelzer, R. Gladstone,

N. R. Golledge, J. M. Gregory, R. Greve, T. Hattermann, M. J. Hoffman, A. Humbert, P. Huybrechts, N. C. Jourdain, T. Kleiner, P. K. Munneke, E. Larour, S. Le clec'h, V. Lee, G. Leguy, W. H. Lipscomb, C. M. Little, D. P. Lowry, M. Morlighem, I. Nias, F. Pattyn, T. Pelle, S. F. Price, A. Quiquet, R. Reese, M. Rückamp, N. J. Schlegel, H. Seroussi, A. Shepherd, E. Simon, D. Slater, R. S. Smith, F. Straneo, S. Sun, L. Tarasov, L. D. Trusel, J. Van Breedam, R. van de Wal, M. van den Broeke, R. Winkelmann, C. Zhao, T. Zhang, and T. Zwinger (2021), Future Sea Level Change Under Coupled Model Intercomparison Project Phase 5 and Phase 6 Scenarios From the Greenland and Antarctic Ice Sheets, *Geophysical Research Letters*, *48*(16), 1–8, doi:10.1029/2020GL091741. 75

Pellicciotti, F., B. Brock, U. Strasser, P. Burlando, M. Funk, and J. Corripio (2005), An enhanced temperature-index glacier melt model including the shortwave radiation balance : development and testing for Haut Glacier d ' Arolla, Switzerland, *Journal of Glaciology*, *51*(May 2016), 573–587, doi:10.3189/172756505781829124. 1

Plach, A., K. H. Nisancioglu, P. M. Langebroek, A. Born, and S. Le clec'h (2019), Eemian Greenland ice sheet simulated with a higher-order model shows strong sensitivity to surface mass balance forcing, *The Cryosphere*, *13*(8), 2133–2148, doi:10.5194/tc-13-2133-2019. 1, 2, 3, 76

Prinz, R., L. Nicholson, T. Mölg, W. Gurgiser, and G. Kaser (2016), Climatic controls and climate proxy potential of Lewis Glacier, Mt. Kenya, *The Cryosphere*, *10*, 133–148, doi:10.5194/tc-10-133-2016. 2

Rennermalm, Å. K., R. Hock, F. Covi, J. Xiao, G. Corti, J. Kingslake, S. Z. Leidman, C. Miège, M. Macferrin, H. Machguth, et al. (2021), Shallow firn cores 1989–2019 in southwest Greenland's percolation zone reveal decreasing density and ice layer thickness after 2012, *Journal of Glaciology*, pp. 1–12, doi:10.1017/jog.2021.102. 76

Robinson, A., R. Calov, and A. Ganopolski (2010), An efficient regional energy-moisture balance model for simulation of the greenland ice sheet response to climate change, *The Cryosphere*, *4*(2), 129–144, doi:10.5194/tc-4-129-2010. 1, 2

Robinson, A., R. Calov, and A. Ganopolski (2011), Greenland ice sheet model parameters constrained using simulations of the Eemian Interglacial, *Climate of the Past*, *7*(2), 381–396, doi:10.5194/cp-7-381-2011. 1, 2

Robinson, A., J. Alvarez-Solas, M. Montoya, H. Goelzer, R. Greve, and C. Ritz (2020), Description and validation of the ice-sheet model Yelmo (version 1.0), *Geosci. Model Dev.*, *13*, 2805–2823, doi:10.5194/gmd-13-2805-2020. 77

Rye, C. J., I. C. Willis, N. S. Arnold, and J. Kohler (2012), On the need for automated multiobjective optimization and uncertainty estimation of glacier mass balance models, *Journal of Geophysical Research*, *117*(F2), 1–21, doi:10.1029/2011JF002184. 2

Saltelli, A., F. Campolongo, and S. Tarantola (2000), Sensitivity Anaysis as an Ingredient of Modeling, *Statistical Science*, *15*(4), 377–395, doi:10.1214/ss/1009213004. 3

Saltelli, A., P. Annoni, I. Azzini, F. Campolongo, M. Ratto, and S. Tarantola (2010), Variance based sensitivity analysis of model output. Design and estimator for the total sensitivity index, *Computer Physics Communications*, *181*(2), 259–270, doi:10.1016/j.cpc.2009.09.018. 3

Sauter, T., and F. Obleitner (2015), Assessment of the uncertainty of snowpack simulations based on variance decomposition, *Geoscientific Model Development*, *8*(3), 3911–3928, doi:10.5194/gmd-8-3911-2015. 3

Sime, L. C., N. B. Karlsson, J. D. Paden, and S. Prasad Gogineni (2014), Isochronous information in a Greenland ice sheet radio echo sounding data set, *Geophysical Research Letters*, *41*(5), 1593–1599, doi:10.1002/2013GL057928. 4

Spear, R. C., and G. M. Hornberger (1980), Eutrophication in peel inlet-II. Identification of critical uncertainties via generalized sensitivity analysis, *Water Research*, *14*(1), 43–49, doi:10.1016/0043-1354(80)90040-8. 3

Tabone, I., J. Blasco, A. Robinson, J. Alvarez-Solas, and M. Montoya (2018), The sensitivity of the greenland ice sheet to glacial–interglacial oceanic forcing, *Climate of the Past*, *14*(4), 455–472, doi:10.5194/cp-14-455-2018. 75

Uppala, S. M., S. B. Healy, M. A. Balmaseda, P. de Rosnay, L. Isaksen, L. van de Berg, A. J. Geer, A. P. McNally, M. Matricardi, L. Haimberger, D. P. Dee, R. Dragani, N. Bormann, H. Hersbach, F. Vitart, S. Kobayashi, U. Andrae, A. C. M. Beljaars, P. Poli, B. M. Monge-Sanz, C. Peubey, J.-N. Thépaut, C. Delsol, E. V. Hólm, A. J. Simmons, M. Köhler, P. Bechtold, P. Berrisford, G. Balsamo, B.-K. Park, M. Fuentes, J. Bidlot, P. Bauer, C. Tavolato, P. Kållberg, and J.-J. Morcrette (2011), The ERA-Interim reanalysis: configuration and performance of the data assimilation system, *Quarterly Journal of the Royal Meteorological Society*, *137*(656), 553–597, doi:10.1002/qj.828. 3, 5

Van de Berg, W. J., M. Van Den Broeke, J. Ettema, E. Van Meijgaard, and F. Kaspar (2011), Significant contribution of insolation to eemian melting of the greenland ice sheet, *Nature Geoscience*, *4*(10), 679–683, doi:10.1038/ngeo1245. 1

Van Den Berg, J., R. van de Wal, and H. Oerlemans (2008), A mass balance model for the Eurasian Ice Sheet for the last 120,000 years, *Global and Planetary Change*, *61*(3-4), 194–208, doi:10.1016/j.gloplacha.2007.08.015. 1

van Griensven, A., T. Meixner, S. Grunwald, T. Bishop, M. Diluzio, and R. Srinivasan (2006), A global sensitivity analysis tool for the parameters of multi-variable catchment models, *Journal of Hydrology*, *324*(1-4), 10–23, doi:10.1016/j.jhydrol.2005.09.008. 3

Vionnet, V., E. Brun, S. Morin, A. Boone, S. Faroux, P. Le Moigne, E. Martin, and J. M. Willemet (2012), The detailed snowpack scheme Crocus and its implementation in SURFEX v7.2, *Geoscientific Model Development*, *5*(3), 773–791, doi:10.5194/gmd-5-773-2012. 1, 76

Walsh, J. E., W. L. Chapman, V. Romanovsky, J. H. Christensen, and M. Stendel (2008), Global climate model performance over Alaska and Greenland, *Journal of Climate*, *21*(23), 6156–6174, doi:10.1175/2008JCLI2163.1. 3

Watanabe, S., S. Kanae, S. Seto, P. J. Yeh, Y. Hirabayashi, and T. Oki (2012), Intercomparison of bias-correction methods for monthly temperature and precipitation simulated by multiple climate models, *Journal of Geophysical Research Atmospheres*, *117*(23), 1–13, doi:10.1029/2012JD018192. 3

Zolles, T., F. Maussion, S. Peter Galos, W. Gurgiser, and L. Nicholson (2019), Robust uncertainty assessment of the spatio-temporal transferability of glacier mass and energy balance models, *The Cryosphere*, *13*(2), 469–489, doi:10.5194/tc-13-469-2019. 2, 3

Graphic design: Communication Division, UiB / Print: Skipnes Kommunikasjon AS

uib.no

ISBN: 9788230856390 (print)
9788230860519 (PDF)